

TRANSIENT KINETIC STUDIES OF CHAR REACTIONS
IN A GRADIENTLESS REACTOR SYSTEM -- CO₂ GASIFICATION

O. Sy and J. M. Calo

Division of Engineering
Brown University
Providence, Rhode Island 02912

1. INTRODUCTION

Although a voluminous literature exists concerning the study of coal char-gas reaction systems, the understanding of the actual mechanisms and the roles of heat and mass transport in the overall conversion process, are still far from complete. One difficulty in determining intrinsic reaction mechanisms in many previous studies can be at least partially attributed to the use of "steady-state" conditions. The results of such experiments can be explained equally well by a few plausible models which all yield roughly the same overall gasification rate. Discrimination among candidate models is difficult under these conditions, and there is no guarantee that the model finally selected actually reflects the true mechanism over a wide range of operating conditions. Also, "steady-state" rate measurements reveal relatively little concerning the detailed sequence of elementary steps that constitutes the intrinsic reaction mechanism.

In addition to difficulties in model discrimination, the types of laboratory reactors which have been used in coal gasification kinetic studies may have also contributed to data interpretation problems that are well known for heterogeneous catalytic systems [e.g., see (1-3)].

The primary objective of the current work is to overcome most of these problems in order to develop a fundamental description of the reaction mechanisms of the heterogeneous coal char-gas reactions using an experimental system and techniques which allow the elementary steps to be better identified. More specifically, the approach involves the application of a "gradientless" reactor system coupled with a supersonic, modulated molecular beam mass spectrometer, and transient response techniques to char gasification kinetic studies. The transient behavior of a reaction system as it proceeds from one steady-state to another upon perturbation of system state variables exhibits characteristics reflective of the nature of the detailed kinetic mechanism. Furthermore, in addition to transient data, the usual steady-state results are available as well. Thus the transient response method is employed as an aid in model discrimination, mechanism determination, and, ultimately, parameter estimation.

The use of an internal recycle, "gradientless" reactor serves a dual purpose: (1) it simplifies the mathematical analysis of the transient data due to the resultant lumped parameter description of the transient response; and (2) it significantly reduces the influence of interphase mass and heat transport gradients. The principal advantages of this type of reactor over other common reactor types have been well documented in the literature [e.g., see (3-11)].

Finally, in order to obtain the transient data, the reactor must be coupled to a responsive analytical technique which allows continuous measurement of the transient product concentrations. Mass spectrometry is one such technique compatible with the transient response method. On-line mass spectrometry has been employed by several researchers in studies of the devolatilization of coal under vacuum conditions (12-14). Rapid sampling while operating at the high pressures relevant to the present study can be accomplished by allowing the product gases after pressure let-down to expand through a sonic orifice as a supersonic, adiabatic free jet into a differentially-pumped vacuum system. The rapid expansion into the vacuum "freezes" the relative compositions of the product gases when the sampled gas attains molecular flow. By skimming the core of the jet, a molecular beam can be formed. The resultant beam is further modulated to discriminate between the in-

stantaneous behavior of the beam species and the same species in the background of the mass spectrometer vacuum envelope (15,16).

The adaptation of these techniques to the current purpose is set forth below. The char-carbon dioxide reaction system is used to illustrate the efficacy of the approach. Other char-gas reaction systems and related studies are being pursued in a similar manner.

2. EXPERIMENTAL

2.1. System Description

A schematic of the experimental apparatus developed for the current transient kinetic studies is presented in Figure 1. Essentially, it consists of: (a) a continuous gas flow, fixed solids, "gradientless" (Berty-type) reactor; (b) an automatic switching gas addition valve network for generating concentration perturbations under conditions of constant flowrate, temperature, and pressure; and (c) a supersonic, modulated, molecular beam mass spectrometer for measuring the transient behavior of the concentrations of the product gases.

A typical experimental run might proceed in the following manner. Steady-state is first established with inert gas (e.g., argon) flowing through the reactor (maintained at the desired temperature and pressure), and with reactant gas (e.g., carbon dioxide) flowing through the purge line. At time zero, the inert gas is instantaneously replaced by the reactant gas now flowing through the reactor, and the reaction is thereby initiated. The switching is done in such a manner as to insure the same volumetric flowrate through the reactor, in spite of the change in gas species. This results in a well-defined step function increase of the reactant to the reactor. The transient response of the reaction system to this perturbation is then monitored with the beam sampling system at the reactor exit.

The experimental system has been designed to operate at conditions relevant to commercial coal gasification conditions (e.g., up to 500 psi at 1400°F, and even higher pressures at lower temperatures, as determined primarily by the manufacturer's specifications for the reactor). Also, the reactor space time (the ratio of the reactor gas phase volume to the volumetric flowrate) can be varied over the range 0.01 - 1.0 min.

The preceding, necessarily brief description is intended to convey only a general overview of the apparatus and its mode of operation. For a thorough discussion of the important and interesting details of the development of the apparatus, and the adaptation of transient kinetic techniques to char gasification, see reference (17).

2.2. System Performance

Reactor mixing performance curves were obtained by imposing step changes in the reactor feed from argon to carbon dioxide at constant volumetric flowrate, pressure, and temperature, and recording the resultant transient response. Due to considerable adsorption of test gases by the char, nonporous 3 mm glass beads were used in the basket for these studies. The resultant data were all clearly exponential, in accordance with well-mixed reactor behavior, and the corresponding time constants were close to expected values. The total gas mixing volume deduced from these experiments was found to be 241.4 cm³, which is quite reasonable in view of the fact that the total internal reactor volume is 275 cm³, of which approximately 30 cm³ is presumed to be dead volume located beneath the impeller.

In order to assess the relative influence of interphase heat and mass transfer on intrinsic chemical kinetic rates, the reactor internal recycle ratio, R , and superficial velocity, v_0 , through the char bed were determined by measuring the pressure drop across the char bed in the same manner as described by Berty (18); i.e., $R = A v_0 / q$, where A is the cross-sectional area of the basket (20.27 cm²) and q is the volumetric flowrate at reactor conditions. For typical experimental conditions with space time $\tau = 15$ s, free gas volume $V_g = 220$ cm³ ($V_g = 241.4$ cm³ - W/ρ_s , where W is the weight of dry char in the basket, ρ_s is the solid density and 241.4 cm³ is the total free gas volume in the reactor from the glass beads experiments), and impeller speed of 2800 RPM, the superficial gas velocity deter-

mined from our calibration is $v_0 = 13.72$ cm/s (0.45 ft/s). With a flowrate of $q = 14.67$ cm³/s the recirculation ratio is $R = 19$, which is sufficient to guarantee good mixing and gradientless operation.

The influence of interphase mass transfer limitation on measured kinetics for a particular set of experimental conditions can be assessed from the Damkohler number, $Da = k_1 C_{s0}(1-\theta)/k_m a_m/RT$, which is the ratio of the reaction rate, (as represented by the kinetic rate constant for the oxygen-exchange reaction; see below), and the effective interphase mass transfer coefficient for CO₂ which can be estimated from the j -factor for interphase mass transfer, j_D (e.g., see (19), p.395). For the experimental conditions used in the current work, it was found that $1 \times 10^{-6} < Da < 9 \times 10^{-4}$. Since $Da \ll 1$, the reaction is definitely not limited by interphase mass transport. The relative importance of intraphase diffusion is considered in the Discussion.

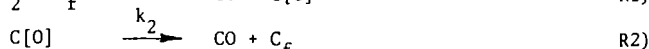
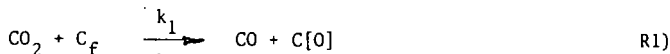
The interphase heat transfer limitation can also be evaluated from the Damkohler number by making use of the Chilton-Colburn analogy between mass and heat transfer in packed beds (e.g., see (19), p. 396). For typical reaction conditions, assuming a heat of reaction of +41.23 kcal/g mol for the overall CO₂ - char gasification reaction, the estimated temperature difference between the surface of the char, T_s , and the bulk fluid, T_b , is $5 \times 10^{-6} < (T_b - T_s)/T_b < 4 \times 10^{-3}$. Thus, for a high operating temperature like 972 K, $(T_b - T_s)$ can be as large as 4°C. Actual temperature differences between the solid and gas in the char bed are expected to be less than this due to radiation. Therefore, it can be conservatively stated that the interphase heat transfer limitation is not significant in the current studies.

Based upon the preceding performance data and numerical estimates, the particle size of the activated coconut (Fischer) char selected for the experiments reported on here was > 14 mesh. With an average particle diameter of about 1.6 mm, the resultant superficial velocity through the char bed at maximum impeller RPM should effectively eliminate interphase heat and mass transfer gradients, and provide a relatively high internal recycle ratio for space times in the range of 12 to 20s, that were found to be optimum for the current experiments.

3. KINETIC MODELING

The general treatment of transient kinetic models is outlined by Bennett (20) and Cutlip et al. (21). In essence, the transient mass balances for the species in the reaction system yield a set of differential equations which defines the model for the particular mechanism assumed. Integration of this system of equations results in the transient curves of the various species, which can then be used for parameter sensitivity studies, and also for parameter estimation by comparison with corresponding experimental data.

In order to illustrate this approach, consider the simple two-step mechanism:



which is imbedded in all known CO₂ gasification kinetic mechanisms, and was found to adequately represent the data in the current work.

If C_{s0} , C_0 , x , θ , and P_i represent, respectively, the active site concentration in g mol/g mol C, the initial total g mol of carbon, the fractional conversion, the fractional surface coverage of the complex, and the partial pressure of species i in the gas phase, the following rate expressions result for the preceding mechanism:

$$r_1 = C_{s0}C_0(1-x)[k_1(1-\theta)P_{CO_2}] \quad 1)$$

$$r_2 = C_{s0}C_0(1-x)[k_2\theta] \quad 2)$$

Assuming a gradientless reactor, a mass balance on each species yields:

$$CO_2: \frac{dP_{CO_2}}{dt} = \frac{P_{CO_2}^{(1-\theta)} - P_{CO_2}}{\tau} - \frac{r_1 RT}{V_g} \quad 3)$$

$$CO_2: \quad \frac{dP_{CO}}{dt} = \frac{(r_1 + r_2)}{V_g} - \frac{P_{CO}}{\tau} \quad 4)$$

$$C[O]: \quad \frac{d\theta}{dt} = \frac{r_1}{C_{so}C_o(1-x)} + \frac{\theta r_2}{C_o(1-x)} \quad 5)$$

$$C: \quad \frac{dx}{dt} = \frac{r_2}{C_o} \quad 6)$$

$$\text{Inert gas (Ar): } P_{Ar} = P_{CO_{2f}} - P_{CO_2} - P_{CO} \quad 7)$$

$$\text{where } \delta = \frac{r_2 RT \tau}{V_g P_{CO_{2f}}} \quad (\text{due to the increase in gas volume upon reaction})$$

P_t = total system pressure, atm

$P_{CO_{2f}}$ = partial pressure of CO_2 in the feed (also total pressure of reactor if feed is pure CO_2), atm

τ = V_g/q ; reactor space time evaluated at reactor conditions, min

V_g = reactor gas phase volume, cm^3

q = volumetric flowrate at reactor conditions, cm^3/min

T = reaction temperature, K

R = universal gas constant, $atm \cdot cm^3 / K \cdot g \text{ mol}$

The units for the rate parameters are $k_1 = [min^{-1} atm^{-1}]$ and $k_2 = [min^{-1}]$. The initial conditions for a pure CO_2 feed at time $t = 0$ are:

$$\begin{aligned} P_{CO_2} &= P_{CO} = \theta = x = 0 \\ P_{Ar} &= P_t \end{aligned} \quad 8)$$

Equations 1 through 8 constitute the model for the reaction system with dependent variables P_{CO_2} , C_{CO} , P_{Ar} , θ , and x , and parameters C_{so} , k_1 , and k_2 .

From simulated CO transient response results, it was found that the active site concentration, C_{so} , has a pronounced effect on the production of CO, but the shape of the transient curve remains relatively unchanged. However, the shape and position in time of the "overshoot" of the CO responses for both mechanisms are quite sensitive to the kinetic rate parameters k_1 and k_2 . The effects of k_1 and k_2 are qualitatively illustrated in Figure 2. It is noted that the "overshoot" is due to large values of k_1 , while the "leveling-off" is associated with large k_2 values.

Once the raw data (i.e., transient curves of the modulated signals for $m/e = 44$ and 28) are corrected to yield the net CO production curve due to reaction (from the fragmentation coefficient measured for CO_2), and then converted to CO partial pressure data (from the relative sensitivity measured for CO and CO_2), the next step is to determine a best parameter set for the proposed mechanism. This is done by minimizing the least squares objective function,

$$\phi = \sum_{k=1}^K \sum_{i=1}^n [(\hat{y}_{ik} - \hat{\bar{y}}_{ik})/y_{ik}]^2 \quad 9)$$

(where the subscript ik represents the i th variable at time k , with:

$i = 1, \dots, n$; the number of variables used in the optimization process,

$k = 1, \dots, K$; the time intervals

y_{ik} = experimental point (partial pressure data),

\hat{y}_{ik} = predicted value from the model,

using a Marquardt-type technique (22), coupled with a Green's function method (23) to determine the necessary first order sensitivity coefficient matrix, $S = \partial y / \partial \beta$. In essence, the parameter estimation procedure consists of solving the $\sim \sim \sim$ equations resulting from minimizing the objective function, Equation 9, based on local linearization of the model about the initial guess parameter set, β . This solution yields the vector of parameter changes, $\Delta \beta_i$, which in turn give $\sim \sim \sim$ the next best estimate of the parameter set to minimize ϕ . This procedure is repeated until the objective function meets an acceptable preset tolerance. In the current work only one variable, P_{CO} , was used in the optimization of the objective function for parameter estimation from the experimental transient data. This was done because this variable is the most sensitive to the particular model used, while P_{CO_2} and P_{Ar} are less so.

4. RESULTS

The CO transient responses for the experimental runs conducted with two particle sizes of activated coconut (Fischer) char are presented in Figures 3 and 4. In these figures, the characteristic "overshoot" of the oxygen-exchange reaction, R1, as well as the "leveling-off" of the transient curves due to the carbon gasification reaction, R2, are clearly evident. As predicted by transient response simulations, smaller space times result in a sharper "overshoot" and a lower quasi-steady-state level of CO at longer times. Higher temperatures favor greater CO production but the "overshoot" becomes progressively less sharp.

The inhibition effect of pressure on gasification is not clearly evident in these figures, but becomes more so upon analysis of the quasi-steady-state gasification rate attained after "leveling-off" of the transient curves. From the stoichiometry of the overall reaction:



For continuous pure CO₂ gas feed, the "steady-state" gasification rate is given by

$$W_{ss} = \frac{-1}{dt} \frac{dC}{dt} = \frac{1}{2C} \frac{d[CO]}{dt} = \frac{P_{CO_{ss}}}{2C_o(1-x)RT} = \frac{P_{CO_{ss}q}}{2C_o RT} \quad 10)$$

for negligibly small carbon conversion (i.e., $x \approx 0$).

Equation 10 can be rearranged to

$$\left(\frac{P_{CO_2}}{W} \right)_{ss} = \left(\frac{2C_o RT}{q} \right) \left(\frac{P_{CO_2}}{P_{CO}} \right)_{ss} \quad 11)$$

The $(P_{CO_2}/P_{CO})_{ss}$ in this expression can be evaluated from the quasi-steady-state values P_{CO_2} obtained at the end of the transient period. A plot of the right-hand side of Equation 11 versus P_{CO_2} at constant temperature is presented in Figure 5. The observed linear dependence P_{CO_2} of the gasification rate on CO₂ partial pressure suggests a "steady-state" rate expression of the form:

$$\frac{P_{CO_2}}{W_{ss}} = \frac{1}{j_1} + \frac{P_{CO_2}}{j_2} \quad 12)$$

or

$$W_{ss} = \frac{j_1 P_{CO_2}}{1 + (j_1/j_2) P_{CO_2}} \quad 13)$$

Equation 13 is the same steady-state rate form observed by Ergun (24), with $j_1 = k_1 C_{so}$ and $j_2 = k_2 C_{so}$, and clearly shows the inhibiting effect of pressure on the gasification rate.

Several models were fit to the transient data: the Blackwood and Ingeme model (25), seven parameters; the Shaw model (26), five parameters; the Mentser and Ergun mechanism (27), five parameters; the Ergun mechanism (24), four parameters; and the two-step mechanism found appropriate in the current work (three parameters). Due to the low levels of CO present in the reactor under the current experimental

conditions, only the latter model fits the data accurately since the others all have CO reaction paths which are superfluous for our data.

The resultant parameter values for the two-step mechanism exhibited distinct Arrhenius temperature dependence. Numerical fits of all the data as a function of temperature yielded the following expressions:

$$k_1 = 6.13 \times 10^{11} \exp \left| \frac{-55,500}{RT} \right| \text{ min}^{-1} \text{ atm}^{-1} \quad (14)$$

$$\text{and } k_2 = 9.98 \times 10^9 \exp \left| \frac{-44,800}{RT} \right| \text{ min}^{-1} \quad (15)$$

Also, for the first time in the same experiment, the concentration of active carbon sites expressed as g mol/g mol C, was determined for the coconut char to be:

$$C_{so} = 1.70 \times 10^{-9} \exp \left| \frac{27,000}{RT} \right| \quad (16)$$

This indicates that the active site concentration has a negative "activation energy". In other words, at higher temperatures, initially active sites become deactivated; viz.,



This deactivation phenomenon agrees with some of the findings of Duval (28) and Blackwood et al. (29), which are discussed further below.

It is of interest to compare the values of the activation energies obtained in the present study for the two steps, R1 and R2, with corresponding values reported in the literature. Table I summarizes the results of previous investigators. It is evident that the apparent activation energy for the two common kinetic steps varies considerably from one study to another; with E_1 ranging from -27 to +76 kcal/g mol and E_2 from -17 to +93 kcal/g mol. This variation can be at least partially attributed to differences in experimental data analysis techniques, as well as the particular reaction mechanism assumed. It should also be noted that in all these studies, the rate parameters are reported as the product of the active site concentration, C_{so} , and the intrinsic rate constant, k . Hence, the apparent activation energies also reflect any variation of C_{so} with temperature. In other words, the difference in the types of char and experimental conditions can account for the wide range of activation energies evident in Table I. As indicated by Johnson (30), C_{so} is expected to decrease with increasing coal rank. In fact, this general trend is substantiated in the case of $k_2 C_{so}$ by the large activation energies observed for the high purity carbon (e.g., Ceylon graphite, Spheron 6 carbon, activated carbon, and graphite) used by Ergun (24) and Mentser and Ergun (27), vis-a-vis the much smaller temperature coefficients found for coconut char by Gadsby et al. (31), Long and Sykes (32), and also in the current work.

Differences in activation energies can also be attributed to presumably catalytic impurities in the char. This effect is especially pronounced (for $k_2 C_{so}$) in the work of Long and Sykes (32) with coconut char where E_2 changed from 38 to 66 kcal/g mol upon removal of mineral impurities with hydrochloric and hydrofluoric acids.

On the other hand, Mentser and Ergun (27) argued that the constant activation energies obtained in their work with different forms of high purity carbon were due to a constant number of active sites, C_{so} , independent of temperature, and thus reflected the true activation energies for the reaction steps. This hypothesis is not at all unreasonable since C_{so} should not decrease indefinitely with coal rank, but rather the active site concentration should attain some constant asymptotic value for the high purity carbons. If the activation energies reported by Mentser and Ergun are the "true" temperature coefficients for R1 and R2 (with $E_1 = 53.0$ kcal/g mol and $E_2 = 58.0$ kcal/g mol), then their results agree reasonably well with the intrinsic activation energies found in the current work ($E_1 = 55.5$ kcal/g mol and $E_2 = 44.8$ kcal/g mol).

Other differences in E_1' and E_2' are probably numerical in origin. For instance, Golovina (33) fitted several simplified forms of the same gasification rate expression to data (i.e., due to possible changes in mechanism at various conditions), and reported different E' values for three different regimes of pressure and temperature. However, the negative activation energies obtained are indicative of improper analysis of kinetic data. In addition, the fact that the same rate form can give rise to different apparent activation energies in different temperature regimes but over the same pressure range (see Table I), as reported by Golovina, also argues against the inherent validity of the proposed rate expression and the reaction rate - controlling zone claimed by the investigator.

The effect of intraphase mass transport resistance on the rate constants is now addressed. First, there was no discernible difference in the gasification rate behavior of the 1.6 mm and 2.68 mm coconut char particles. Also, the resultant model parameters for the two-step mechanism exhibit essentially the same temperature dependence for both particle sizes. However, chars generally exhibit a polymodal pore size distribution with most of the internal surface area available in pores of molecular dimensions (super micropores) (34). Thus, even though the insensitivity to particle size indicates no bulk diffusional limitation (i.e., in the macropores), if diffusion in the micropores were the limiting resistance to char gasification, particle size would not necessarily have any effect; i.e., the characteristic size of the microporous material in both particle sizes is similar. In addition, micropore diffusion is known to be activated (35). Thus if its rate is comparable to the kinetic rate, or rate-controlling, its activation energy would be included in the overall apparent activation energy.

The diffusion parameter (diffusion time constant) of CO_2 in the micropores of WYODAK 35 x 60 char at 800°C is given by Debelak and Malito (36) as $D/r^2 = 1.68 \text{ min}^{-1}$ for fresh char (i.e., $x = 0$). The coconut char gasification rate at 800°C and 1 atm in pure CO_2 , as given by Equation 13 with the rate parameters reported here, is $1.16 \times 10^{-3} \text{ min}^{-1}$. Thus, if the microporous structure of the WYODAK and coconut chars are at all similar, the observed gasification rate is too small by three orders-of-magnitude to be micropore diffusion-controlled. Even at the highest possible constant asymptotic gasification rate (i.e., at high pressure) of $4.02 \times 10^{-3} \text{ min}^{-1}$ at 800°C , the reaction is still definitely reaction rate-controlled.

Based on these observations, it is concluded that the activation energies for the parameters k_1 and k_2 found in the present study are intrinsic and in agreement with the general trend reported in the literature.

The negative "activation energy" exhibited by the active site concentration is consistent with the results of Duval (28), who presented strong evidence that active sites on a graphitic lattice disappear spontaneously with reaction temperature by a process termed thermal "healing" or "annealing". Thus, in effect, active sites are subjected to two modes of depletion: reaction with a gas phase molecule and thermal neutralization. Boulanger (37) also noted the same effect in carbon - CO_2 and carbon-steam systems. A similar trend was reported by Blackwood et al. (29) and Johnson (30) in studies of the effects of coal-char preparation temperatures. Blackwood et al. (29) correlated their results for hydrogen gasification rate constants in terms of $k = k^* \exp(E_p/RT_p) \exp(-E_g/RT_g)$, where T_g and T_p are the gasification and char preparation temperatures, respectively. For brown coal chars gasified in hydrogen at 25 atm with $T_p = T_g$, these workers found $E_p = 20 \text{ kcal/g mol}$. It is noted that there is a direct analogy between $T_p = T_g$ in these char reactivity studies and conditions in the current work whereby the coconut char was held at the reaction temperature in an argon atmosphere for relatively long periods of time prior to imposing the concentration step change to reactant CO_2 . Thus, the temperature dependence of C_{S0} found by Blackwood et al. (29) agrees well with that found by Duval (28) and in the present study. Blackwood et al. (29) proposed that the decreasing reactivity with increasing temperature is due to rearrangement of the carbon structure into a more stable ring

lattice, thereby reducing the availability of free π electrons for the formation of complexes at edges, and stabilizing previously unstabilized bonds.

6. CONCLUDING REMARKS

The efficacy of applying the experimental apparatus and transient response techniques to heterogeneous char-gas reactions has been successfully demonstrated for CO₂ gasification. This approach promises to be a valuable tool for determining mechanisms and rate parameters for direct use in modeling, design, and analysis of new or existing gasification and related systems. A similar approach is being taken in studying gasification reactions with other gases and mixtures.

ACKNOWLEDGEMENT

The authors gratefully acknowledge the support of the U. S. Department of Energy under Grant Nos. DE-FG22-80PC30211 and DE-FG22-81PC40786. However, any opinions, findings, conclusions, or recommendations expressed herein are those of the authors and do not necessarily reflect the views of DOE.

REFERENCES

- (1) Carberry, J. J., *Ind. Eng. Chem.* **56**, 39 (1964).
- (2) Bennett, C. O., Cutlip, M. B., and Yang, C. C., *Chem. Eng. Sci.* **27**, 2255 (1972).
- (3) Mahoney, J. A., *J. Catal.* **32**, 247 (1974).
- (4) Kobayashi, H., and Kobayashi, M., *Catal. Rev.-Sci. Eng.* **10**, 138 (1974).
- (5) Bennett, C. O., *Ibid.* **13**, 121 (1976).
- (6) Yang, C. C., Cutlip, M. B., and Bennett, C. O., in *Catalysis*, Hightower, J. W., Ed., vol. 1, *Proceedings of the Fifth International Symposium Congress on Catalysis*, p. 14-279, Miami, Fla. (1972).
- (7) Berty, J. M., Preprint No. 41F, 70th Annual Meeting of AIChE, New York, N. Y., Nov. 13-17, 1977.
- (8) Tajbl, D. G., Simons, J. B., and Carberry, J. J., *Ind. Eng. Chem. Fund.* **5**, 171 (1966).
- (9) Paspek, S. C., Varma, A., and Carberry, J. J., *Chem. Eng. Edn.* **14**, 78 (1980).
- (10) Halladay, J. B., and Mrazek, R. V., *J. Catal.* **28**, 221 (1973).
- (11) Brown, C. E., and Bennett, C. O., *AIChE J.* **16**, 817 (1970).
- (12) Joy, W. K., Ladner, W. R., and Pritchard, E., *Fuel* **49**, 26 (1970).
- (13) Juntgen, H., and van Heek, K. H., *Ibid.* **47**, 102 (1968).
- (14) Meyer, R. T., and Lynch, A. W., *High Temp. Sci.* **4**, 283 (1972).
- (15) Fenn, J. B., and Anderson, J. B., *Fourth International Symposium on Rarefied Gas Dynamics*, Section 8, p. 311, Toronto (1964).
- (16) Calo, J. M., and Bailey, A. D., *Rev. Sci. Instrum.* **45**, 1325 (1974).
- (17) Sy, O., "Transient Kinetic Studies of Char-Gas Reactions in a Gradientless Reactor: CO₂ Gasification," Masters Dissertation, Princeton University, May 1982.
- (18) Berty, J. M., *Chem. Eng. Progr.* **70**, 78 (1974).
- (19) Smith, J. M., *Chemical Engineering Kinetics*, McGraw Hill, N. Y. (1981).
- (20) Bennett, C. O., *AIChE J.* **13**, 890 (1967).
- (21) Cutlip, M. B., Yang, C. C., and Bennett, C. O., *Ibid.* **18**, 1073 (1972).
- (22) Marquardt, D. W., *J. Soc. Ind. Appl. Math.* **11**, 431 (1963).
- (23) Kramer, M. A., J. M. Calo, and H. Rabitz, *Appl. Math. Model.* **5**, 432 (1981).
- (24) Ergun, S., *J. Phys. Chem.* **60**, 480 (1956).
- (25) Blackwood, J. D., and Ingeme, A. J., *Aust. J. Chem.* **13**, 134 (1960).
- (26) Shaw, J. T., *Fuel* **56**, 134 (1977).
- (27) Mentser, M., and Ergun, S., *U. S. Bur. Mines Bull.* **644** (1973).
- (28) Duval, X., *J. Chim. Phys.* **47**, 339 (1950).
- (29) Blackwood, J. D., McCarthy, D. J., and Cullis, B. D., *Aust. J. Chem.* **20**, 1561, 2525 (1967).
- (30) Johnson, J. L., *Kinetics of Coal Gasification*, Wiley, N. Y. (1979).
- (31) Gadsby, J., Long, F. J., Sleightholm, P., and Sykes, K. W., *Ibid.* **A193**, 357 (1948).
- (32) Long, F. J., and Sykes, K. W., *J. Chim. Phys.* **47**, 362 (1950).

- (33) Golovina, E. S. Carbon 18, 197 (1980).
- (34) Gan, H., Pandi, S. P., and Walker, P. L., Jr., Fuel 51, 272 (1972).
- (35) Walker, P. L., Jr., Fuel 59, 809 (1980).
- (36) Debelak, K. and Malito, J. T., "Effective Diffusivity in Coals as a Function of Conversion," presented at the 56th Colloid and Surface Science Symposium, Blacksburg, VA, June, 1982.
- (37) Boulangier, F., Duval, X., and Letort, M., Proceedings of the Third Conference on Carbon, p. 257, Pergamon Press, N. Y. (1959).

T (°C)	P (atm)	k ₁ C	k ₂ A exp(-E ₂ /RT)
--------	---------	------------------	---

Reference	Carbon Type	Summary of Kinetic Parameters (this work)				Summary of Kinetic Parameters (literature)	
		$T(^{\circ}\text{C})$	$P(\text{atm})$	$A_1 = A_2 \exp(-E^*/RT)$	$A_1(\text{min}^{-1})$	$E^*(\text{kcal/gmol})$	$k_{\text{iso}} = A_2 \exp(-E^*/RT)$
							$A_2(\text{min}^{-1})$
1. (31)	coconut char	700-850	0.01 - 1	7.6×10^9	58.8	2.4×10^9	28.7
2. (32)	coconut char	700-800	0.07 - 0.2	7.6×10^{10}	58.8	3.6×10^3	38.0
		with impurities extracted		3.8×10^{10}	68.4	2.3×10^8	66.0
3. (24)	activated carbon (a)	700-1000	1	-	-	8.5×10^8	59.0
	activated carbon (b)	900-1150	1	-	-	8.28×10^7	59.0
	ceylon graphite (c)	1000-1400	1	-	-	1.55×10^7	59.0
4. (29)	coconut char	790-870	2-40	2.7×10^{11}	76.0	1.13×10^{12}	76.0
5. (27)	Spheron 6	750-850	1	1.54×10^6	53.0	5.15×10^7	58.0
6. (30)	high volatile bituminous coal char (Pittsburgh, seam)	870-980	1-35	3.56×10^3	28.4	3.42×10^{10}	65.0
7. (33)	graphite	1380-1530	1	4.7×10^8	75.0	-	-
	"	"	3-10	4.7×10^8	75.0	23.5	18.0
Note:			2-40	4.7×10^8	75.0	1.9×10^6	56.5
$A_1 = \left \frac{R}{2 \pi \text{ min atm}} \right $		1730-1927	1	3.8×10^{-4}	-27.0	-	-
		"	3-10	3.8×10^{-4}	-27.0	67.2	24.5
		"	20-40	3.8×10^{-4}	-27.0	0.17	-3.0
$A_2 = \left \frac{R}{\text{cm}^2 \text{ min}} \right $		2030-2330	1	9.5×10^2	40.0	-	-
		"	3-10	9.5×10^2	40.0	7.1×10^{-3}	-17.0
		"	20-40	9.5×10^2	40.0	3.0	12.5
8. (38) summary of various chars		-	-	-	32.5 to 61.7	-	17.9
9. Present work	activated coconut char	680-770	8-30	1.0×10^3	28.5	17.0	17.9

Note:

$$A_1 = \left| \frac{g}{\text{cm}^2 \text{ min atm}} \right|$$

$$A_2 = \left| \frac{E}{2 \sin} \right|$$

8 (3A) SUMMARY

9. Present activities
Work

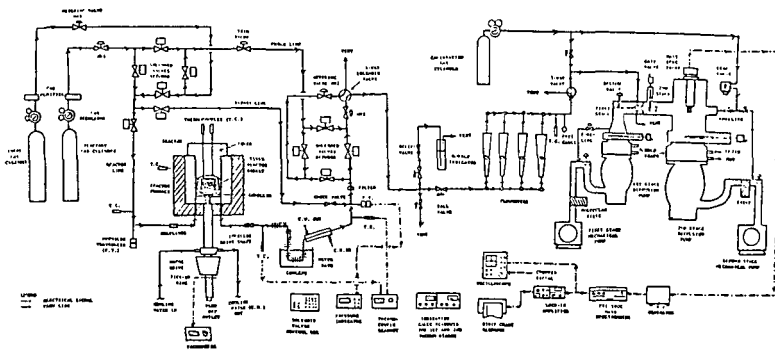


Figure 1. Schematic of the experimental apparatus for transient kinetic studies.

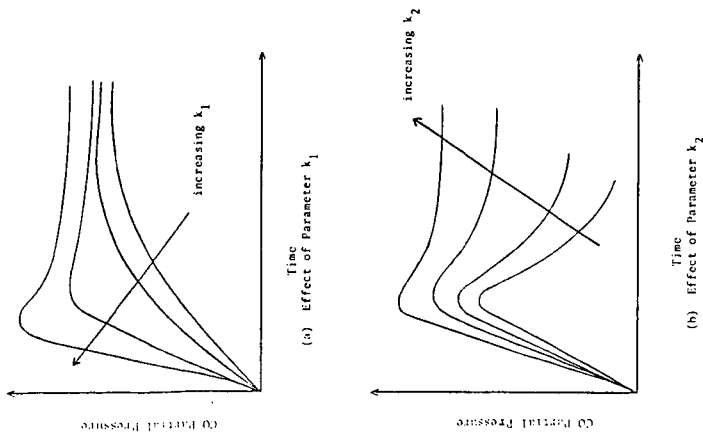


Figure 2. Sensitivity of CO transient response to parameters k_1 and k_2 - qualitative behavior.

Figure 3. Experimental transient response of CO partial pressure versus model predictions for CO₂ gasification of activated coconut char using the two-step mechanism (1.6 atm, 36.1925g, 4.3 cm bed height).

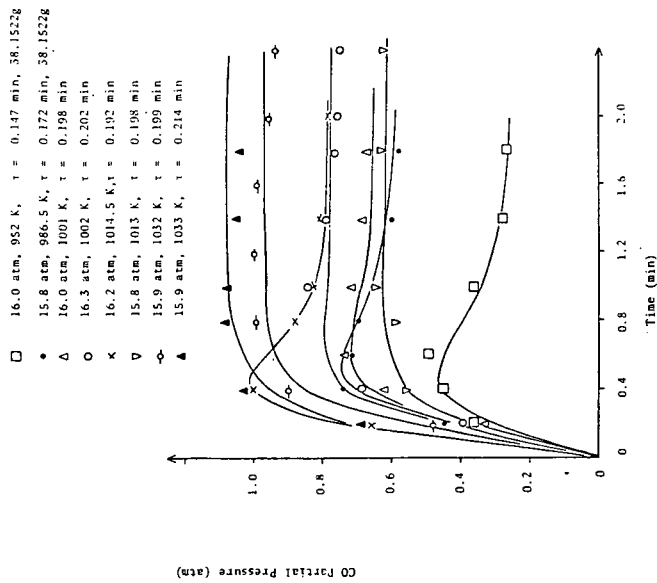


Figure 3. Experimental transient response of CO partial pressure and CO₂ production for CO₂ poisoning of activated charcoal using the two-step mechanism (2.68 mm, 39.036g, 4.3 cm bed height).

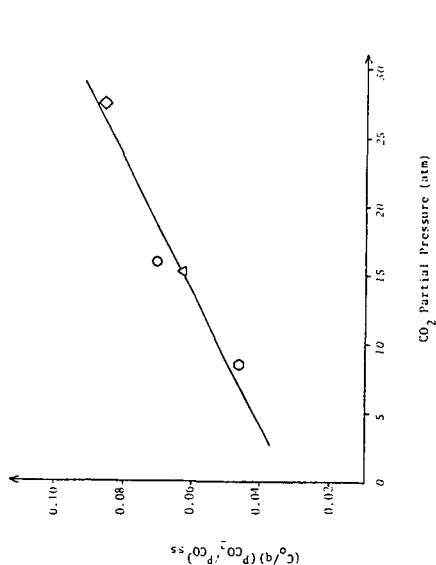
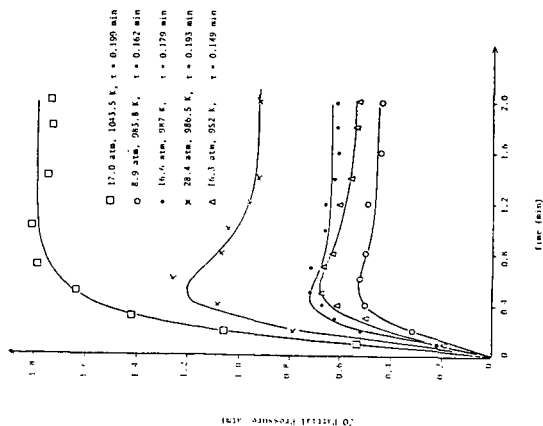


Figure 5. Quasi-steady-state gasification rate as a function of CO₂ partial pressure: (a) 1.6 mm activated coconut char, 39.036g, 4.3 cm bed height, 16.6 atm, 986.5 K, $\gamma = 0.18$ min; (b) 1.6 mm activated coconut char, 38.152g, 4.3 cm bed height; Δ $P = 15.8$ atm, $\gamma = 0.17$ min.

REACTION OF HIGH VELOCITY ATOMIC OXYGEN WITH GRAPHITE

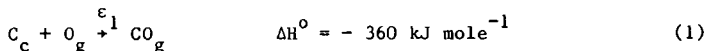
G. S. Arnold, R. K. Herm, and D. R. Peplinski

Chemistry and Physics Laboratory,
The Aerospace Corporation
El Segundo CA, 90245

Atmospheric bombardment of a spacecraft in low Earth orbit (LEO) presents a regime of gas-surface chemistry which has been the subject of very little laboratory investigation. The predominant atmospheric species in LEO (200-800 km) is ground state, neutral atomic oxygen (1). Although the ambient temperature is not extremely high ($\sim 10^3$ K), the 8 km sec^{-1} orbital velocity of the spacecraft causes oxygen atoms to strike the satellite's surfaces with an average collision energy of $5 \times 10^2 \text{ kJ mole}^{-1}$ ($\sim 5 \text{ eV}$). At the altitude at which the space shuttle operates ($\sim 240 \text{ km}$) the flux of atomic oxygen striking surfaces normal to the craft's velocity vector is of the order of $8 \times 10^{14} \text{ cm}^{-2} \text{ sec}^{-1}$. (1) The phenomenology of oxygen atom-surface interactions at such a collision energy is completely unstudied in the laboratory. The lack of experimentation in this area owes not to any assumption that such chemistry is fundamentally uninteresting, but rather reflects the difficulties inherent in reproducing in the laboratory the 8 km sec^{-1} impact velocity.

The details of oxygen atom surface interactions at orbital velocity are of particular interest for the prediction of the integrated effects of long-term exposure of materials to the LEO atmosphere. The unique opportunity which the shuttle orbiter provides to recover a variety of materials from LEO has highlighted the need for such an understanding. Organic polymers, including polyimides, polyesters, and polyurethanes, have been observed to erode at significant rates (2). A silver surface 2100\AA thick was completely oxidized (3). Osmium and graphite surfaces exposed to the atmosphere were completely removed (3,4).

The reaction of atomic oxygen with graphite:



is well known and so initially one does not find the removal of graphite surfaces by atmospheric oxygen to be particularly surprising (5). The rate at which graphite was removed was, however, quite unexpected. On the third shuttle flight (STS-3), a graphite surface estimated to be 10^{-4} in. thick was completely removed. The total time of direct exposure of the surface to the atmosphere was approximately 9 hours. If reaction 1 were responsible for the removal of the graphite, then it must have been occurring with a probability in excess of 0.8 per oxygen atom collision.

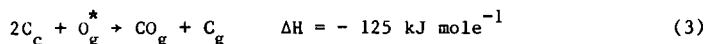
Reference 5 reports that the variation with surface temperature of the probability of reaction 1, ϵ_1 , for the case of oxygen atoms impacting at thermal velocities is given by:

$$\epsilon_1 = 0.63 e^{-1160/T} \quad (2)$$

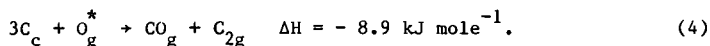
The temperature of the graphite exposed on STS-3 is expected not to exceed 420K, a temperature at which the Arrhenius expression given above predicts a value of ϵ_1 of 0.04. Even though the estimate of reaction probability on orbit is based on data which are somewhat less precise than might be desirable, the difference between prediction and observation is substantial.

Such a discrepancy in predicted and observed reaction probabilities indicates the possibility that the high translational energy of oxygen atoms striking graphite surfaces on orbit results in the enhancement of the probability that an oxygen atom removes a carbon atom on impact (as compared to the thermal oxidation of graphite by

O atoms). It is instructive to note that if one includes the translational energy of the atomic oxygen in one's accounting, channels for the removal of carbon atoms in addition to reaction 1 are at least thermodynamically allowed. Two of these reactions are:



and



Thus the oxidation of graphite was selected as the initial subject for investigation in a new facility constructed specifically for the study of high energy oxygen atom surface chemistry. In addition to providing further insight into a gas-surface interaction of great fundamental and practical interest, such experimentation serves as the prototype for the investigation of the oxidation of spacecraft materials by high energy atomic oxygen.

Figure 1 shows a schematic representation of the beam apparatus designed for the investigation of high energy oxygen atom surface chemistry. The vacuum system is comprised of four chambers. The first three are stainless steel boxes, 18 in. cubed, sealed with Buna-N "O-Rings". The first is pumped by an unbaffled 16 in. oil diffusion pump (Varian VHS-400). Each of the second and third chambers is pumped by a 10 in. oil diffusion pump (Consolidated Vacuum Corp.), topped with a liquid nitrogen cooled trap (Mt. Vernon Research Corp.), and an electro-pneumatically operated, viton-sealed gate valve (Vacuum Research Manufacturing Corp.). The fourth chamber uses crushed metal seals and is pumped by a high-speed turbomolecular pump (Balzers TPU 510).

The oxygen atom beam source (described below) is housed in chamber 1. The source is recessed into chamber 1 in order to minimize the distance from source to target thereby delivering the maximum available beam flux to the target. A Beam Dynamics Inc. model 2 nickel skimmer, 0.90 mm orifice diameter, connects chambers 1 and 2. Chambers 2 and 3 act as buffers to aid in the reduction of pressure between the source and the target. A beam chopper and beam flag which aid in the characterization of the beam are mounted in chamber 2. The second chamber also provides space for installation of a low resolution slotted disk velocity filter, which may be used when it is desirable to prevent light from the beam source from falling upon the target.

The solid target is contained in the fourth chamber, which is recessed into the third chamber to minimize source to target distance. A quadrupole mass spectrometer (Extranuclear Laboratories) is provided for characterization of the atomic beam and also for identification of the volatile products of bombardment of the target.

The production of a beam of neutral atomic oxygen of sufficient velocity and intensity for this program requires advances in the state-of-the-art of beam source technology. Indeed, one major reason for the scarcity of experimental data on atomic oxygen-surface interactions at high energies (~ 5 eV) is the difficulty in building a reliable, fast, high-intensity O atom beam source. Figure 2 shows the source constructed here to achieve such a beam. The source is a modified, commercially available plasma torch. The modifications include attachments for a water-cooled nozzle, through which the atomic beam expands into the vacuum system, and exhaust channels to dispose of excess torch gas. The torch operates in the non-transferred mode, i.e., the electric arc is confined within the torch. A plasma is formed in

* O^* indicates translational excitation of 480 kJ mole^{-1} .

helium by a dc arc. A small amount of O_2 (~ 2% of the total gas flow) is injected downstream of the arc into the gas flow, where it is thermally dissociated into oxygen atoms by the hot helium. The high temperature and the isentropic expansion provide for the oxygen atom velocity, which results in a supersonic beam. A similar source has been reported by Air Force Geophysics Laboratories (6).

The arc source has been tested with pure He, He/ O_2 mixtures, He/Ar/ O_2 mixtures, and Ar/ O_2 mixtures as a function of torch power. Tests with O_2 indicate that oxidation of electrodes does not take place even at high torch current levels. He, Ar, O_2 , and O atom beams have been detected using the mass spectrometer. Conversion of molecular oxygen into atoms is determined from relative mass peak signals (measured by the quadrupole mass spectrometer), I_O/I_{O_2} , by the formula of Miller and Patch (7).

$$y = \frac{N_O}{N_{O_2}} = P \left(\frac{\sigma_{O_2}}{\sigma_O} \right) \left(\frac{1}{\eta} \frac{I_O}{I_{O_2}} - 1 \right) \quad (6)$$

where N_O/N_{O_2} is the inferred number density ratio of O to O_2 , P is the probability of dissociative ionization, σ_O/σ_{O_2} is the ratio of electron impact ionization cross sections, I_O/I_{O_2} is the ratio of mass spectrometer signals of O and O_2 with the torch on, and η is the I_O/I_{O_2} ratio with the torch off. The per cent dissociation is given by:

$$\%D = 100 y/(y + 2).$$

As one can see from figure 3, the per cent dissociation of O_2 into O ranges from ~ 30 to 48% for a 2.55% O_2 in Ar mixture, to ~ 15 to ~ 19% for various O_2 in He/Ar mixtures. These per cent dissociation translate into source temperatures of 3000-3200°K for O_2 in Ar, and 2700-2850°K for O_2 in He/Ar mixtures. Although not shown, tests made using pure He also show a lower dissociation. The greater efficacy of argon in dissociating O_2 probably owes to increased energy deposition in Ar, which flows more slowly through the torch (0.63 STP ℓ sec⁻¹ Ar, 2.1 STP ℓ sec⁻¹ He).

Results will be reported of measurements of the rate of volatilization of graphite by high velocity atomic oxygen in order to determine if the apparent enhancement of this rate on orbit is real. Mass spectral measurement of the products of high velocity O atom bombardment of carbon will be described as well.

References

1. A. E. Hedin, Tables of Thermospheric Temperature, Density and Composition Derived from Satellite and Ground Base Measurements, Laboratory of Planetary Atmospheres, Goddard Space Flight Center, Volumes 1, 2, and 3 (January 1979).

A. E. Hedin, C. A. Reber, G. P. Newton, N. W. Spencer, H. C. Brinton, H. G. Mazer, and W. E. Pottes, "A Global Thermospheric Model Based on Mass Spectrometer and Incoherent Scatter Data MSIS 2, Composition," J. Geophys. Res. **82**, 2148-2156 (1977).

A. E. Hedin, J. E. Salah, JH. V. Evans, C. A. Reber, G. P. Newton, H. W. Spencer, D. C. Kayser, D. Alcayde, P. Bauer, L. Cogger, and J. P. McClure, "A Global Thermospheric Model Based on Mass Spectrometer and Incoherent Scatter Data 1, N₂ Density and Temperature," J. Geophys. Res. **82**, 2139-2147 (1977).
2. Lubert J. Leger, "Oxygen Atom Reactions with Shuttle Materials at Orbital Altitudes," NASA TM 58246, May 1982.
3. R. Linton, NASA MSFC, private communication.
4. G. B. Murphy and S. D. Shawhan, "Initial Results: The Measurements of the Shuttle's plasma environment on STS-3," 12th Space Simulation Conference, Pasadena CA. 17-19 May 1982.
5. Chul Park, "Effect of Atomic Oxygen on Graphite Ablation," AIAA Journal **14**, 1640 (1976) and references cited therein.
6. J. A. Silver, A. Freedman, C. E. Kolb, A. Rahbee and C. P. Dolan, "A supersonic nozzle beam source of atomic oxygen produced by electric discharge heating," Accepted for Publication, Rev. Sci. Instrum.
7. D. R. Miller and D. F. Patch, "Design and Analysis of a High Intensity Fast Oxygen Atom Source Rev. Sci. Instrum. **40**, 1566 (1969).

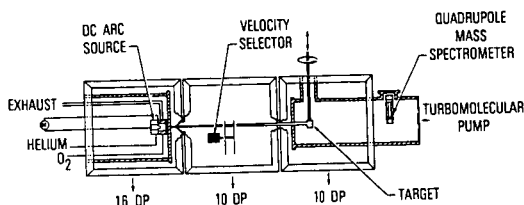


Figure 1. High energy oxygen atom surface chemistry apparatus.

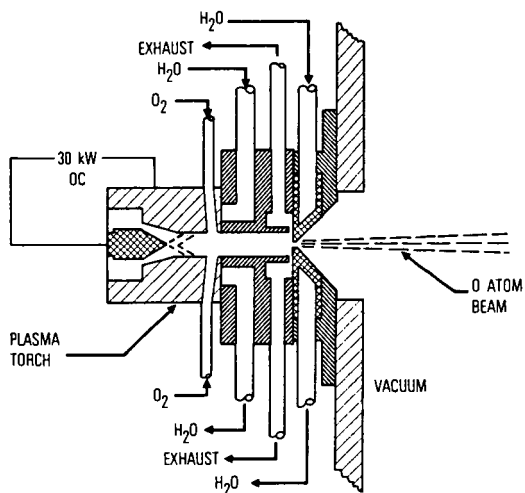


Figure 2. DC plasma arc atomic beam source.

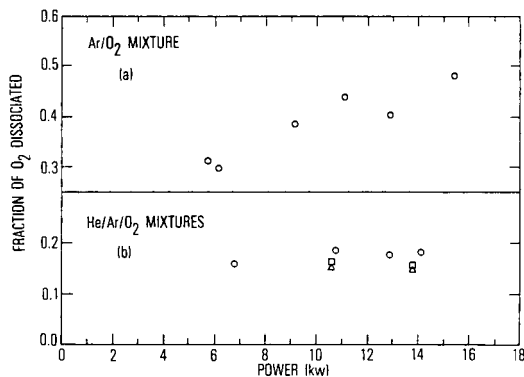


Figure 3.

Dissociation efficiency for O_2 in gas mixtures as a function of arc source power consumption: (a) 2.55% O_2 in Ar, (b) (o) 2.2% O_2 , 5.9% Ar, 91.9% He; (e) 1.5% Ar, 92.6% He; and (Δ) 2.9% O_2 , 5.9% Ar, 91.2% He.

Structure Changes During Carbon Methanation Reactions

J. Sentiesteban^{*}, S. Fuentes^{*} and M.J. Yacaman^{**}

^{*}Instituto de Fisica UNAM, Mexico, 20 DF

^{**}Physics Department, West Virginia University

1. INTRODUCTION

The reaction of carbon methanation on graphite surfaces containing platinum particles was studied using electron microscopy, gas chromatography and thermogravimetry. In the electron microscope, the weak beam thickness fringes ⁽¹⁾ and topographic refraction images ⁽²⁾ were used. In addition the STEM microdiffraction technique to obtain crystallographic information from individual particles ⁽³⁾ was employed.

2. ACTIVITY RESULTS

Figure 1 shows the results for the activity for methane production as function of the temperature. Below 700°C the methane concentration is undetectable. It starts to increase at this temperature and a maximum is obtained at 800°C. At 850°C the reaction approaches the thermodynamic equilibrium and the concentration is reduced. However at 900°C it increases again. The TEM showed that at this temperature channeling on the graphite surface starts to be produced. ⁽³⁾ Below this temperature the particles produced only pits in the surface.. Figure 2 shows a topographic image of the channels. Irregular large particles are extremely active in this reaction since they produce large channels and therefore remove more carbon from the surface. The weak beam image picture shows that the particles are very rough in shape. They

are flat platelets with a thickness of about 100 Å. A typical example is shown in Figure 3. It was found that well faceted particles did not produce any channeling and therefore they were inactive for the reaction. Particles in the size range below 100 Å produced regular channels moving along $\langle 11\bar{5}0 \rangle$ directions of the graphite in most cases, in agreement with the findings of Baker et.al⁽³⁾ and Tomita and Tamai⁽⁴⁾. However large irregular particles produced irregular channels not oriented along specific directions. The channeling always started along edges or steps on the graphite surface. The activation energy and reaction rate was determined by chromatography in the 700-800°C range and by thermogravimetry in 800-900°C interval. The reason for this was that at high temperatures, the methane was decomposed in the post-reaction zone, producing an error in the chromatographic measurements. The values found were 43.5 ± 4 KCal/mol and $0.0415 \text{ gr}(\text{CH}_4) / \text{hr gr}(\text{PT})$ for the activation energy and reaction velocity respectively in the 700-800°C interval and 44.0 ± 4 KCal/mol and $0.026 \text{ gr}(\text{CH}_4) / \text{hr gr}(\text{PT})$ for the 800-900°C interval. These results suggest that the reaction mechanism is the same for the whole range of temperatures. Microdiffraction experiments indicated that particles had an FCC structure corresponding to a cubo-octahedron. However in many cases a complex pattern was obtained not corresponding to an FCC structure. This was probably a carbide or an oxide. It was not possible to identify this phase univocally and more experiments are being carried out. The reaction appears to be produced on the interface Pt-graphite and is always related to pitting or channeling. The rate determining step seems to be the break of the C-C bond on the graphite surface. The main rate of the catalyst is to reduce the activation energy for the breaking of the C-C bond. The ability of the particles to remove carbon seems to be related to its surface roughness.

REFERENCES

1. M.J. Yacaman and T. Ocana, Phys. Stat. Sol. A) 42, 571 (1977).
2. A. Gomez, P. Hernandez and M.J. Yacaman, Surf. and Interf. Anal. 4, 120 (1982).
3. R.T.K. Baker, R.D. Sherwood and J.A. Dumesic, J.Catal 66, 56 (1980).
4. A. Tomita and Y. Tamai, J. Catal. 27, 293 (1972).

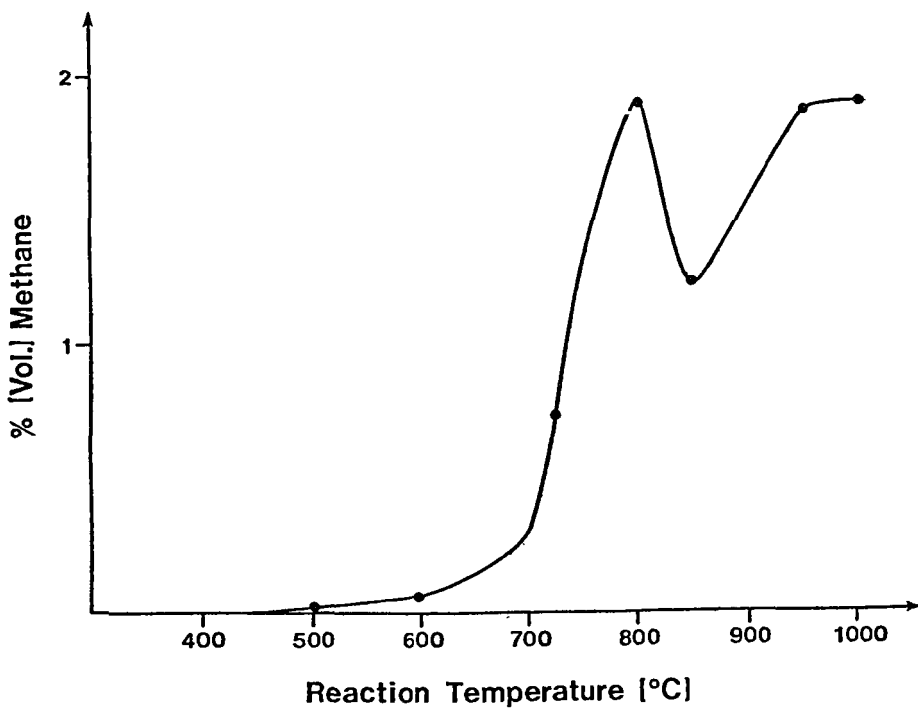


Figure 1. Concentration of methane as a function of the temperature.



Figure 2. Topographic image of channeling in graphite surfaces.



Figure 3. Weak beam image of a large particle showing rough surfaces.

DIRECT INVESTIGATION OF REACTING COALS BY
DIFFUSE REFLECTANCE INFRARED SPECTROMETRY

Peter R. Griffiths, Shih-Hsien Wang, Issam M. Hamadeh,
Paul W. Yang and David E. Henry

Department of Chemistry, University of California,
Riverside, California 92521

Introduction

A few years ago we showed that it was possible to measure the diffuse reflectance (DR) infrared spectrum of solids at high signal-to-noise ratio (SNR) with no sample preparation required other than pulverization (1). The key factors in our design were the use of a Fourier transform infrared (FT-IR) spectrometer incorporating a mercury cadmium telluride (MCT) detector, and the design of a highly efficient optical configuration for collecting diffusely reflected radiation and passing it to the detector. At that time, we suggested that the study of coal might be among the more important applications of DR spectrometry, although we initially believed that in order for good spectra to be obtained it was necessary to grind the samples with about ten times their weight of an alkali halide diluent (2). Subsequently, we demonstrated that equally good spectra could be obtained when no diluent was added, and several applications of DR infrared spectrometry to coal chemistry were described in a recent publication from this laboratory (3). Today it is possible to obtain commercial accessories for DR spectrometry for most commonly used FT-IR spectrometers from at least four different sources.

In view of the structural information potentially obtainable from the infrared spectra of neat powdered coals, we have studied the feasibility of monitoring the chemical changes which occur while reactions are taking place. This work necessitated two instrumental developments before truly useful data could be obtained. These were the construction of a cell and optical configuration suitable for the study of gas-solid reactions at high temperature and the further refinement of the assignment of infrared spectra of coals, especially after resolution enhancement.

Optics and Cell

The first DR infrared spectra measured during a reaction were described by Niwa *et. al.* (4,5). Their spectra were measured on a grating spectrometer and had a very low SNR. Subsequently (6), we described a small cell for controlling the atmosphere around a heated powder which could be installed in the optics reported in our first paper on DR spectrometry (1). Although the spectra measured with this cell had a far higher SNR than those of Niwa *et. al.*, the cell still had several disadvantages, in that it had to be very small, its temperature could not be raised above about 200°C, and temperatures had to be estimated rather than measured directly. The optical efficiency was reduced by the window geometry and, in addition, a substantial fraction of the radiation reaching the detector had never interacted with the sample, leading to a high level (~20%) of stray light.

Subsequently, a superior cell was introduced by Harrick Scientific Corporation (Ossining, N.Y.) with improved upper temperature limits, optical efficiency and stray light specifications. However, this cell still had one significant drawback for the study of reacting coals, in that it had only one inlet/outlet gas line, so that if tars were formed they would condense on the windows, completely obscuring the infrared beam from the detector.

To circumvent this problem and to permit improved operating specifications, a completely redesigned cell was constructed. Separate inlet and outlet gas lines were installed; the use of a wide-bore outlet tube permitted a vacuum of 10^{-4} torr to be obtained. The base of the sample cup is fritted so that inert or reactive gases can be drawn through the sample, preventing tar deposits on the window. The

input beam and diffusely reflected output beam are passed through a single 50cm diameter KCl window. The sample is heated by a nichrome wire coiled around the cup. The temperature of the sample can be measured by a thermocouple inserted into the powdered coal, and temperatures up to 600°C (1100°F) have been reached, which should allow the study of most important reactions of coals. To avoid overheating, the body of the cell is water-cooled.

To accommodate this cell, we designed a fundamentally different optical configuration for DR infrared spectrometry, which permits a large cell to be installed with little or no loss in optical efficiency. If a non-absorbing sample (such as powdered KCl) is placed in the cell, the SNR of the interferogram measured with an FT-IR spectrometer operating at full throughput (0.06 cm² steradian) with a medium-range MCT detector ($\lambda_{\text{max}}=15\mu\text{m}$) can be so large in the region of the centerburst that the dynamic range of the analog-to-digital converter may be exceeded unless a screen is placed in the beam. This cell and optics are described in details in the Ph.D. dissertation of Hamadeh (7), and are shown schematically in Figure 1.

Resolution Enhancement

Absorption bands in the infrared spectra of coals may be rather broad, so that detailed chemical information may be masked by the overlap of neighboring bands. Conversion of the spectrum to the second, or even the fourth, derivative has permitted the separation of small shoulders in the spectra of coals (3,6,8) but the interpretation of second- and fourth-derivative spectra is made difficult by the possibility that secondary lobes from intense sharp peaks may be mistaken for a real spectral feature in complex spectra. An alternative, and we believe preferable, technique for resolution enhancement where the effect of secondary lobes should be minimized is Fourier self-deconvolution (FSD). Here the absorption spectrum is converted to its Fourier transform, multiplied by an exponential function, and truncated if necessary to remove the high frequency noise components. The inverse transform then yields a spectrum in which the width of all spectral features has been reduced (9). Care must be taken, however, to avoid the use of an exponent in the multiplier which is too large since side-lobes will be generated which are analogous to those of second-derivative spectra.

To illustrate the potential of Fourier self-deconvolution in coal spectrometry, the progressive resolution enhancement of the spectrum of an oxidized low volatility bituminous coal in the region of the carbonyl stretching bands is shown in Figure 2. In the upper spectrum it can be seen that side-lobes have been generated and the noise level of the spectrum is increased to the point that it is difficult to distinguish a real feature from a noise spike. We have recently developed a technique to determine the optimum level of resolution enhancement consistent with an acceptable noise level and side-lobes (10), and we believe that the degree of resolution enhancement of all spectra shown or used in subsequent sections of this paper is quite conservative, and could probably have been improved upon if there optimization procedures had been applied rigorously.

Spectral Assignments

This increased resolution leads to some benefits and some problems. The benefits are obvious when the newly resolved bands can be unequivocally assigned to definite vibrational modes. For example, the spectra of most coals contain two bands between 3000 and 2800 cm⁻¹; these may be assigned to the symmetric and asymmetric stretching modes of aliphatic C-H groups. Each band often shows evidence of being composed of two unresolved or partially resolved components which can be completely resolved by FSD; these components can be assigned to vibrations of methylene and methyl groups. By studying the ratio of the intensities of these bands, the relative rates of reaction of CH₂ and CH₃ groups can be monitored, for example during air oxidation (vide infra).

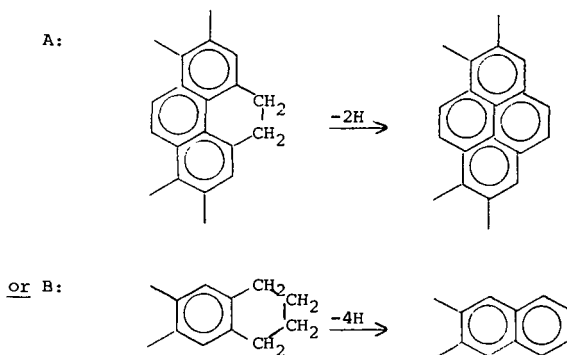
The disadvantage of the enhanced information content is encountered when the newly resolved spectra cannot be interpreted with certainty. In Figure 2, as many as nine bands may be resolved in the carbonyl stretching region alone. Some of these, e.g. the two anhydride bands at 1845 and 1775 cm^{-1} , are easily assigned. Others, especially the bands between 1735 and 1675 cm^{-1} , are much less easy to assign with any degree of certainty.

We are hoping to increase the certainty of these band assignments by correlating the infrared spectra with both solution-phase ^1H and solid-phase ^{13}C NMR spectra. The correlating of solution-phase ^1H spectra of that fraction of each coal soluble in pyridine- d_5 with the diffuse reflectance spectrum of the solute remaining after complete evaporation of the solvent is certainly useful, but one can never be sure that the structure of the coal remains unchanged after solvent elimination. The SNR of CP-MAS ^{13}C NMR spectra measured on a 60 MHz spectrometer was too low to permit useful conclusions to be made, and we are hoping that spectra to be measured on a 90 MHz spectrometer with a wide magnet gap prove more helpful.

Low Temperature Oxidation

The potential of DR spectrometry for monitoring coal reactions will be illustrated by the low temperature (150°C) air oxidation of a low volatile bituminous coal. This reaction is very slow - much slower than the types of reactions which we ultimately hope to study (which can have half-lives of only a few seconds) - but the data still give a good indication of the type of results which can be obtained. Deconvolved spectra measured at different times after oxidation was initiated are shown in Figure 3. The increase in absorption around 1700 and 1250 cm^{-1} is evident, showing that oxygen reacts to form both double and single carbon-oxygen bands, with C=O formation being the more rapid reaction. The existence of anhydride groups is not obvious in the early spectra, but the 1845 cm^{-1} band builds up rapidly after a few days, indicating that oxidation to carboxylic acids is an initial step, followed by condensation of neighboring $-\text{CO}_2\text{H}$ groups when their concentration is sufficiently high.

The increase in aromaticity can be inferred from a plot of the ratio of the intensity of the aromatic C-H stretching band at 3070 cm^{-1} to that of the symmetric methyl stretching band (2872 cm^{-1}) against time of oxidation, see Figure 4. The mechanism of this reaction can be inferred from a plot of the ratio of the intensities of the asymmetric methylene and methyl stretching mode against time of oxidation, see Figure 5. The faster rate of disappearance of CH_2 groups indicates that one possible mechanism by which aromaticity is increased is by oxidative dehydrogenation of hydroaromatic methylene groups:



In Reaction A, an aromatic ring with two neighboring C-H groups would be formed whereas in Reaction B the newly formed aromatic ring would have four neighboring C-H groups. It is possible to determine which reaction has the higher probability by studying the spectral region between 950 and 650 cm^{-1} . Three strong bands of approximately equal intensity may be observed in this region, at approximately 880, 815 and 760 cm^{-1} . These bands are due to the aromatic out-of-plane C-H deformations, and may be assigned as follows, after Bellamy (11):

880 cm^{-1} band: Isolated C-H groups, i.e. 1,2,3,4,5-pentasubstituted ring; 1,2,3,5 and 1,2,4,5-tetrasubstituted ring; 1,2,4, trisubstituted ring (in conjunction with 815 cm^{-1} band).

815 cm^{-1} band: Two neighboring C-H groups, i.e. 1,2,3,4-tetrasubstituted ring; 1,2,4-trisubstituted ring (in conjunction with 880 cm^{-1} band); para-disubstituted ring.

760 cm^{-1} band: Four neighboring C-H groups, i.e. ortho-substituted ring.

An increase in the intensity of the 815 cm^{-1} band relative to that of the 760 cm^{-1} band on dehydrogenation would indicate that Reaction A is favored over Reaction B, and vice versa. In Figure 6, it is shown that the rate of increase of the 760 cm^{-1} band is greater than that of the 815 cm^{-1} band, indicating that Reaction B is favored. It is noteworthy that this type of conclusion also gives an indication of the structure of low volatility bituminous coals, since the dimethylene structural unit in the reactant for Reaction A has been generally believed to be more prevalent in coals of this rank than the tetramethylene hydroaromatic unit in the reactant for Reaction B.

Conclusions

We believe that these data indicate the feasibility of monitoring structural changes occurring during reactions such as oxidation, pyrolysis and hydrogenation, with or without catalysts present, in situ by diffuse reflectance infrared spectrometry. Our current cell allows reactions to be studied at temperatures as high as 600°C. Reaction products may be continuously swept out of the cell, permitting characterization by a wide range of other instrumental techniques. Reactions occurring at high pressure are less easy to monitor at this time, but it should not be too difficult to redesign the cell so that pressures to 1000 psig are permissible.

References

1. M. P. Fuller and P. R. Griffiths, Anal. Chem., **50**, 1906 (1978).
2. M. P. Fuller and P. R. Griffiths, Amer. Lab., **10**(10), 69 (1978).
3. M. P. Fuller, I. M. Hamadeh, P. R. Griffiths and D.E. Lowenhaupt, Fuel, **61**, 529 (1982).
4. M. Niwa, T. Hattori, M. Takahashi, K. Shirai, M. Watanabe and Y. Murakami, Anal. Chem., **51**, 46 (1979).
5. T. Hattori, K. Shirai, M. Niwa and Y. Murakami, Anal. Chem., **53**, 1129 (1981).
6. P.R. Griffiths and M. P. Fuller, in Advances in Infrared and Raman Spectroscopy, Vol. 9, (R. Clark and R. Hester, eds.), Wiley-Interscience, New York (1982), pp. 63-127.
7. I. M. Hamadeh, Ph.D. dissertation, Ohio University, Athens, Ohio (1982).
8. P. C. Painter, R. W. Snyder, M. Starsinic, M. M. Coleman, D. W. Kuehn and A. Davis, Appl. Spectrosc., **35**, 475 (1981).
9. J. K. Kauppinen, D. J. Moffatt, H. H. Mantsch and D. G. Cameron, Appl. Spectrosc., **35**, 271 (1981).
10. W. J. Yang and P. R. Griffiths, unpublished results (1982).
11. L. J. Bellamy, "The Infrared Spectra of Complex Molecules," Chapman and Hall, London (1954).

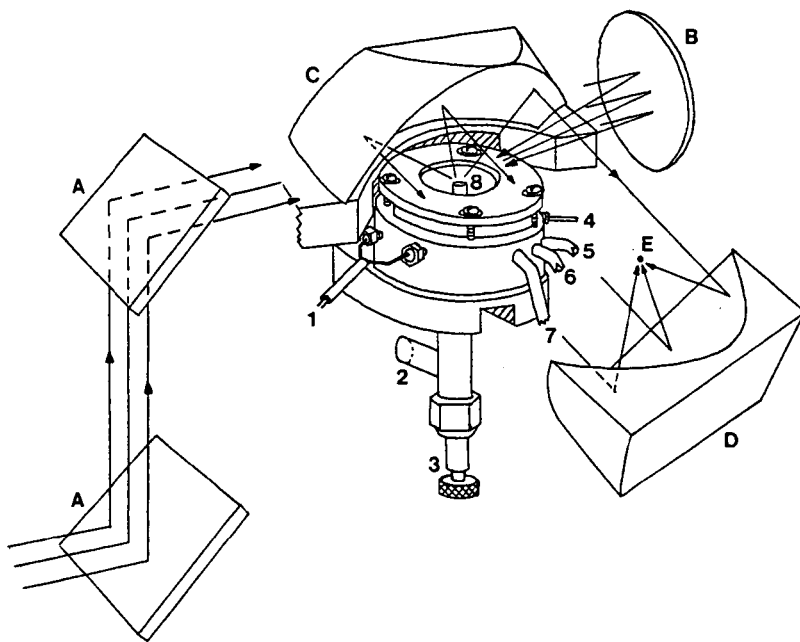


Figure 1: Schematic of cell designed for the study of gas-solid reactions. The level of the collimated beam from the interferometer is raised by the two plane mirrors (A) and focused onto the sample by the off-axis paraboloidal mirror (B). The diffusely reflected beam is collected and collimated by the paraboloidal mirror (C) and refocused by the other segment of the same paraboloidal blank (D) onto a downward-looking MCT detector at E. The components of the cell are as follows: (1) Heater leads, (2) Line to vacuum pumps, (3) Screw for sample removal, (4) Gas inlet line, (5) (6) Water inlet and outlet lines, (7) Manometer connection, (8) Sample.

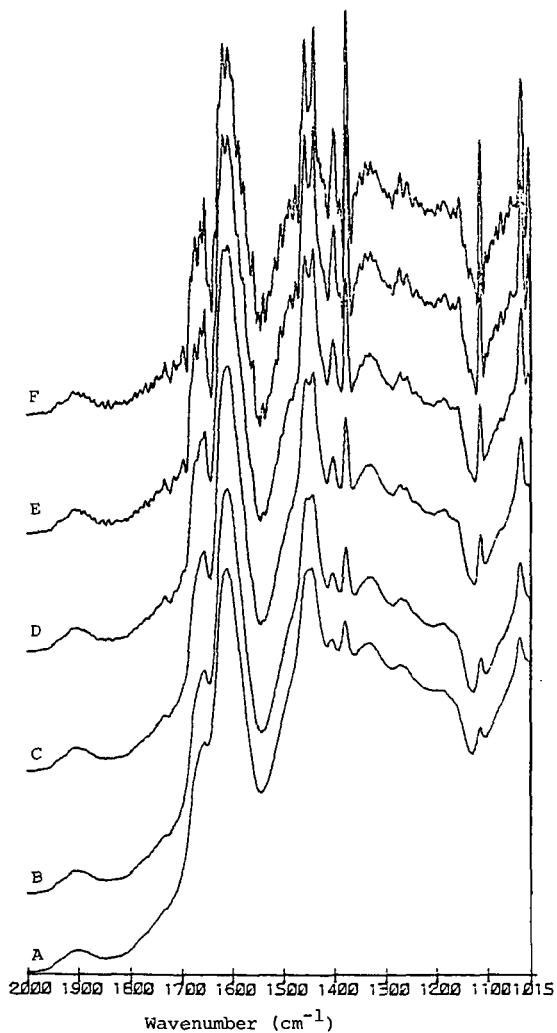


Figure 2: Effect of progressive resolution enhancement of the DR spectrum of a low volatility bituminous coal. The original spectrum is the lowest trace (A). Spectra used in this paper were computed with the parameter used for spectrum D.

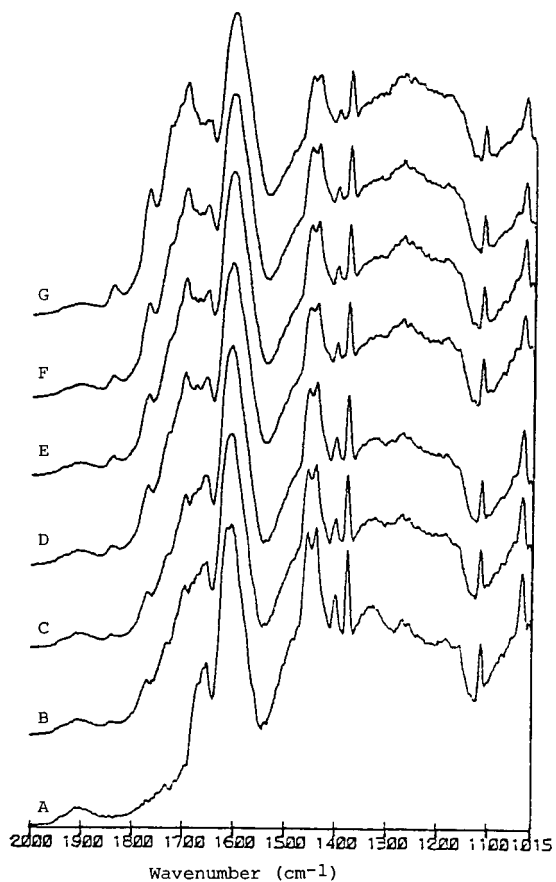


Figure 3: Resolution-enhanced spectra of a low volatility coal subjected to 150°C air oxidation for (A), 0; (B), 2; (C), 4; (D), 6; (E), 8; (F), 10; (G), 12 days.

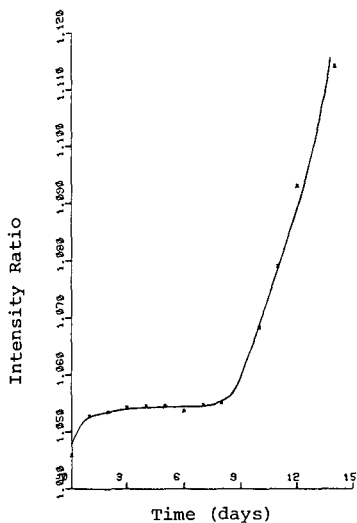


Figure 4

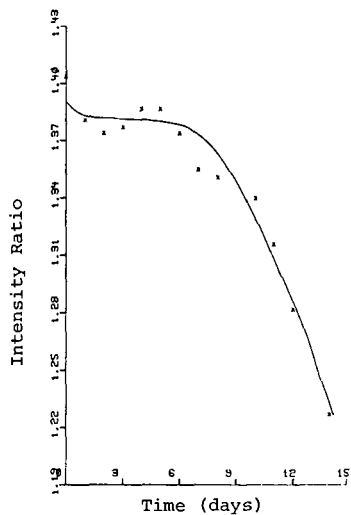


Figure 5

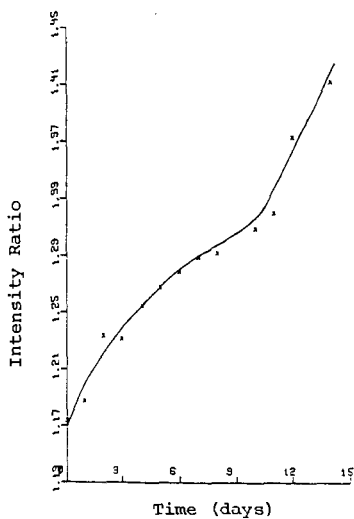


Figure 6

Figures 4, 5 and 6: Plots of ratio of band intensities in the DR spectra of a low volatility coal (PSOC 620, Bedford Co., PA) against time of oxidation at 150°C.

Figure 4: Aromatic C-H stretch (3070 cm⁻¹) vs symmetric methyl stretch (2872 cm⁻¹);

Figure 5: Asymmetric methylene stretch (2920 cm⁻¹) vs asymmetric methyl stretch (2962 cm⁻¹);

Figure 6: 760 cm⁻¹ aromatic C-H out-of-plane deformation vs 815 cm⁻¹ band.

THE IDENTIFICATION AND CHEMISTRY OF SPECIES RESULTING FROM
THE RAPID PYROLYSIS OF SMALL COAL PARTICLES IN VACUUM
AND IN THE PRESENCE OF REACTIVE GASES

R.H. Hauge, L. Fredin, J. Chu and J.L. Margrave

Department of Chemistry, Rice University, Houston, Texas 77251

INTRODUCTION

The various experiments in this study are designed to produce data from reactors which emphasize the early stages of coal gasification and its reactions with auxiliary gases by bringing the coal quickly up to reaction temperature under conditions where highly reactive gas phase intermediates can exit rapidly from the reaction zone. They are then deposited on a 15K reflective surface with a large excess of inert gas where further reaction is rapidly quenched. The products when isolated in a non-interactive solid such as nitrogen, argon, or even dry air exhibit well-defined spectra which allow the precise measurement of isotopic shifts and peak positions. Free radicals and other reactive species can be detected by characteristic infrared spectra. The presence of intermediates is also monitored with a fast time response quadrupole mass spectrometer. The combination of mass spectrometry and matrix isolation infrared spectroscopy serves as an effective probe for the existence of transient gaseous reaction intermediates.

The types of data obtained from the studies include:

- (1) Structural data for new species and suggested reaction pathways from isotopically-substituted reactants.
- (2) Information on the dependence of various gas products formed on rates of heating, reactant gases, and coal particle size.

The question as to whether the reactions of particular primary building blocks of coal lead to specific products is studied by adding the molecular species, i.e., various polycyclic aromatics (PCA's) to the coal or as a reactant gas and noting the effect on product distribution.

EXPERIMENTAL

A new matrix isolation system has been designed to allow both mass spectrometric and matrix isolation infrared studies of highly reactive transient species. Close coupling with differentially pumped systems permits the detection of species evolving from samples exposed to pressure pulses of various gases up to one atmosphere. The system is integrated into a high resolution Fourier transform spectrometer which covers the spectral range from the far i.r. to the near i.r. (100 microns to 1 micron). The design has seventy available deposition surfaces. This large number of surfaces is very valuable in attempts to detect small changes which occur due to changed reactor conditions. The increased accuracy of infrared difference spectroscopy can be used to great advantage with a large number of samples which result from small changes in reactor conditions. The combination of mass spectrometric and matrix isolation spectra greatly increase the likelihood of positive species identification. Three quartz crystal

infrared. Results from this study are presented in Figure 5.

At 146C, coal devolatilization can be characterized by evolution of CO_2 , CH_4 , H_2O , and CO . At an increased temperature of 326C, light hydrocarbon gases such as C_2H_4 and C_2H_6 are observed along with CH_4 , CO_2 , CO and H_2O . Most of these light hydrocarbons are devolatilized between 326 and 605C. A similar behavior has been noted by Solomon and co-workers. /1,2/ At 1038C, a new peak at 1525 cm^{-1} appears which has not yet been identified.

An interesting observation is that CO_2 seems to reach maximum yield at low temperatures and remains relatively constant at higher temperatures. However, CO appears to increase with higher temperatures and does not reach a maximum at the highest temperature studied.

Rapid Pyrolysis of Illinois #6

Studies of rapid pyrolysis of coal granules, using the pulsed flow reactor and the coal granule inlet valve described in Figure 3 indicate results similar to those for slow pyrolysis. However, rapid pyrolysis of Illinois #6 powder gives a much more complex IR spectrum with two new peaks appearing at 1180 and 1328 cm^{-1} . These two peaks are predominant and always occur simultaneously. Their relative intensities are always the same, indicating that they are due to a single species.

A comparison of rapid pyrolysis of Illinois #6 granules versus powders is illustrated in Figure 6.

Two other coals beside Illinois #6 were studied, Western Kentucky and Upper Freeport as shown in Figure 7. Western Kentucky is a high moisture and high oxygen content coal while Upper Freeport is a low moisture and low oxygen content coal. Both types of coal gives results similar to Illinois #6 when their powders are rapidly pyrolyzed. Absorptions at 1180 and 1328 cm^{-1} are predominant over the methane absorption for both coals studied. This indicates that the species responsible for 1180 and 1328 cm^{-1} is common to all coals during rapid pyrolysis.

Rapid Pyrolysis of Oxidized Illinois #6

Illinois #6 powder was oxidized by heating in an oven at 190C. Samples taken after one hour and after 18 hours of heating were rapidly pyrolyzed through the pulsed flow reactor. Figure 8 shows the predominant gaseous products to be CO_2 , CO and H_2O , as expected for oxidized coal. Slight traces of CH_4 and the species responsible for 1180 and 1328 cm^{-1} are also observed. This indicates that the presence of the unidentified intermediate species is not dependent upon the extent of oxidation of the coal samples. It is, however, reduced in yield which indicates the species is not due to oxidation of the coal sample.

Rapid Pyrolysis of Illinois #6 with D2016 and D2018

The effect of gaseous water on rapid pyrolysis of Illinois #6 granules was studied by the addition of D2016 and D2018. Gaseous deuterated water was pre-mixed with argon and pulsed through the reactor immediately after coal granules were dropped into the hot reactor zone. Results, shown in Figure 9, suggest that oxygen from

mass monitors are mounted on the cold trapping block. They serve as very sensitive quantitative monitors of the beam density striking the trapping surface. A detailed schematic of the MI-MS apparatus is shown in Figures 1 and 2.

Figure 3 presents a schematic diagram of a pulsed flow reactor for coal granules and coal powders. The reactor contains three sections. The first section, A, contains the coal granule inlet valve. The second section, B, contains the hot reactor zone, resistively heated through a nichrome wire wrapped around the outside of the quartz tube. It is separated from the cold (15K) copper matrix isolation surface by a small amount of quartz wool inserted in the tube. Coal granules are introduced into the hot reactor zone by simply dropping them in through valve A. A two-way valve is then pulsed open which causes an inert gas, argon, to carry the gaseous products through the quartz wool and onto the 15K copper surface of the matrix isolation apparatus. Approximately 15 grains of coal were used for each trapping.

The third section, C, is used for introduction of coal powders into the hot reactor zone. It contains a fluted glass column, separated from the hot reactor zone by two two-way valves. The inert carrier gas, argon, is let in from the bottom, passing the frit, creating a simulated fluidized bed of coal powder. Coal powder along with the inert gas is pulsed into the hot reactor zone by sequentially pulsing open each of the two-way valves. Gaseous products are carried by the excess inert gas onto the 15K matrix isolation surface to be studied by infrared spectroscopy. Usually 50-100 pauses of coal powder were used for each trapping.

PULSED FLOW VERTICAL HEATER REACTOR

A schematic drawing of the vertical heater reactor is shown in Figure 4. This reactor is very similar to the pulsed flow reactor described in Figure 3, except that the design allows the gaseous products to be trapped directly onto the matrix surface without formation of tars along the sides of the tube as in the case for the previous reactor. The hot reactor zone is placed in the matrix isolation chamber. It consists of a quartz tube with a small opening near the bottom of the tube which is inserted into a vertical tantalum heater. The tantalum heater also has a small opening on the side facing the matrix isolation surface. A small piece of quartz wool is placed into the quartz tube so that it just covers the opening. This prevents particles from being blown onto the matrix surface and keeps them in the hot reactor zone.

Coal powder is pulsed into the heater in the same way as described for the previous pulsed flow reactor. In general, pyrolysis is carried out over a temperature range of 120 to 1000 C, in vacuo. Argon has been used as the inert carrier and matrix gas.

RESULTS

Slow Pyrolysis of Illinois #6 Powder

Coal particles (250 mesh) are placed in the vertical quartz tube described in Figure 4 and slowly heated from 146C to 1038C. Gaseous products obtained at different intervals of temperature are trapped with argon, introduced from a separate inlet tube, onto the 15K copper matrix isolation surface and subsequently examined through

the water ends up as CO and CO₂, as seen by the presence of CO18 and CO16O18 in the reaction with D2O18. However, no deuterated methane is evident in either reactions.

DISCUSSION

To date our work has shown that the product gaseous species from pyrolysis are very dependent on coal particle size. As might be expected, the larger particles tend to produce the smaller alkanes and alkenes as a result of secondary pyrolysis. Rapid pyrolysis of the smaller particles produces new species which are thought to be more representative of the species resulting from initial bond breaking steps. One species in particular produces strong features at 1328 and 1180 cm⁻¹. Insufficient reference data has prevented the identification of this species as yet but it is hoped that studies of model compounds and additional mass spectrometric information will allow identification of this significant reaction intermediate. It is also clear that improved control of particle size and the amount of coal injected per pulse will greatly aid our interpretation of product distributions. Of course, this also applies to studies of reactions with gases such as water, hydrogen and carbon dioxide. Preliminary work with a small gas recirculating system in which selected coal particle sizes are entrained with reactant and inert gases indicates that a much improved pulsed coal injection system is possible. It is expected that considerable additional data of product distributions correlated to particle size, temperature and reactant gas will be available in the near future.

REFERENCES

1. P.R. Solomon, "The Evolution of Pollutants During Rapid Devolatilization of Coal", Rep. R76-952588-2, United Technologies Research Center, East Hartford Conn. 1977, Rep. NSF/RA-770422, NTISPB, 278496/AS, 1977.
2. Adv. in Chem. Series, 192, Coal Structure, Ed. M.L. Gorbaty and K. Ouchi, Chap. 7, "Coal Structure and Thermal Decomposition", P.R. Solomon.

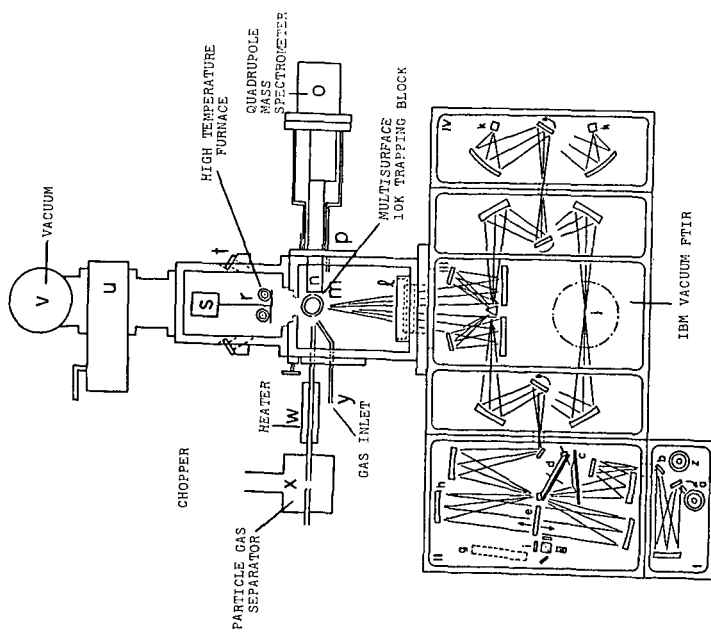


FIGURE 1

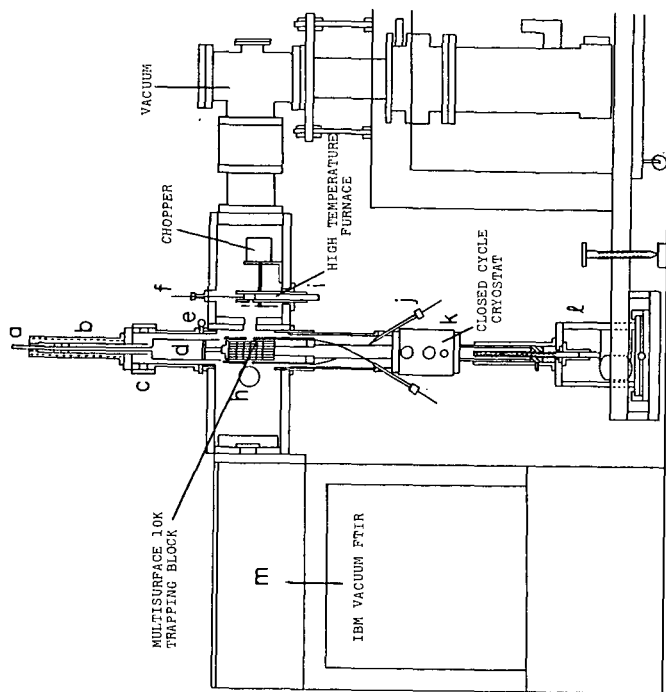


FIGURE 2

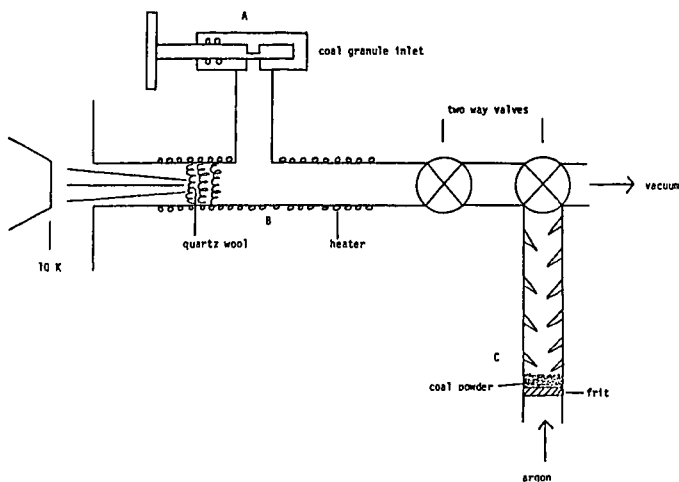


Fig. 3. PULSED FLOW REACTOR

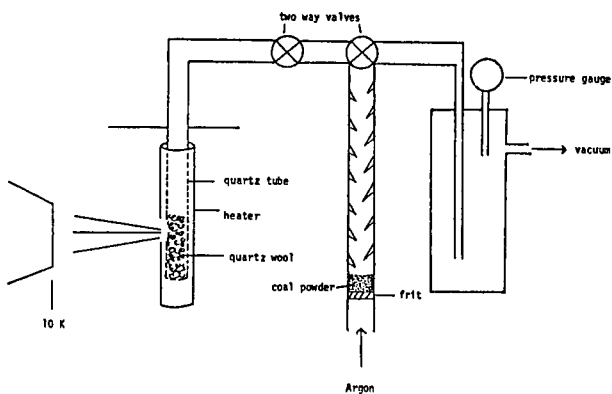


Fig. 4. PULSED FLOW VERTICAL HEATER REACTOR

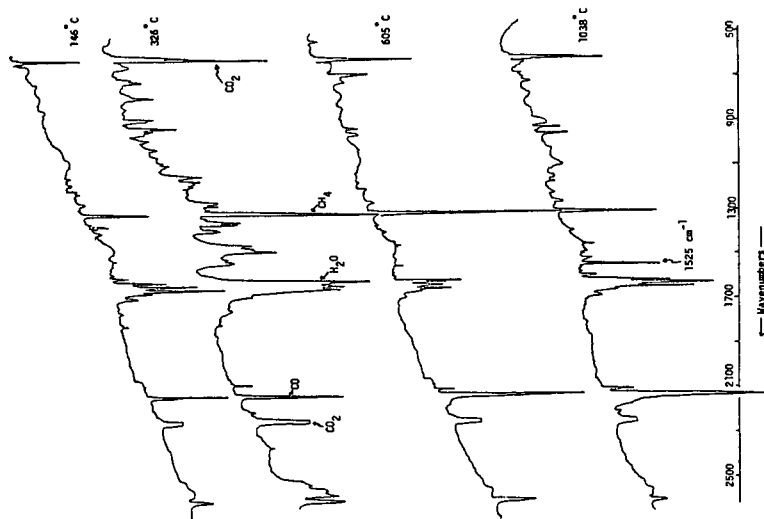


Fig. 5. Slow Pyrolysis of Illinois #6 Powder

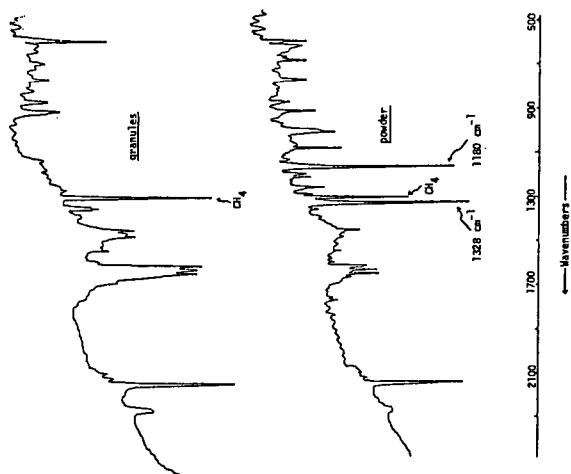


Fig. 6. Rapid Pyrolysis of Ill. #6 at -1000°C

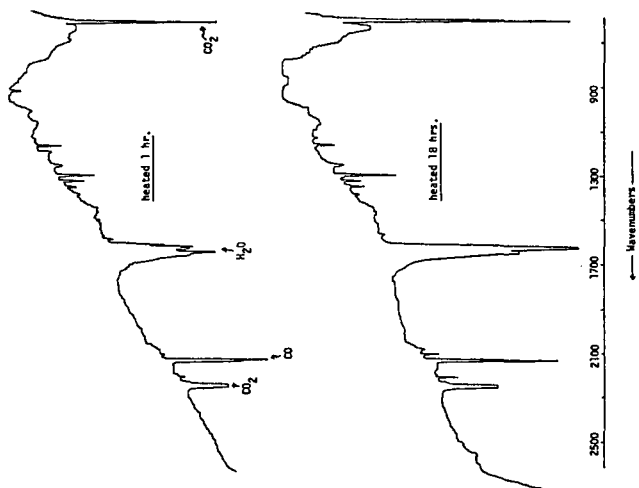


Fig. 8. Rapid Pyrolysis of Oxidized J11. #6

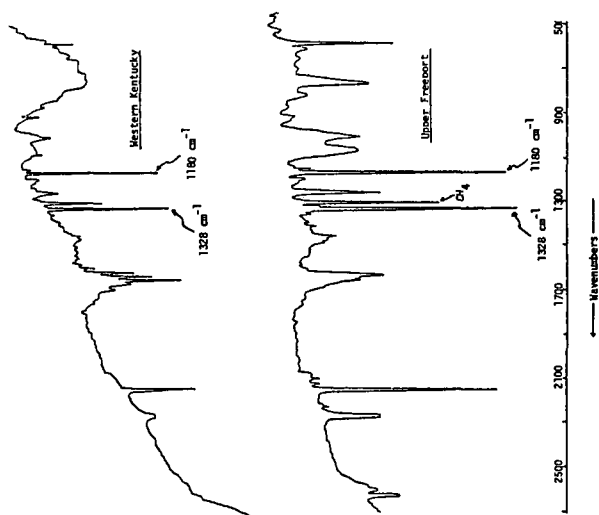
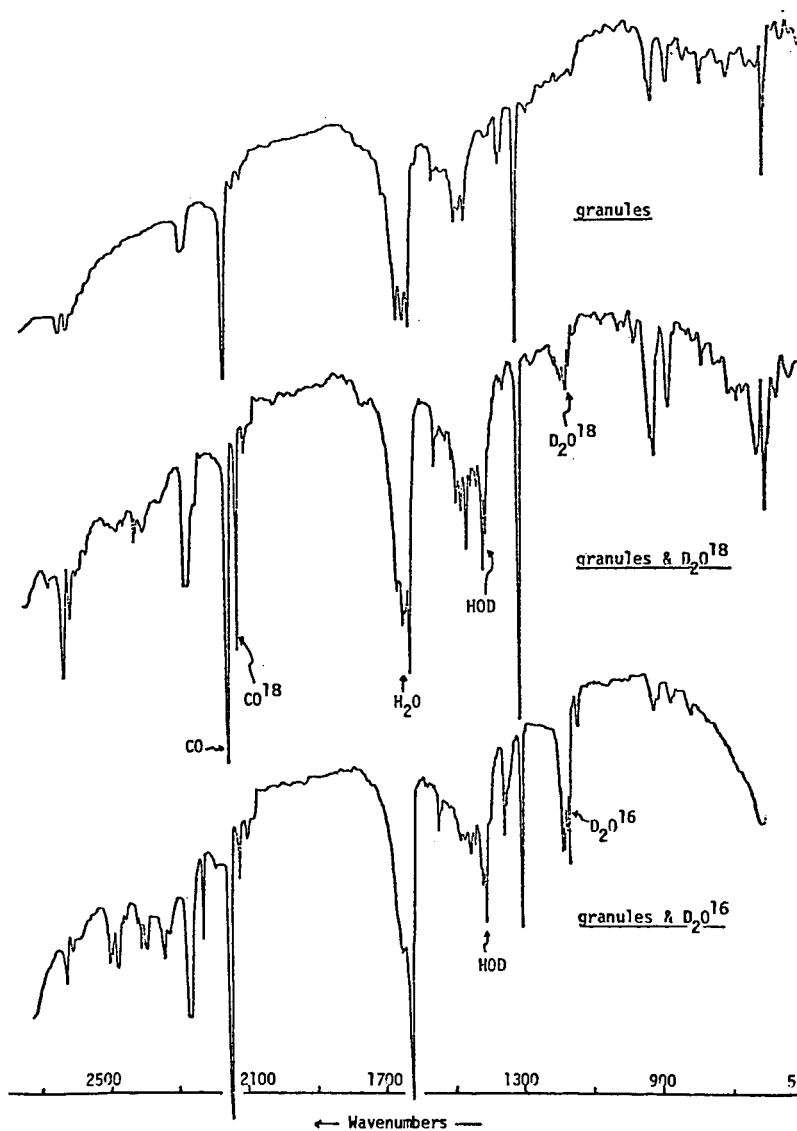


Fig. 7. Rapid Pyrolysis of Other Coals at 1000°C

Fig. 9. Rapid Pyrolysis of Ill. #6 with D_2O^{16} & D_2O^{18}



CHEMISTRY AND STRUCTURE OF COALS: AIR OXIDATION STUDIES
RELATED TO FLUIDIZED BED COMBUSTION

E. L. Fuller, Jr., N. R. Smyrl, R. W. Smithwick III, and C. S. Daw*

Oak Ridge Y-12 Plant
Union Carbide Corporation,
Nuclear Division
Oak Ridge, Tennessee 37830

Efficient use of coals as feedstocks and thermal energy requires comprehensive understanding of the physical and chemical structure of the starting materials and the changes wrought in the processing steps. Diffuse Reflectance Infrared Fourier Transform (DRIFT) spectroscopy is being developed^{1,2} as a facile, nondestructive, rapid, highly informative means of measuring and monitoring the chemical structure of coals

Figure 1 shows how well the DRIFT technique can be used to rank coals with respect to the hydroxyl content and hydrocarbon type and content for unweathered powders of the greater maturity increasing from top to bottom. Figure 2 shows the wealth of information as related to carbonyl content, polynuclear aromaticity and mineral type and mineral content for the various coal powders and the simulated end members of the coalification process (cellulosic fibers and graphite).

Figure 3 is an example where the changes due to oxidation are readily discerned. This partial oxidation involved loss of the aliphatic hydrogen ($2800-3000\text{ cm}^{-1}$) and simultaneous carbonyl formation ($1600-1900\text{ cm}^{-1}$) with little or no loss of hydroxyl ($3600-2000\text{ cm}^{-1}$), aromatic hydrogen ($3200-3000\text{ cm}^{-1}$), polynuclear carbon ($1650-1550\text{ cm}^{-1}$), nor polyaromatic hydrogen ($900-700\text{ cm}^{-1}$). Studies of catalytic effects due to inorganic constituents are facilitated by DRIFT as shown in Figure 4 where quantitative measures are obtained for the amount and nature of argillic components inherent in and/or admixed with the run of the mine coals.

The DRIFT technique uses the coal as a solid piece and/or as powder with no mulling agents (CCl_4), support medium (KBr), or other extraneous materials that can contribute erroneous spectral features and serve as barriers for *in situ* reaction studies. Figures 5 and 6 illustrate the additional information that one can obtain by noting spectral changes wrought on oxidation. The dehydrogenation process involves oxidation of only the aliphatic hydrocarbon initially and only at the latter stages the oxygen attack involves unsaturated olefinic and aromatic species

(3035 cm^{-1}). Also there is little or no loss of phenolic, carboxyl alcoholic, etc. entities (3650-2400 cm^{-1}) until the later stages of reaction. Figure 6 shows more details of the oxygen insertion process where the initial oxidation forms somewhat isolated carbonyls (1705 cm^{-1}) with higher degrees of reaction progressively forming analogs of carboxylic acids (1745 cm^{-1}), acid anhydrides (1775 cm^{-1}) and organic carbonates (1845 cm^{-1}) as a synergetic continuum of oxygen enrichment prior to the final evolution as gaseous carbon dioxide. Steady state conditions seem to prevail where the process proceeds continuously at the steady state concentrations noted in the upper difference spectrum. DRIFT spectroscopy uniquely allows one to monitor the concentration of virtually all of the entities required to fully elucidate the oxidation mechanism proposed by batch techniques.^{3,4} Additional details of interpretation and experimental techniques are given elsewhere.

Mercury porosimetry, vapor sorption, microscopy, and helium picnometry aid appreciably in our heat and mass transport modelling under conditions relevant to fluidized bed reactors of the Tennessee Valley Authority. The original rigid structure of the coal swells and expands as volatile bubbles grow and flow out of the tarlike mass where the -3+4 mesh particles are introduced into the hot (1500°F) reactor. The volatiles burn vigorously and the residual char slowly burns away to leave residual ash. Data will be given to show the nature of the porosity (internal/external, open/closed, macro/micro, etc.) as determined by the various techniques and the relevance to existing and proposed processes.

ACKNOWLEDGMENTS

The Oak Ridge Y-12 Plant is operated by Union Carbide Corporation's Nuclear Division for the Department of Energy under U.S. Government Contract W-7405-eng-26. *C. S. Daw is located at the Oak Ridge National Laboratory.

REFERENCES

1. Smyrl, N. R. and Fuller, E. L., Jr.; *Chemistry and Structure of Coals: Diffuse Reflectance Infrared Fourier Transform (DRIFT) Spectroscopy of Air Oxidation in Coal-Coal Products: Analytical Characterization Techniques* edited by E. L. Fuller, Jr., American Chemical Society, 1982.
2. Fuller, M. P., Hamadeh, I. M., Griffiths, P. R., and Lowenhaupt, D. E.; *Diffuse Reflectance Infrared Spectrometry of Powdered Coals*, Fuel, 61, 529 (1982).

3. Bouwman, R. and Frericks, I.; *Low Temperature Oxidation of a Bituminous Coal: Infrared Spectroscopic Study of Samples from a Coal Pile*, Fuel, 59, 309 (1980).
4. Keifer, J. R., Novicky, M., Akhtar, M. S., Chughtai, A. R., and Smith, D. M.; *The Nature and Reactivity of Elemental Carbon (Soot) Surface as Revealed by Fourier Transform Infrared (FTIR) Spectroscopy*, Pro Intl. Soc for Opt. Eng., 289, 184 (1981)

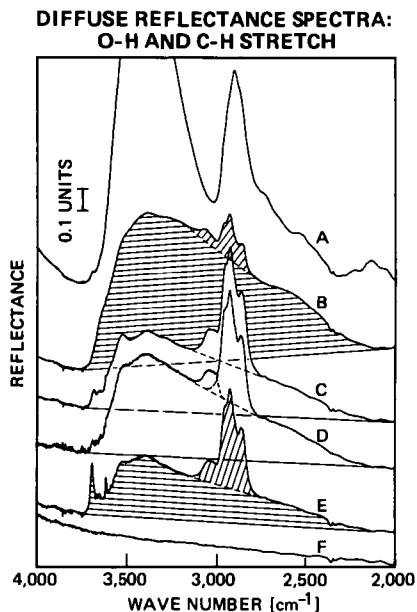


Figure 1. Hydrogen stretch region of DRIFT spectra of; A. cellulosic fibers, B. Lignite, C. Subbituminous Coal, D. C-bituminous coal, E. A-bituminous coal, and F. Graphite. All samples are equilibrated with 30 ppm moisture in the argon purge.

DIFFUSE REFLECTANCE SPECTRA

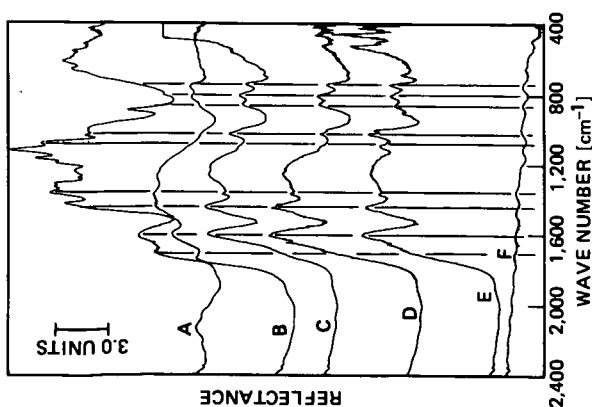
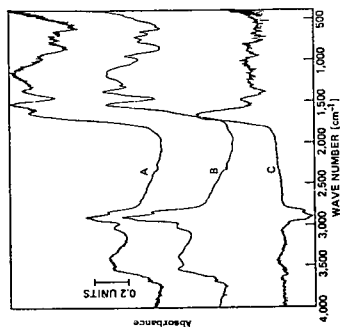
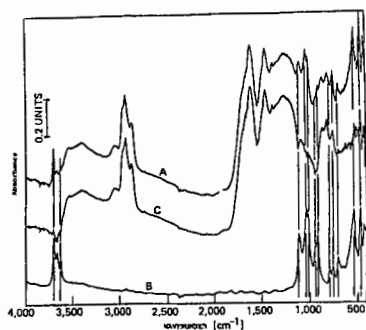


Figure 2. Low energy DRIFT Spectra: Legend Same as Figure 5. Vertical lines (left to right) denote characteristic bands for (1) carbonyl, (2) polynuclear aromatic rings, (3) methylene, (4) mineral, and (5) aromatic hydrogen groups, respectively.



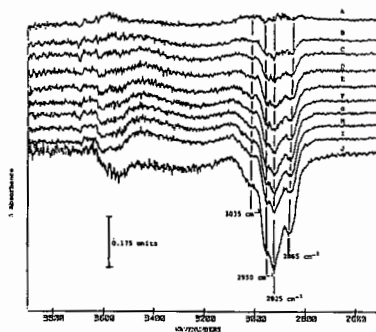
DRIFT Spectra of Wyodak Coal.
A. Sample after ~ 24 hr of oxidation in 2.7 kPa at 393°C
B. Dried unoxidized sample
C. Difference Spectrum (A-B)

Figure 3. DRIFT Spectra. A. Partially oxidized coal powder 1 hour, 2.7 kPa of air at 393°C. B. Original coal powder dried in vacuum at 400°C. C. A-B with no scaling factor to show the changes due to oxidation.



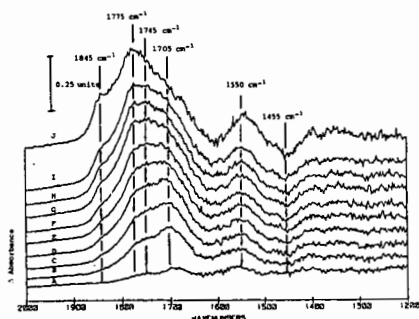
DRIFT spectra.
A. Bruceton Coal
B. Kaolin in KCl (2.0%)
C. Difference spectrum (A - 0.7404B)

Figure 4. Correction for Minerals. A. DRIFT spectrum for powdered coal. B. DRIFT spectrum of 20% kaolin dispersed in powdered KCl. C. A-0.7404B for each of the individual 3600 data points.



DRIFT Difference Spectra in the 2800-3000 cm^{-1} region of Oxidized Hydrot Coal (1900-1500 cm^{-1}).
A. 1 min E. 45 min I. 2 hr
B. 5 min F. 1 hr J. 17.5 hr
C. 15 min G. 1.5 hr
D. 30 min H. 1.75 hr

Figure 5. DRIFT Difference Spectra for ca 19 hours continuous oxidation of coal. These difference spectra show the loss of hydrogen from C-H and, in later stages, OH units of coal.



DRIFT Difference Spectra in the 1200-1800 cm^{-1} region of Oxidized Hydrot Coal (1900-1500 cm^{-1}).
A. 1 min D. 30 min G. 1.5 hr J. 17.5 hr
B. 5 min E. 45 min H. 1.75 hr
C. 15 min F. 1 hr I. 2 hr

Figure 6. DRIFT Difference Spectra for Carbonyl Region. The amount and nature of the oxygenated species changes markedly. A general increase in carbonyls is noted and shift to higher frequencies is evident.

Solid-Solid Contacting in Catalyzed Gas-Char Reactions

D. C. Baker

Shell Development Company
Houston, TX 77001

and

A. Attar

Department of Chemical Engineering
North Carolina State University, Raleigh, NC 27650

Introduction

Coal char samples that are used for gas-carbon reaction studies can possess a wide range of porosities depending upon preparation techniques. In general, the char may be classified as non-porous, slightly porous, or highly porous. The total particle reaction rate is a summation of the intra-particle reaction rate and the external surface reaction rate and is dependent upon the type of char under investigation, viz.

$$r_{\text{meas}} = (\eta A^{\text{int}} + A^{\text{ext}}) r_{\text{true}} \quad (1)$$

where r_{meas} is the measured total particle reaction rate, r_{true} is the true reaction rate, A^{int} and A^{ext} are the internal and external surface areas, respectively, and η is the effectiveness factor.

Further elaborations on the total particle reaction rate arise in gas-carbon reactions when reaction at specific sites warrants the inclusion of an internal and external active site density, C_t , and when r_{true} applies to a complex reaction path such as gasification, viz. char- CO_2 gasification,

$$r_{\text{meas}} = (\eta A^{\text{int}} C_t^{\text{int}} + A^{\text{ext}} C_t^{\text{ext}}) \frac{k_1(\text{CO}_2)}{1 + \frac{k_1}{k_3}(\text{CO}_2) + \frac{k_{-1}}{k_3}(\text{CO})} \quad (2)$$

It is often difficult to determine when the effectiveness factor is approximately unity for complex reaction paths, consequently rate expressions simpler than equation (2) are often used. For example, Jalan and Rao¹ assumed a first order reaction rate with respect to CO_2 during char- CO_2 gasification. Also note that in the case of equation (2) only "apparent" activation energies can be obtained from Arrhenius plots of r_{meas} vs. $1/T$ since k_1 , k_{-1} , and k_3 all depend on T , and even this approach is invalid if the surface areas and site densities are not constant with respect to temperature and the time duration of the experiment.

When a solid catalyst is introduced onto char, the catalyst contacting with char must be considered since it may be (a) limited to a small portion of the external char surface area, (b) contacted with the entire external char surface area, but excluded from internal pores, or (c) contacted with the entire external and internal char surface areas. The consequences of catalyst contacting on measured reaction rates and measured activation energies need to be realized when interpreting experimental data since these measurements often are taken as the main basis for speculating on catalytic mechanisms.²⁻⁴

Analysis

It has been proposed that certain catalysts in gas-carbon reactions act only to increase the density of active sites (i.e. C_t in equation (2)).⁵ Assuming this type of catalysis prevails, Table 1 summarizes, for several initial reaction conditions and for several conditions of catalyst contacting, the changes in measured reaction rates and measured activation energies which occur when a solid catalyst is introduced onto char. As shown in Table 1, the initial uncatalyzed reaction conditions may be in the regime of kinetic control ($\eta=1$), intra-particle diffusional control ($\eta<1$), or external diffusional control (i.e. proportional to the difference in bulk and surface concentrations and film thickness). When a solid catalyst is introduced, the catalyzed reaction conditions depend on the porosity of the char and the extent of catalyst contacting (i.e. catalyst penetrates internal pores or catalyst excluded from internal pores). The interplay between initial uncatalyzed reaction conditions and extent of catalyst contacting during catalytic gasification can lead to measured activation energies increasing, decreasing, or remaining constant with catalyst application. An interesting case is where the measured activation energy increases with the introduction of a solid catalyst. In such a case a slightly porous char has an uncatalyzed total particle reaction rate initially made up of nearly equivalent external and internal (diffusion controlled) reaction rates. Introduction of a catalyst, which is excluded from internal pores but which contacts the entire external surface area, can lead to the external surface reaction rate overwhelming the intra-particle reaction rate and consequently increasing the measured activation energy.

In reviews of catalyzed gas-carbon reactions, it is often noted that the measured activation energy may decrease with introduction of a catalyst as the system becomes diffusion controlled.⁶ However, similar physical reaction considerations are usually not given to the case where the measured activation energy increases with introduction of a catalyst. Measured activation energies have been reported to increase, decrease, and remain constant for catalyzed gas-carbon reactions relative to the uncatalyzed reactions.^{2-5,7} It is interesting to note that catalyst contacting alone may explain these differences.

Results Using Non-porous Char

In a recent study, Baker⁸ presented results on the catalyzed char- CO_2 surface exchange of oxygen. Such a system was originally studied

by Orning and Sterling.⁹ The char that was used in this study was non-porous thereby eliminating the need for considerations of both intra-particle reaction rates and internal catalyst contacting. By employing a unique pulsing technique, the CO₂ molecules could be followed through a char-packed microdifferential reactor without the use of radioactive tracers which were extensively used in earlier studies.⁹⁻¹² The experimental system is depicted in Figure 1. Proper choice of pulse size, pulse residence time, and reactor temperature and pressure, permitted measurements of the char-CO₂ oxygen exchange reaction for uncatalyzed char, as well as char catalyzed with alkali and alkaline earth carbonates, viz.



where C_f is a free active exchange site which can accept oxygen from gaseous CO₂ and C_o is an oxygen occupied active exchange site. The total density of active exchange sites is given by

$$\text{C}_t = \text{C}_o + \text{C}_f \quad (4)$$

Figure 2 presents some of the data from the study. A detailed discussion and analysis is provided by Baker⁸ and by Baker and Attar.¹³ By initially purging the system with CO, all the active sites were converted to free active sites. Consequently, the reaction rate at low surface oxide formation is given by

$$r_{\text{meas}} = A^{\text{ext}} \text{C}_t^{\text{ext}} k_1 (\text{CO}_2) \quad (5)$$

which allows direct measurement of k₁(T). Since negligible gasification occurred, the surface area and active site density, as given in equation (5), remained constant throughout the experiments.

The data which are plotted in Figure 2 indicate the possibility that the activation energy for k₁ at low surface oxide formation, 214 kJ/mole, is the same for catalyzed and uncatalyzed char. Mentser and Ergun determined a similar value of 222 kJ/mole for uncatalyzed carbon black.¹⁴ At high surface oxide formation the back reaction cannot be neglected, viz.



and this leads to curvature in the Arrhenius data.^a The differences in measured reaction rates for different catalysts is attributed to differences in the density of active sites, C_t^{ext}. Surface areas, A^{ext}, were essentially equivalent for all samples.

At present, the data do not allow discrimination between the degree of catalyst contacting at the char surface for the various carbonates (calcium, sodium, and potassium) and their intrinsic capability to generate active sites on the char surface. However, the data do point out some similarities between catalyzed and uncatalyzed gas-char reactions which are not accounted for in many of the proposed catalytic gasification mechanisms that are based mainly on differences in measured "apparent" activation energies.

^a Statistically meaningful data could only be obtained at conversions of >3% and the back reaction became noticeable at conversions of 10%, thus limiting the conversion range for activation energy determinations.

Conclusions

Solid-solid contacting may affect the measured reaction rate and measured activation energy during catalyzed gas-carbon reactions. The measured activation energy may increase, decrease, or remain constant with the introduction of a solid catalyst. Data for a non-porous char indicated an identical first step in catalyzed and uncatalyzed char gasification. That is, CO_2 exchanged oxygen with the char surface, apparently at active site locations. The activation energy for this reaction, 214 kJ/mole, was similar for catalyzed and uncatalyzed char, however, the reaction rates differed by orders of magnitude. The catalytic effect for the alkali and alkaline earth carbonates was attributed to differences in the density of active sites. Whether the different catalyzed rates were due to different degrees of external contacting or to true differences in catalytic properties was not resolved in this study.

REFERENCES

1. Jalan, B. P. and Y. K. Rao, Carbon, 16, 175-184, 1978.
2. Veraa, M. J. and A. T. Bell, Fuel, 57, 194-200, 1978.
3. McKee, D. W., Carbon, 17, 419-425, 1979.
4. McKee, D. W., Fuel, 59, 308-314, 1980.
5. Otto, K., L. Bartosiewicz and M. Shelef, Fuel, 58, 565-572, 1979.
6. McKee, D. W., Physics and Chemistry of Carbon (Ed. P. L. Walker, Jr.), 16, 1-118, 1981.
7. Guzman, G. L. and E. E. Wolf, Ind. Eng. Chem. Process Des. Dev., 21, 25-29, 1982.
8. Baker, D. C., Ph.D. Dissertation, Univ. of Houston, 1981.
9. Orning, A. A. and E. Sterling, J. Phys. Chem., 58, 1044-1047, 1954.
10. Bonner, F. and J. Turkevich, J. Am. Chem. Soc., 73, 561-564, 1951.
11. Ergun, S., J. Phys. Chem., 60, 480-485, 1956.
12. McKee, D. W. and J. T. Yates, J. Catalysis, 71, 308-315, 1981.
13. Baker, D. C. and A. Attar, submitted for publication to Fuel.
14. Mentser, M. and S. Ergun, U.S. Bur. of Mines, Bull. No. 664, 1973.

Table 1. Changes in Measured Rate (r_m) and Activation Energy (E_m) with Catalyst Application to Char

Initial Reaction Conditions						
	Non-Porous Char		Slightly Porous Char		Highly Porous Char	
			Catalyst Penetrates Internal Pores	Catalyst Excluded From Internal Pores	Catalyst Penetrates Internal Pores	Catalyst Excluded From Internal Pores
Kinetic Control	r_m	Increase				
	E_m	No Change or Decrease				
Intraparticle Diffusional Control	r_m	NA	Increase			
	E_m		Decrease	Increase	Decrease	
External Diffusional Control	r_m	No Change				
	E_m					

NA - Not Applicable

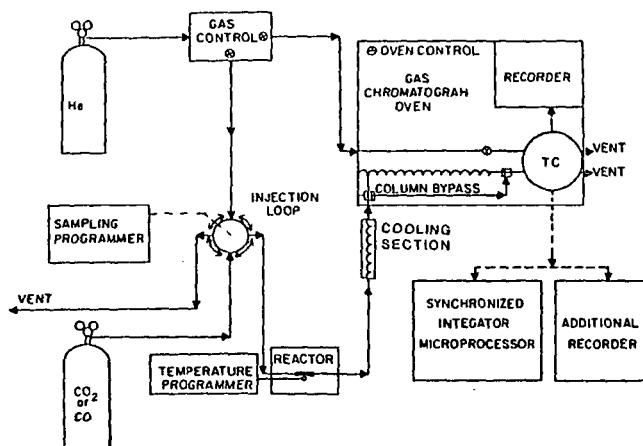


FIGURE 1
SYSTEM FOR STUDYING CHAR-CO₂ SURFACE EXCHANGE OF OXYGEN⁸

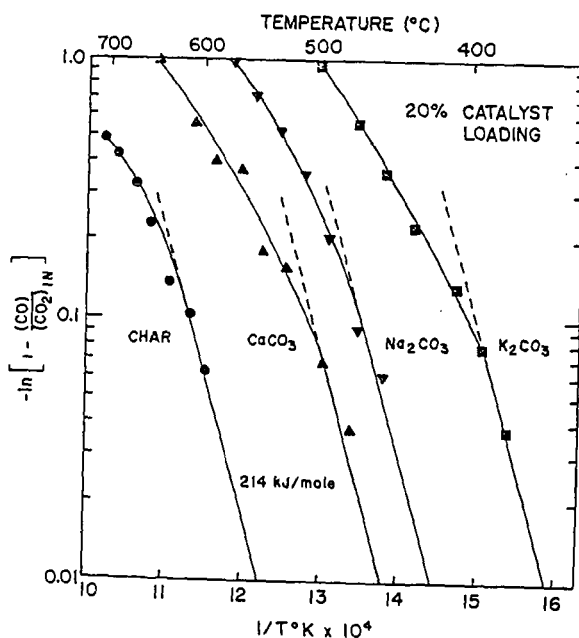


FIGURE 2
ARRHENIUS-TYPE DATA FROM CHAR-CO₂ SURFACE EXCHANGE OF OXYGEN⁸

A STUDY OF THE ROLE OF ALKALI METAL SALTS AS CHAR GASIFICATION CATALYSTS BY KNUDSEN CELL MASS SPECTROMETRY

Bernard J. Wood, Robert D. Brittain, and K. H. Lau

Materials Research Laboratory, SRI International
333 Ravenswood Avenue, Menlo Park, CA 94025

INTRODUCTION

Although there is much current interest (1, 2) in the high-temperature reaction of oxidizing gases with carbons admixed with alkali metal salts, there is no consensus on the chemical mechanisms that comprise the process. There is general agreement that the carbon and the salt chemically interact at modest temperatures to form a catalytically active state or reactive intermediate for the oxidation reaction. The nature of this state or intermediate, however, is disputable. To search for the identity of this intermediate and to elucidate its role in catalyzing the gasification or oxidation of carbon, we have employed Knudsen cell mass spectrometry to examine the gaseous species in equilibrium with carbon-alkali metal salt admixtures at elevated temperatures.

EXPERIMENTAL

Knudsen cell mass spectrometry is a technique which reveals the gaseous species in equilibrium with a solid or liquid phase, alone or in the presence of added gases. The material of interest is loaded into the Knudsen cell, a small cylindrical container made of refractory material, with an orifice that is a very small fraction of the cell's total surface area. The cell is situated in a high vacuum system so that the orifice is in line-of-sight with a mass spectrometer ion source. An electrical resistance heating element permits the cell to be heated to high temperatures. Gaseous species formed in the cell, or introduced through an inlet tube, collide, on the average, thousands of times with the contents of the cell before they escape through the orifice. Consequently, these species can be considered to be in chemical and thermal equilibrium with the solid/liquid phases in the cell when they emerge from the orifice and are detected by the mass spectrometer. A shutter, which can be moved over the orifice, permits the cell effusate to be distinguished from the ambient gases in the vacuum system. The general experimental technique and our apparatus have been described in the literature (3, 4). In our experiments we used 100 mg samples of pure alkali metal salts or of salts admixed with Illinois No. 6 coal char or Spheron-6 channel black in Knudsen effusion cells fabricated from platinum and from graphite. We determined the relative partial pressures of vapor components by measuring their ion intensities with ionizing energies 3 to 3.5 eV greater than their respective appearance potentials, to avoid contributions to the ion signals by alternative fragmentation processes in the mass spectrometer. The absolute vapor pressure of each species was calculated by the equation,

$$P = k(I^+)(T)/\sigma \quad 1)$$

where T is the Temperature in Kelvins, σ is the relative ionization cross-section, and k is an instrumental constant.

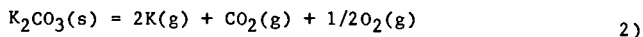
The particular systems of interest in this study were K_2CO_3 mixed with Spheron-6 or char, Cs_2CO_3 mixed with Spheron-6, and KBr mixed with Spheron-6. The effects of added H_2O , CO_2 , CO on vapor species abundances above the K_2CO_3 admixtures were investigated in separate runs. The relative abundances of the vapor species above the pure alkali metal salts in platinum cells, were also determined.

RESULTS

Equilibrium Gaseous Species

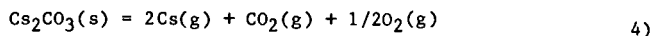
Pure Salts

On the basis of the observed ions and their relative intensities (Table 1), we conclude that the major vapor species over $K_2CO_3(s)$ are $K_2CO_3(g)$, $K(g)$, $CO_2(g)$, and $O_2(g)$. The neutral $K_2O(g)$ appears only at high temperature in negligible amount. The vaporization processes of K_2CO_3 , in the observed temperature range can be written as follows:



The enthalpy, ΔH , for Reaction 2 was calculated from the temperature dependence of the intensities of the gaseous ions. The value obtained, 247 (+/- 5) kJ/mol, is in agreement with the value of 251 kJ/mol calculated from JANAF data (5). The derived enthalpy of Reaction 3 was 291 kJ/mol.

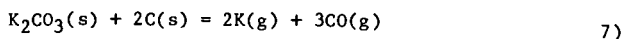
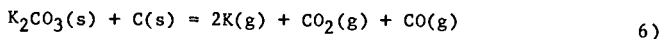
The vaporization of Cs_2CO_3 was found to proceed by analogous reactions:



Enthalpies of vaporization were calculated from the temperature dependence of Cs^+ and $Cs_2CO_3^+$ in the temperature range 930 to 1051 K. For Reaction 4 the experimental enthalpy was $\Delta H = 240.3$ (+/- 3) kJ/mol compared to 248.7 kJ/mol calculated from the JANAF tables (5). The enthalpy of the sublimation reaction was 251.9 (+/- 3) kJ/mol.

Carbon-Salt Admixtures

Over an admixture of K_2CO_3 and coal char (8 wt% K, mole ratio K/C = 0.029), observed in the temperature range 723 to 973 K, the only identifiable vapor species were $K(g)$, $CO(g)$, and $CO_2(g)$, suggestive of carbothermic reduction of the inorganic salt:



The temperature dependence of vapor pressures for $K(g)$, $CO(g)$, and $CO_2(g)$ is given in Table 2. The vapor pressures of $K(g)$ above the K_2CO_3 -char sample and the pure K_2CO_3 sample are plotted in Figure 1 along with the equilibrium lines calculated from JANAF data (5) for Reactions 2, 6, and 7. The pressures of $K(g)$ above the mixture of salt with char are intermediate between those for the pure salt and for the two reduction reactions.

In a similar manner the vaporization behavior of pure Cs_2CO_3 and mixtures with Spheron-6 and coal char were investigated. A sample of Cs_2CO_3 admixed with Spheron-6 (25 wt% Cs, mole ratio Cs/C = 0.033) was studied in the temperature range 729-1059 K. The major species observed were Cs(g) , CO(g) , and $\text{CO}_2\text{(g)}$, but the CO_2^+ and the CO^+ signals decreased continuously with time (Table 3). CSOH(g) was also observable in the vapor at very low partial pressures. The temperature dependence of partial pressures of the observed species above the mixture is given in the order in which data were taken in Table 3. Successive points at the same temperature demonstrate the time behavior of the signals for each species. The material removed from the Knudsen cell at the conclusion of this experiment was pyrophoric.

To provide a clue to the composition of the solid that remained in the cell, another sample of the Cs_2CO_3 -Spheron-6 mixture was heated in a separate vacuum system at 800 K overnight. A portion of this vacuum-heated mixture was transferred into a capillary tube under an argon atmosphere and analyzed by X-ray diffraction. A crystalline diffraction pattern was observed but could not be identified.

In separate experiments, the equilibrium pressure of Cs above pure Cs_2CO_3 , 8 wt% Cs_2CO_3 in char, 25 wt% Cs_2CO_3 in char, and 25% Cs_2CO_3 in Spheron-6 was observed. The results of these experiments are plotted in Figure 2, along with the calculated values for vaporization of the pure solid and for a possible carbothermic reduction reaction. The pressure of Cs above the Spheron-6 samples is observed to be approximately one order of magnitude higher than that above the pure salt, while the Cs pressure over the 8 wt% mixture with char is two orders of magnitude lower than that of the pure salt. Increasing the weight loading of Cs in the sample to 25% is accompanied by an increase of the Cs vapor pressure by an order of magnitude. X-ray diffraction analysis of the residual solid removed from the Knudsen cell revealed the presence of cesium aluminum silicate, CsAlSiO_4 , among other unidentified lines.

In marked contrast to the results for the carbonate-carbon systems, samples of pure KBr and KBr admixed with Spheron-6 (4 wt% K; mole ratio K/C = 0.014) behaved identically with respect to the vaporization of K-containing species; KBr sublimation was the only observable reaction involving potassium in both samples.

Effect of Added Gases

The effects of added H_2O , CO , and CO_2 upon vapor pressure of K(g) above a Spheron-6 admixture with K_2CO_3 was investigated in the graphite Knudsen cell. Effects on the K^+ signal level were studied in the temperature range 900-1100 K. During addition of the reactant gas the total pressure in the mass spectrometer was increased by a factor of 10 to approximately 1×10^{-4} Pa. Substitution of Ar(g) for the reactive gases had no effect on the K^+ signal, indicating that there was no dynamic flow effect on the performance of the Knudsen cell. Addition of CO(g) caused an immediate, completely reversible K^+ signal depression by 10-20%. This behavior would be expected by the effect of the law of mass action on Reactions 6 and 7. $\text{CO}_2\text{(g)}$ addition resulted in immediate depression of the K^+ level by 10% followed by a slower decrease as flow continued. When CO_2 input was discontinued, only partial recovery of the K^+ signal level occurred. A similar pattern in K^+ signal depression was observed upon addition of $\text{H}_2\text{O(g)}$. A blank run, with pure K_2CO_3 in the graphite cell at 1000 K, exhibited measurable pressures of K(g) and CO(g) , indicative of some interaction between K_2CO_3 and the cell. However, the addition of H_2O or CO_2 had no effect on levels of CO^+ and H_2^+ . The K^+ signal level was depressed by about 15% during H_2O flow, but returned to the same level after the flow was terminated. The depression of K^+ during H_2O flow is accounted for in part by the appearance of KOH^+ in the effusate at about 1% of the intensity of K^+ .

As mentioned above, KBr(g) was the only K-containing vapor species detected over an admixture of KBr and Spheron-6. The addition of H_2O to the Knudsen cell gradually depressed the pressure of KBr(g) ; over a period of 1800 s the KBr^+ signal dropped to 50% of its initial value. At $T = 945 \text{ K}$ in the presence of H_2O , a K^+ peak, associated with K(g) by its appearance potential, appeared in the mass spectrum and began to grow steadily. Termination of the H_2O supply caused this peak to decrease.

DISCUSSION

Comparison of the equilibrium pressures of K(g) and Cs(g) over the respective carbonates with those observed over admixtures of the carbonates and Spheron-6 or char, indicates that there is a strong chemical interaction between the salts and the carbon at elevated temperature. This interaction is not simply carbothermic reduction of the salt, as evidenced by the disparity between the calculated and the measured vapor pressures of K(g) (Figures 1 and 2). It seems likely that, in the observed temperature range, a discrete chemical compound is formed with a thermodynamic activity of the alkali metal greater than that of the carbonate but substantially below that of the pure element. The Knudsen cell data give no direct clue to the structure of this solid or liquid phase, but they do suggest that oxygen is a component because oxygen-containing gaseous species (CO and CO_2) are observed to be in equilibrium with the substance. The suppression of the pressure of molecular KBr(g) coupled with the appearance of K(g) over a KBr -Spheron admixture upon the addition of H_2O , is further evidence of an essential role of oxygen in the formation of the compound. The clear X-ray diffraction pattern obtained from the Cs_2CO_3 -Spheron sample that had been heated under vacuum is indicative of a crystalline material. This pattern could not be associated with a specific chemical structure, but it was definitely not produced by Cs_2CO_3 , CsOH , Cs_2O , nor by a Cs-graphite intercalation compound. Such structures have been suggested as intermediates in the alkali-metal catalyzed steam gasification of coal chars (2).

At high temperatures in the absence of an external source of oxygen, the alkali metal Spheron admixtures exhibit a gradual loss of oxygen as evidenced by the diminution in CO and CO_2 partial pressures (Tables 2 and 3). Accompanying this process, the alkali metal partial pressures increase slightly, indicative of an increase in activity with the change in oxygen stoichiometry. An opposite change occurs when the mixture is exposed to an oxidizing gas (steam or CO_2).

Based on these considerations, we propose that the chemical species formed by the interaction of alkali metal carbonates and carbon at high temperatures is a non-stoichiometric oxide that contains an excess of the metal as ions and also in a dissolved state. Metal-rich Cs-O compounds, with stoichiometries corresponding to Cs_4O and Cs_7O , have been characterized as crystalline solids at room ambient temperatures (6). At high temperatures they melt into liquid phases comprised of a higher oxide containing excess Cs (7). Information on the K-O system is available only for higher oxygen stoichiometries (8), but, by analogy, we would expect all alkali metal-oxygen systems to behave similarly.

The role of the alkali metal additive as a gasification catalyst is probably critically dependent on the formation and action of such an oxide phase. We suggest that during gasification the catalyst forms a liquid oxide film distributed over the surface of the char or carbon. (There is considerable evidence that catalyst melting does occur (10)). The composition of the film is determined by a dynamic balance between a reducing process at the carbon interface and an oxidizing process at the surface in contact with the gaseous reactant, H_2O or CO_2 . At the catalyst/char interface, the anions in the catalyst react with the carbon to form an intermediate, such as a phenolate (11) that subsequently splits out CO . The anions are replenished by reaction between the oxidizing gas and the oxide at the gas/catalyst

interface. Net transport of oxygen from gas to carbon occurs by diffusion of the species in the molten catalyst film.

The presence of mineral constituents (typically SiO_2) in most coal chars complicates this picture by providing an alternative reaction path for the alkali metal salt additives. The interaction of these minerals with an alkali metal is illustrated strikingly in the case of the Cs_2CO_3 -char admixture. The equilibrium partial pressure of Cs(g) over this sample is significantly lower than over pure Cs_2CO_3 . Thus, the Cs activity in the solid phase is highly suppressed, as would be the case if it were chemically combined in a very stable compound, such as the CsAlSiO_4 detected in the X-ray pattern of the residue. However, the low intensity of this pattern considered together with the variation in equilibrium Cs(g) pressure with the Cs content of the sample (Figure 2), suggests that all the Cs is not tied up as a discrete crystalline compound of fixed composition. It is more likely that the Cs is dissolved in an amorphous mineral glass, in which its activity is a function of its concentration.

ACKNOWLEDGMENT

This work was supported by the U.S. Department of Energy, Morgantown Energy Technology Center. The X-ray diffraction measurements were made by Eldon Farley.

REFERENCES

1. D. W. McKee, Chem. Phys. Carbon, 16, 1 (1981).
2. W-Y. Wen, Catal. Rev.-Sci. Eng., 22, 1 (1980).
3. D. L. Hildenbrand, J. Chem. Phys., 48, 3657 (1968); 52, 5751 (1970).
4. K. H. Lau and D. L. Hildenbrand, J. Chem. Phys., 71, 1572 (1979).
5. JANAF Thermochemical Tables, NSRDS-NBS 37, Second Edition, U.S. Government Printing Office, Washington, D.C. (1971).
6. A. Simon, Struct. Bonding, 36, 81 (1979).
7. C. F. Knights and B. A. Phillips, J. Nucl. Mat., 84, 196 (1979).
8. A. J. Leffler and N. M. Wiederhorn, J. Phys. Chem., 68, 2882 (1964).
9. D. W. McKee, Carbon, 20, 59 (1982).
10. B. J. Wood, K. M. Sancier, D. R. Sheridan, B. L. Chan, and H. Wise, "The mechanism of Catalytic Gasification of Coal Char," Quarterly Report No. 4, Dept. of Energy Contract No. DE AC21-80MC14593, SRI International, Menlo Park, CA, November 15, 1981.
11. C. A. Mims and J. K. Pabst, ACS Div. Fuel Chem. Preprints, 25 (3), 258 (1980).

Table 1
APPEARANCE POTENTIALS AND RELATIVE INTENSITIES OF
IONS IN MASS SPECTRUM OF K_2CO_3

Ion	AP(eV)	Temperature (K)	Neutral Precursor	$I^R(AP + 3 \text{ eV})$ at 1153 K
K^+	4.3 ± 0.3	1121	K	1035
CO_2^+	13.7 ± 0.3	1121	CO_2	285
$C_2CO_3^+$	6.1 ± 0.3	1153	K_2CO_3	0.3
K_2O^+	7.8 ± 0.5	1068	K_2CO_3	2.0
K_2O^+	5.2 ± 0.5	1153	K_2O	0.03 ^a
O_2^+	11.9 ± 0.3	1153	O_2	33

^aMeasured at AP + 2 eV to eliminate the fragment contribution from K_2CO_3 .

Table 2
PARTIAL PRESSURES OF GASEOUS SPECIES ABOVE
 K_2CO_3 -CHAR ADMIXTURE AT VARIOUS TEMPERATURES

Temperature (K)	Partial Pressures (kPa × 10 ⁴)		$CO_2(g)$
	$K(g)$	$CO(g)$	
720	0.001	0.5	0.06
788	0.015	0.24	0.2
871	0.19	1.9	1.56
909	1.2	38.	15.1
952	5.17	53.1	2.43
978	9.68	-	-
875	0.63	1.5	0.22

Table 3
PARTIAL PRESSURES OF GASEOUS SPECIES ABOVE
 Cs_2CO_3 -SPHERON-6 ADMIXTURES

Temperature (K)	Partial Pressure (kPa × 10 ⁵)			
	$Cs(G)$	$CO(g)$	$CO_2(g)$	$(CsOH(g))$
397	0	0	0.16	0
421	0	0	8.01	0
549	0	0	5.22	0
727	0	0	18.4	0
727	0	0	5.3	0
729	<0.001	0.25	1.56	0
826	0.002	3.14	14.5	0
857	0.002	3.00	4.42	0
886	0.005	3.92	2.13	0
886	0.014	1.73	0.36	0
935	0.065	9.35	1.43	0.001
936	0.33	3.77	0.11	0.001
936	0.31	1.80	0.09	0.001
992	1.41	7.96	0	0.003
1059	4.98	15.50	0	0.005
972	0.76	0.36	0	0.002

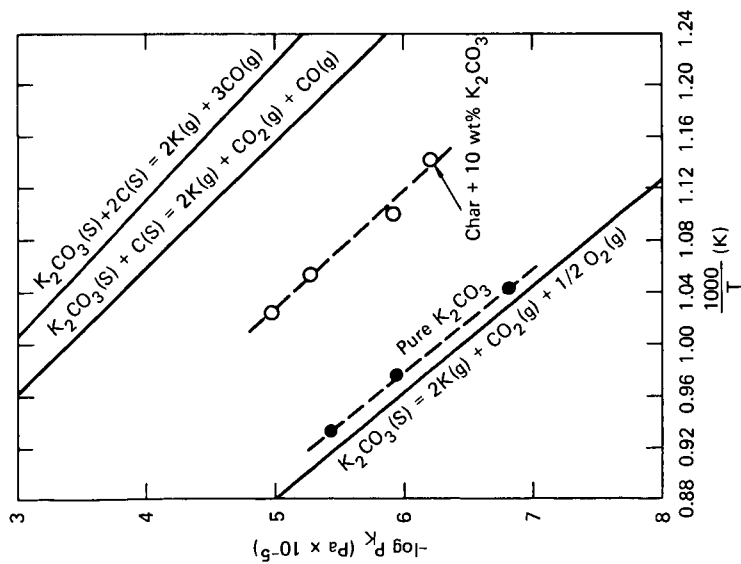


FIGURE 1 COMPARISON OF THE CALCULATED K VAPOR PRESSURES WITH EXPERIMENTAL DATA

JA-2202-12

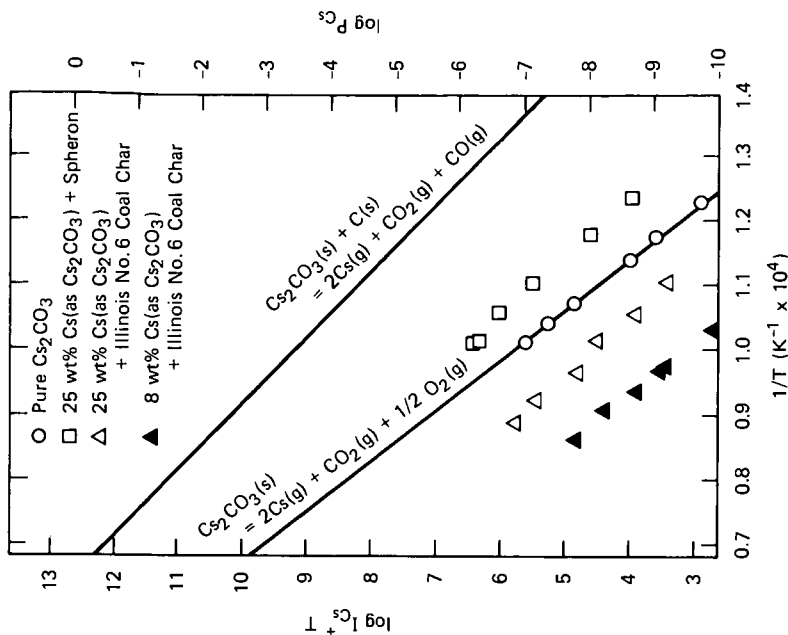


FIGURE 2 COMPARISON OF CALCULATED EQUILIBRIUM C_s PRESSURES WITH EXPERIMENTAL DATA

JA-2202-48

EFFECTS OF CATALYSTS AND CO₂ GASIFICATION ON THE ESR OF CARBON BLACK. II.

Kenneth M. Sancier

SRI International
Menlo Park, CA 94025

INTRODUCTION

In a previous paper, we reported some preliminary results of an in situ esr study of a K₂CO₃-carbon black mixture as a function of temperature and steam gasification.^[1] We found that (1) heating the mixture in helium above 600 K produced irreversible broadening of the esr line, which did not occur for carbon black alone, (2) the broadened line had a shape broader than Lorentzian, and (3) under steam gasification conditions, the esr line width decreased in proportion to the steam concentration.

In the present paper, we report further results from in situ esr studies of (1) the thermal interaction between carbon black and various salts and (2) effect of CO₂ gasification conditions. Also, we used the esr technique^[2] to provide information on changes in the electrical conductivity of a sample that may relate to the mechanisms of the thermal and gasification reactions.

EXPERIMENTAL

The specifications of the carbon black (Spheron-6, Cabot Corporation) and the esr apparatus have been described.^[1] The samples consisted of a mixture of 3 wt% carbon black in a given salt that was mechanically ground with a mortar and pestle. The only diluent of the carbon black was a given salt. All the salts were of reagent quality. The amount of sample mixture examined by esr was adjusted so that a known mass of carbon black was present, between 3 and 6 mg.

Carbon dioxide gasification was performed by using premixed gases containing and 0, 4.1, 7.9, and 15.8 vol% CO₂ in helium. A switching valve was used to select the desired gas mixture to flow over the sample in the quartz reactor mounted in the high temperature esr sample heater.

The techniques for measuring changes in the relative electrical conductivity of a sample resulting from temperature changes or chemical changes have been described elsewhere.^[2] Briefly, a change in electrical conductivity of a sample is approximately proportional to two electrical conductivity parameters, ΔI_P^{-1} and ΔI_D , that can be measured during an esr measurement. I_P is the peak height of the resonance signal of a reference sample (0.1% pitch in KCl, Varian), which was situated in the auxiliary cavity of a dual rectangular cavity (TE₁₀₄); the sample was situated in the other cavity, which has the sample heater accessory. ΔI_P^{-1} calculated from the differences in the values of I_P^{-1} referring to two different conditions of the sample, e.g., temperature. I_D is the bias current of the crystal diode detector of the microwave bridge, and ΔI_D is the change in this current resulting from a change in the electrical conductivity of the sample. By connecting a recorder to the crystal diode current meter, it was possible to record ΔI_D as a function of time during gasification experiments. The parameter

ΔI_p^{-1} is suitable for measuring relatively large changes in electrical conductivity, such as those arising from heating a sample. The parameter ΔI_p is useful for following smaller changes in the electrical conductivity of a sample, e.g., arising from a chemical change associated with CO_2 gasification.

Free radical concentrations were measured by using a computer to store the esr data and to calculate the first moments of the first derivative curves. The results were normalized for cavity sensitivity using I_p , gain, rf modulation amplitude settings (typically 0.1 mT), and mass of carbon. Microwave power incident on the sample cavity was 1 mW.

RESULTS

For convenience, the results of the in situ esr measurements made on several salt-carbon black mixtures will be subdivided into two parts: thermal effects and CO_2 gasification effects.

Before each series of esr measurements with a given sample, oxygen was desorbed from the carbon by heating the sample in the esr reactor cell at about 500 K for 5 min while helium flowed through the cell. The value of the esr line width measured at room temperature was about 7.0 mT (70 gauss) before the desorption and about 0.15 mT after the desorption. The esr line was symmetric for all the salt-carbon black mixtures.

Various samples were tested for microwave power saturation, and none was detected for sample temperatures examined in the range from 290 to 800 K and for microwave power levels incident on the sample in the range of 0.1 to 40 MW; the upper value was limited by the electrical conductivity of the samples.

Thermal Effects

The thermal interaction between a salt and carbon black heated in helium were investigated by studying a series of potassium halide-carbon black mixtures. Alkali metal halides are less active catalysts than K_2CO_3 for gasification of carbonaceous materials.^[3,4] For comparison, a K_2CO_3 carbon black mixture was included. Also included was a mixture of carbon black with CaO which is expected to be a relatively poor gasification catalyst^[3,5] and has relatively low electrical conductivity at elevated temperatures. Hence, the CaO serves as a diluent to decrease microwave skin depth effects so that the esr properties of carbon black alone can be studied.

To determine the effects of heating the mixtures in helium we measured three esr parameters simultaneously: variations in the free radical concentration, line width, and ΔI_p . Measurements were made at successively higher temperatures (Figures 1a and 2a), but before progression to each next higher temperature, a measurement was made at 290 K (Figures 1b and 2b).

The free radical concentrations uncorrected for Curie's law were essentially independent of both the measurement temperature and the type of salt, within the accuracy of these measurements. The values of I_p , which were used to normalize the free radical concentrations for changes in cavity sensitivity, varied by a factor of about 10 over the temperature range studied, indicating the importance of such a correction.

The esr line width began to increase at temperatures above 850 K, and the magnitude of the increase was strongly dependent on the anion of the salt (Figure 1a). When the sample was cooled to room temperature the line width decreased. An irreversible effect is evident by the fact that a significant fraction of the line broadening produced at higher temperatures was retained upon cooling the samples (compare Figures 1a and 1b). In general, the effect on line width and the magnitude of the irreversible effects for the salts decreased in the following order: $\text{KBr} \approx \text{KCl} \approx \text{KI} > \text{K}_2\text{CO}_3 \approx \text{KF} > \text{CaO}$.

The electrical conductivity parameter, ΔI_p^{-1} , generally increased with heating temperature, and with few exceptions was almost independent of the type of salt mixed with carbon black (Figure 2a). The results of the measurements at 290 K, after cooling from a given higher temperature, also indicate that an irreversible increase in the electrical conductivity for some salts had been produced thermally (compare Figures 2a and 2b). Measurements on two salts, K_2CO_3 or KCl , in the absence of carbon black show that the ΔI_p^{-1} parameter has a very small temperature dependence, increasing less than 10% as the temperature was raised from 300 to 1200 K.

Comparison of Figures 1 and 2 suggests that there is a qualitative similarity in the way the heating temperature affects the two parameters, line width and ΔI_p^{-1} . A test of the relationship between line width and ΔI_p^{-1} is shown in Figure 3, which is a replot of the results in Figures 1a and 2a. The curves drawn in Figure 3 indicate that line width has a monotonic relationship to ΔI_p^{-1} , but that the functional dependence may be different for different salts.

CO_2 Gasification Effects

At elevated temperatures when He gas passing over a sample was switched to He containing CO_2 (15.8%), the line width decreased and the free radical concentration increased as shown in Figures 4 and 5, respectively. Before the CO_2 gasification measurements, the sample was thermally equilibrated at a given temperature for about 20 min. However, the line width and free radical concentration continued to change slowly, probably the result of slow irreversible changes caused by CO_2 as discussed above. Therefore, to separate the slow thermal changes from the rapid changes produced by CO_2 , we switched the gas flowing over the sample at a given temperature, 800 or 850 K, back and forth between He and He containing CO_2 . The sequence of the measurements is indicated by the numbers beside the data points in Figures 4 and 5. These results show that CO_2 had a greater effect at the higher temperature for both line width and free radical concentration. Also, at a given temperature the magnitude of the effect tended to become limited at concentrations of CO_2 greater than about 4%; e.g., see the line width dependence at 850 K in Figure 4. This behavior is probably due to a diffusion-limited process.

It was of interest to determine whether CO_2 gasification conditions altered the electrical conductivity of the sample, but the electrical conductivity parameter, ΔI_p^{-1} , exhibited a very small and almost imperceptible response. Therefore, the more sensitive electrical conductivity parameter, ΔI_D , was used. The recorded value of ΔI_D is shown in Figure 6, which shows the changes that occurred as the gas passing over the sample at 855 K was switched between He and 15.8 % CO_2 in He. Although the sample was initially in He the positive slope of ΔI_D indicates that the sample was not stable although it had been thermally equilibrated. However, it is clear from the recording that CO_2 caused the value of ΔI_D

to decrease (electrical conductivity decrease) and that subsequent exposure to He caused the value of ΔI_D to increase.

The observed values of the line width are marked in Figure 6 at three points in time. The results show that the line width changed reversibly when the sample was alternately exposed to He and CO_2 . Also, the decrease in line width correlates with the decrease in the electrical conductivity of the sample, as was the case in the study of thermal effects discussed earlier.

When carbon black alone and mixtures of carbon black with the potassium halides or with CaO were exposed to CO_2 gasification conditions at 850 K, very small or no changes were observed to occur in line width, free radical concentration, or in electrical conductivity (ΔI_D).

The correlation between an increase in the value of ΔI_D and an increase in electrical conductivity was established by noting that both ΔI_D and ΔI_P^{-1} changed in the same way for large enough changes in electrical conductivity, e.g., as produced by an increase of sample temperature.

DISCUSSION

In the previous paper^[1] some suggestions were made to account for those changes occurring in the esr spectra due to a thermal interaction between carbon black and K_2CO_3 and due to steam gasification. The additional experimental information obtained in the present esr study, pertaining to various other salts and a study of CO_2 gasification, provides a broader basis for interpreting the mechanisms of the thermal and gasification reactions.

Thermal Effects

Two mechanisms were suggested^[1] to account for the esr line broadening resulting from heating a mixture of salt and carbon black: (1) increased electrical conductivity and (2) unresolved hyperfine splitting (hfs) due to an interaction between the magnetic moment of the unpaired electron and that of the nucleus of the cation of the salt. The current results suggest that the increase in line width is related to the increase in the electrical conductivity because of the observed proportionality between the line width and the change in the electrical conductivity parameter for a series of salt-carbon black mixtures heated to various temperatures (Figure 3). In the following discussion, the relationship between these two parameters is examined in detail.

We postulate that some sort of complex is formed between certain salts and carbon black to account for the increase in the electrical conductivity and esr line width resulting from heating mixtures of salts and carbon black being significantly greater than the increase when the individual components are heated. Generally, an increase in electrical conductivity is due to an increase in the concentration or mobility of the charge carriers. Since the free radical concentration of the salt-carbon black mixtures was insensitive to temperature, it appears that charge carriers (conduction electrons or holes) are mainly responsible for the observed esr signal, whereas π -electrons would obey Curie's law. If the esr measurements detect all the charge carriers, then the observed increase of the electrical conductivity with increase in temperature is due mainly to an increase in charge carrier mobility.

We propose a series of reactions to account for the effect of the electronic properties of the solid. First, elemental metal atoms are produced by carbon reduction of the cation of the salt (e.g., K^+);^[6] Second, an extended aromatic structure develops by loss of hydrogen and polymerization of the carbonaceous material,^[7,8] and this polymerization could possibly be catalyzed by a salt or a metal atom. Third, a complex is formed between an aromatic structure and the ions or atoms of the salt. For example, such a complex could involve metal ions or atoms which (1) substitute for the hydrogens of CH or OH groups of the aromatic structure,^[9] (2) interact electrostatically with the π -orbitals of the extended aromatic structure,^[10] or (3) form a kind of intercalation compound with the available graphite-like structures, although such compounds are usually not expected to be stable at gasification temperatures.

For most salts studied, the changes in the esr parameters are largely irreversible, indicating that the salt-carbon black complex is stable. The greater effects produced by the alkali metal salts than by CaO or Al_2O_3 ^[1] are probably due to the greater ease with which carbon can reduce the alkali metal cations.

Based on the concepts suggested above, we propose that the observed line broadening results from relaxation effects that occur in the salt-carbon black complex when the unpaired electrons observed by esr experience the inhomogeneous fields developed near the sites at which a salt (e.g., the metal atom or cation and the anion) interacts with the aromatic carbon structure. Since these sites are nonuniformly distributed, the unpaired electrons in a conduction band or in π -orbitals experience different environments, resulting in inhomogeneous broadening of the esr line. The observed line shape, which is broader than Lorentzian, probably results from a superposition of two or more Lorentzian lines representing different environments.

Gasification Effects

Gasification by either steam^[1] or CO_2 of a salt-carbon black sample results in the same qualitative changes in the three esr parameters: a decrease in the line width, a decrease in the electrical conductivity, and an increase in the free radical concentration. Therefore, it appears that a single mechanism could account for the changes in the esr spectra that occur during gasification conditions.

We suggest that steam or CO_2 reacts with the salt-carbon complex and fragments carbon-carbon bonds of aromatic rings. As a result, the unpaired electrons will experience a decreased resonance path and less interaction with the atoms or ions of the salt that were associated with the aromatic ring before fragmentation. In other words, the unpaired electron will experience fewer regions with inhomogeneous fields, and therefore the esr line width should decrease.

Also as a result of the fragmentation of the aromatic rings the steady-state concentration of free radicals will be increased. Although these free radicals are probably unstable and will react with CO_2 or polymerize to produce a more stable structure, other radicals will be produced continuously by the gasification reaction.

The *in situ* esr results clearly indicate that for a salt to promote catalytic gasification, both the cation and anion of a salt must interact with the carbon structure. That is, switching to CO_2 gasification conditions caused changes in

the esr parameters only for salts with catalytic activity, e.g., salts with an alkali metal cation and a non-halide anion. Evidently, the character of the salt-carbon complex determines catalytic activity.

However, the changes in the esr parameters produced by thermal effects do not appear to correlate with the catalytic activity of the salts. For example, large increases in both line width and electrical conductivity occurred upon heating mixtures of carbon black with either of two salts, K_2CO_3 or KCl, which have widely different catalytic activities.

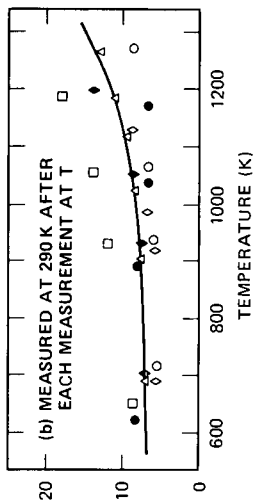
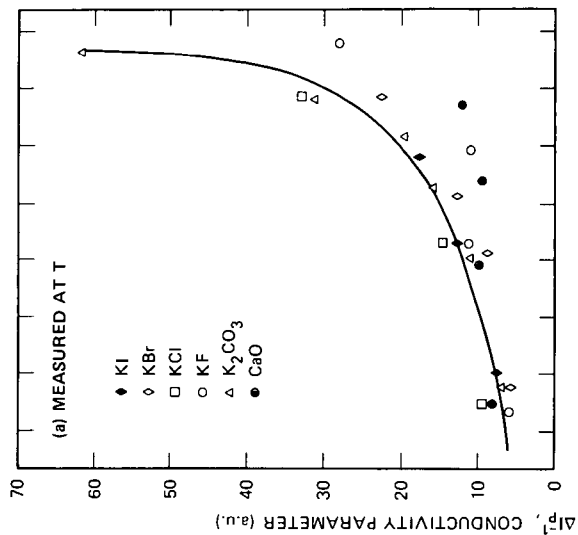
To elucidate the mechanism of catalytic gasification, we plan to consider the information developed by esr along with that obtained by other techniques being pursued in our laboratory.

ACKNOWLEDGMENTS

The author is grateful to his colleagues Bernard Wood and Henry Wise for valuable discussions and to Steven Leach and Robert Brittain for computer programming for the esr studies. He also acknowledges valuable discussions with L. S. Singer and J. Uebbersfeld. The research was supported by the U. S. Department of Energy under Contract No. DE AC21-80MC14593.

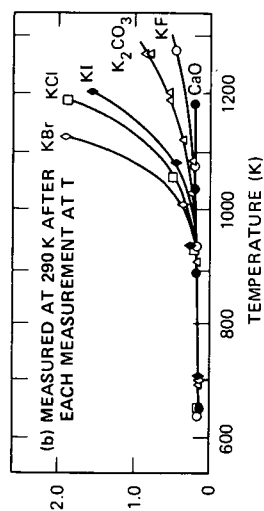
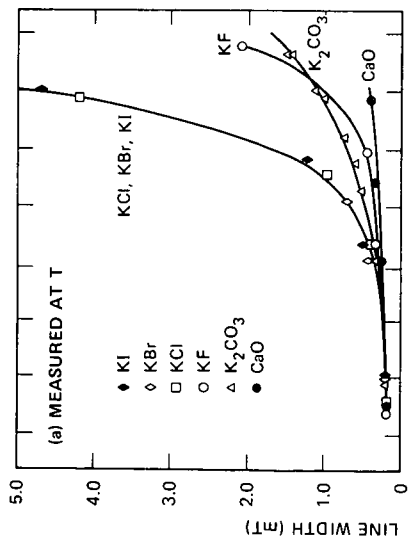
REFERENCES

1. K. M. Sancier, Fuel, in press.
2. M. Setaka, K. M. Sancier, and T. Kwan, J. Catal. 16, 44 (1970).
3. M. J. Veraa and A. T. Bell, Fuel, 57, 194 (1978).
4. D. W. McKee, C. L. Spiro, P. G. Kosky, and E. J. Lamby, ACS Fuel Division Reprints, 27(1), 74 (1982).
5. E. J. Hippo, R. G. Jenkins, and P. L. Walker, Jr., Fuel, 58, 338 (1979).
6. D. A. Fox and A. H. White, Ind. Engng. Chem., 23, 259 (1931).
7. S. Mrozowski, Carbon, 6, 841 (1968).
8. L. S. Singer and I. C. Lewis, Appl. Spectroscopy, 36, 52 (1982).
9. C.A. Mims and J. K. Pabst, Proc. International Conf. Coal Science, Dusseldorf, 730 (1981).
10. N. L. Holy, Chem. Rev., 74, 243 (1974).



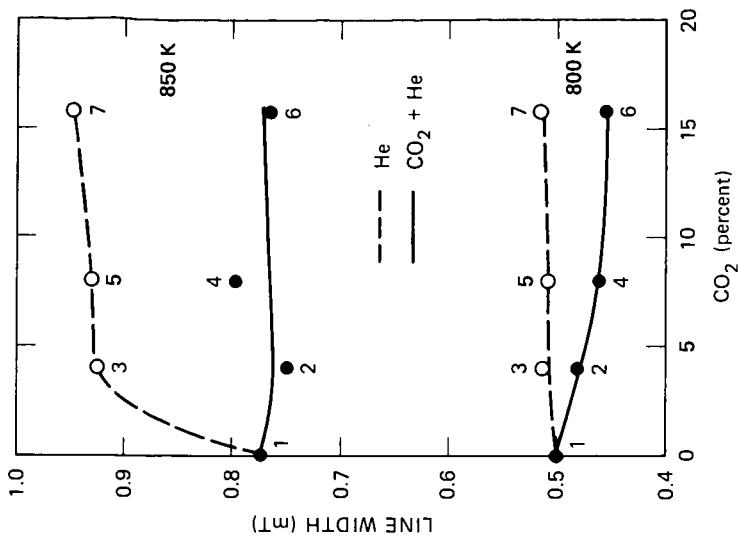
JA-2202-50

FIGURE 2 EFFECT OF TEMPERATURE ON ESR ELECTRICAL CONDUCTIVITY PARAMETER OF SALT-CARBON BLACK MIXTURES
3 wt% carbon; heated in helium.



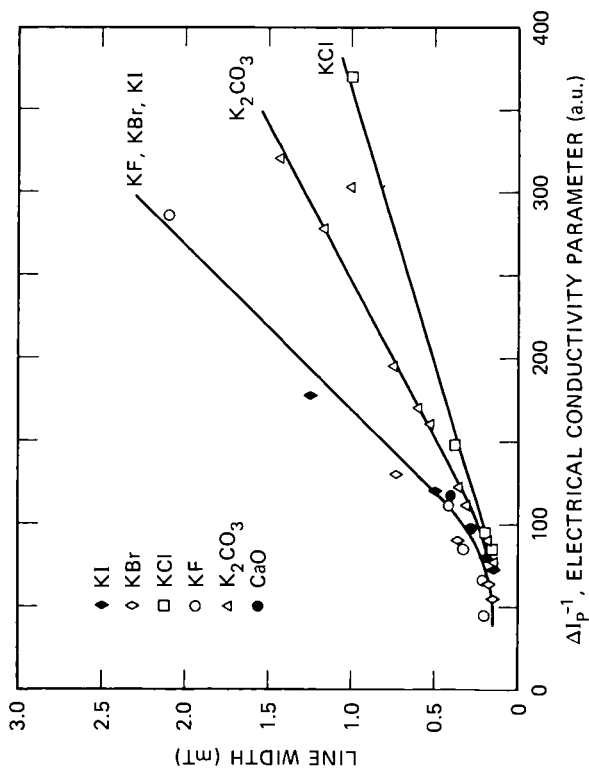
JA-2202-43

FIGURE 1 EFFECT OF TEMPERATURE ON ESR LINE WIDTH OF SALT-CARBON BLACK MIXTURES
3 wt% carbon; heated in helium.



JA-2202-45

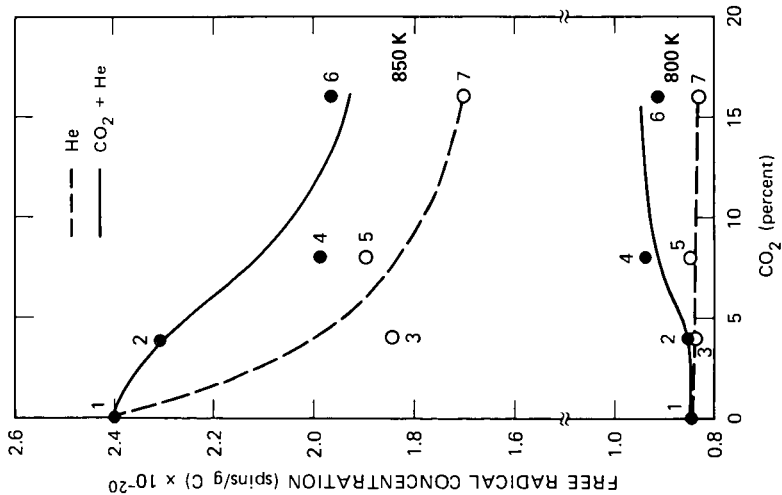
FIGURE 4 EFFECT OF CO₂ ON ESR LINE WIDTH OF K₂CO₃-CARBON BLACK MIXTURE 3 wt% carbon; numbers identify sequence of measurements.



JA-2202-51

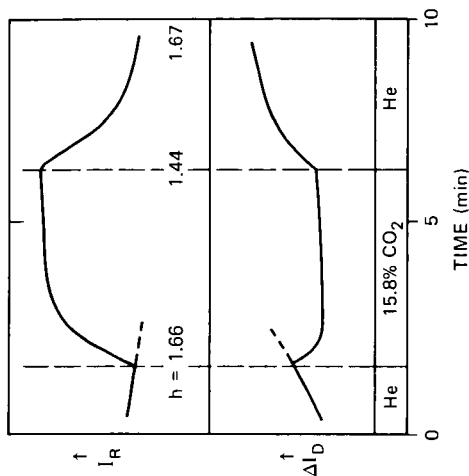
FIGURE 3 RELATIONSHIP BETWEEN ESR LINE WIDTH AND ESR ELECTRICAL CONDUCTIVITY PARAMETER OF POTASSIUM SALT-CARBON BLACK MIXTURES

3 wt% carbon; heated in helium. Replot of Figures 2a and 3a.



JA-2202-46

FIGURE 5 EFFECT OF CO₂ CONCENTRATION ON FREE RADICAL CONCENTRATION IN K₂CO₃-CARBON BLACK MIXTURE 3 wt% carbon; numbers identify sequence of measurements.



JA-350543-18

FIGURE 6 EFFECT OF CO₂ GASIFICATION ON ESR PARAMETERS OF CARBON — K₂CO₃ (8 wt% K) MIXTURE AT 855 K

I_R — Peak intensity of radical signal
 ΔI_D — Detector current
 h — Line width (mT)

CONTROLLED ATMOSPHERE ELECTRON MICROSCOPY STUDY OF THE
 K_2CO_3 - CATALYZED GRAPHITE - H_2O REACTION

C. A. Mims, R. T. K. Baker, J. J. Chludzinski,

Exxon Research and Engineering Co.
P.O. Box 45, Linden, NJ 07036

and

J. K. Pabst

Exxon Research and Engineering Co.
P.O. Box 4255, Baytown, TX 77520

Controlled atmosphere electron microscopy has provided unique insight into the details of the mode of catalytic attack of carbons by reactive gases (1). Many of the systems investigated show graphite gasification to occur at the interfaces between discrete catalyst particles and edges of the graphite layer planes. Graphite is removed in these cases by the formation of channels through the graphite sheets. Some catalysts (e.g. Mo (2)) display increased tendency to wet the reactive graphite surface and therefore exhibit a stronger interaction.

Alkali salts are perhaps the best known catalysts for gasification of carbon and have been extensively studied. Several investigators have provided evidence that potassium salts react readily with the carbon substrate to form surface salt complexes (3). We undertook this study in part to see if the morphology of K_2CO_3 - catalyzed attack would reflect this strong surface bonding.

EXPERIMENTAL METHOD

All experiments were performed in the controlled atmosphere microscope (4). Pure, thin specimens of Ticonderoga graphite were mounted on heating stages and impregnated by a fine mist of 0.1% K_2CO_3 solution. Water vapor was admitted to the controlled atmosphere cell from a wet argon stream. The behavior was monitored as the sample was taken by steps through heating and cooling cycles to temperatures as high as 800°C. Higher temperatures than this were avoided to minimize the amount of catalyst vaporization. Several successful runs on different samples make up the data base.

RESULTS

Initial heating cycle in H₂O

We paused for sufficient time (15 min) at each temperature during the initial heating program to detect slow changes in the specimen and catalyst morphology. Up to temperatures of 550°C the only change noticed was the gathering of particles of K₂CO₃ on the edge of the specimen (see Figure 1a). The particles generally had liquid-like shapes with contact angles suggestive of attractive (wetting) interaction. When the temperature was raised above 550°C the particles slowly, or more rapidly at higher temperature, disappeared from the graphite edge. The sequence of photographs in Figure 1 shows this occurrence over the span of approximately 2 minutes at 670°C. That catalyst remained on the specimen after the particles disappeared was shown by the subsequent gasification behavior of the graphite. Therefore we believe that the disappearance of the particles reflects spreading of the salt to a thin film on the graphite surface rather than evaporation.



Onset of gasification

Almost simultaneously with the disappearance of the catalyst particles, attack of the edges of the graphite specimen became evident. The edges began receding at many places along the entire edge, at first showing as a series of irregular notches. Soon the notches took on a hexagonally faceted appearance (see Figure 2). The rate of edge recession at 550°C was too slow to be readily apparent in real time but increased with increasing temperature. The rates were much faster than the uncatalyzed rate at the same conditions, reflecting the fact that catalyst had remained on the sample. The edge recession eventually involved the entire specimen edge with hexagonal faceting throughout.

We analyzed films of the experimental runs to derive rates of edge recession. Reactive edges exhibit a reproducible and characteristic recession rate which is general for all features on a given sample. These rates for one run are plotted in Figure 3. Data are shown for both increasing temperature sequence and decreasing temperature sequence. We observed no hysteresis in the rates for a complete cycle of temperature.

DISCUSSION

The morphology of the K₂CO₃ catalyst during gasification is striking confirmation of strong interaction between the catalyst and the edges of the graphite lattice. The interfacial bonding is strong enough to compete with the cohesive bonding within the bulk salt and effectively disperse the catalyst along the active edge. Surface salts groups such as phenoxide analogs have been identified on less ordered carbons impregnated with alkali catalysts and quenched from gasification conditions (3c). These surface salts are thought to be responsible for the high dispersion of alkali catalysts on carbons such as coal char and also explain the reproducibility of the catalytic effect of potassium salts on these materials.

Hexagonal faceting of the gasifying graphite edge reflects a preferential reaction of one crystallographic orientation over another. J. M. Thomas exploited this feature very elegantly in optical microscopy (5). The facets in this study are aligned parallel to the $\langle 1120 \rangle$ set of crystal directions. This can be determined by noting the orientation of the facets with respect to twin bands along the $\langle 1010 \rangle$ direction which are usually present in graphite specimens. One such twin boundary appears in Figure 2. The K_2CO_3 catalyzed reaction thus exposes the "zig zag" presentation of the surface. This orientation must be less reactive than other orientations, for example the "armchair" or  or  configuration. This is perhaps not surprising in that the $\langle 1120 \rangle$ orientation presents one uncondensed carbon atom per ring exposed at the edge whereas the $\langle 1010 \rangle$ orientation presents two uncondensed carbons together. The latter might a priori be expected to be the more reactive and would explain the results obtained here. Thomas did see a dependence of the orientation of etch pits in the graphite- O_2 reaction on reaction conditions.

The activation energy derived from the edge recession data (35 kcal/mol) is lower than that observed by McKee and Chatterji for K_2CO_3 on graphite (52.2 kcal/mol (6)). Direct comparison is difficult because in neither study is the reactant gas composition (particularly the H_2 partial pressure) well characterized. Furthermore very different pressures were used in the two studies.

CONCLUSIONS

We have seen microscopic evidence of strong interaction between potassium catalyst and the reactive edges of graphite. This interaction is thought to be driven by the formation of surface salt bonds. The spreading of the catalyst which results from this strong interaction provides high dispersion and efficient use of the catalyst. The hexagonal faceting provides additional insight into the reactivity of proposed surface ensembles.

REFERENCES

- 1 R. T. K. Baker, to be published.
- 2 R. T. K. Baker, P. S. Harris, D. J. Kemper and R. J. Waite, Carbon **12**, 179 (1974).
- 3 a. F. J. Long and K. W. Sykes, J. Chem. Phys. **47**, 361 (1950).
b. C. A. Mims, and J. K. Pabst, Proc. Int. Conf. on Coal Sci. 1981 p. 730 (verlag Gluckauf GmbH, Essen).
c. C. A. Mims and J. K. Pabst, J. Am. Chem. Soc. to be published.
- 4 R. T. K. Baker and P. S. Harris, J. Sci. Instrum. **5**, 793 (1973).
- 5 J. M. Thomas in Chemistry and Physics of Carbon (P. L. Walker, ed.) vol. 1 p. 122, Marcel Dekker (NY) (1965).
- 6 D. W. McKee and D. Chatterji Carbon **16**, 53 (1978).

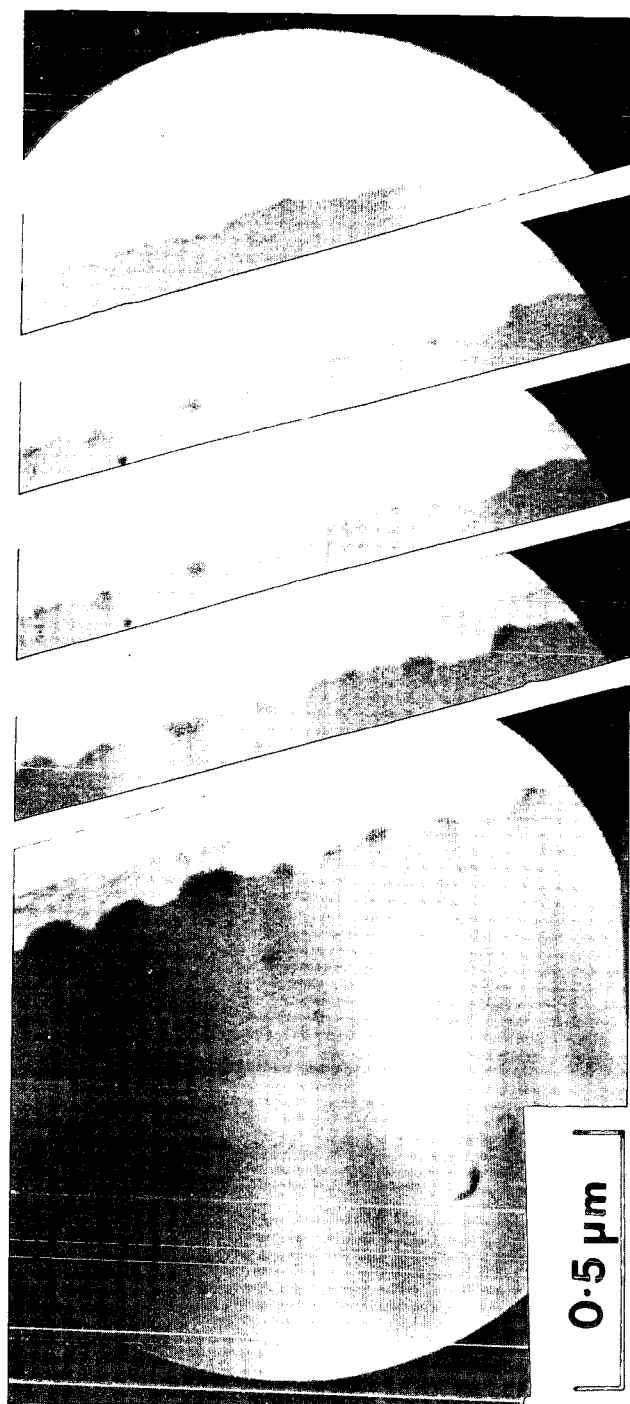


Figure 1. Sequence of photographs taken from the CAEM video display showing the progressive disappearance of droplet-like particles of K_2CO_3 on the edge of graphite at $670^\circ C$ in water vapor. The sequence spans 120 seconds.



Figure 2. Photograph of video display showing active edge of graphite while reacting at 715°C in H_2O . General motion of features was from left to right. The remnant of the original edge (E) can be seen as well as a twin band (T).

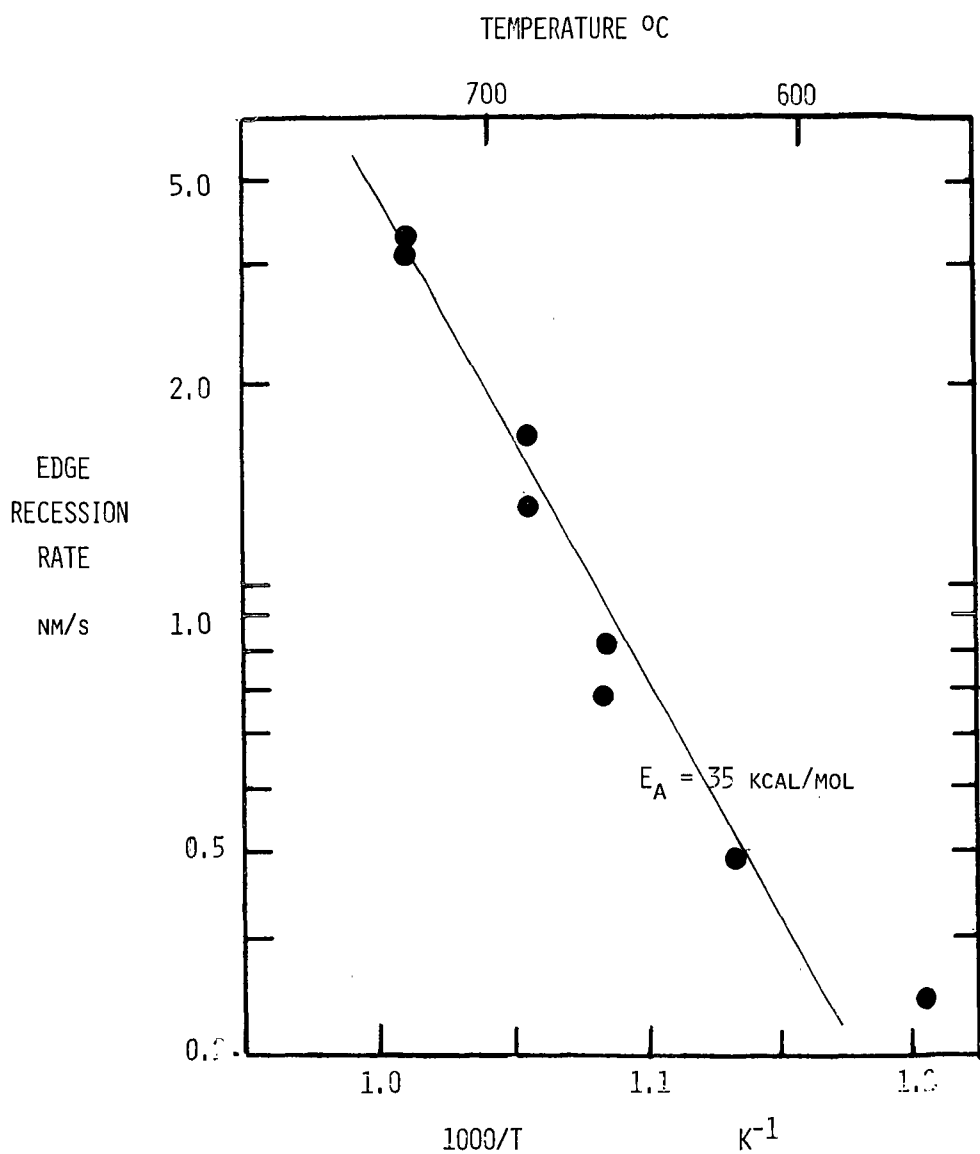


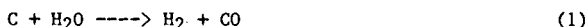
Figure 3. Arrhenius plot of catalyzed edge recession rates measured on a single graphite sample. Data points are the average of many features. Data for ascending and descending temperature sequence are shown at several temperatures

LOW TEMPERATURE METHANE PRODUCTION BY THE CATALYZED REACTION OF
GRAPHITE AND WATER VAPOR

F. Delanny, W. T. Tysoe, G. Yee, R. Casanova, H. Heineman and G. Somarjai

Materials & Molecular Research Division
Lawrence Berkeley Laboratory
and
Department of Chemistry
University of California
Berkeley, California 94720

The gasification of carbon (coal) by reaction with water vapor is usually conducted at a temperature higher than 1200K. This reaction exhibits an apparent activation energy of the order of 50 kcal/mole. It is catalyzed by various salts of alkali metals, especially potassium [1,2]. At these high temperatures, the main products are CO and H₂, according to the reaction



The simultaneous production of CH₄ has also been reported [3] especially when the reaction temperature is lowered. The relatively high temperature would, however, facilitate the decomposition of most hydrocarbons that could have been produced.

Our research is focussed on finding suitable catalysts for the low temperature production of low molecular weight hydrocarbons from the reaction of carbon (coal) with water vapor. It has been reported recently that potassium hydroxide, potassium carbonate and several other alkali metal hydroxides catalyze the production of methane in the temperature range from 500 to 600K with an apparent activation energy of about 11 kcal/mole [4]. In order to gain more insight into the mechanism of this production, this study has been extended by

- i) using two different reactors to accomodate either graphite single crystals or graphite powder,
- ii) extending the temperature range up to 1075K,
- iii) varying of the reactor vapor pressure, and
- iv) investigating other catalysts: calcium oxide and transition metals.

Graphite single crystals were obtained by cleavage from a larger piece of highly oriented pyrolytic graphite (HOPG) from Union Carbide Corporation. They were mounted on the manipulator of a UHV system, in firm contact with a gold foil that could be heated resistively. The sample was accessible to surface analysis by AES, XPS, ion sputter cleaning and mass spectrometry. It could also be isolated within a high pressure cell where it was exposed to water vapor and/or other gases for chemical reaction. The products were analyzed by gas chromatography. This apparatus has been described in more detail elsewhere [4].

*On leave from the Groupe de Physicachimie Minérale et de Catalyse, Université Catholique de Louvain, Belgium.

Pure graphite powders were reacted with water in a fixed bed reactor made of a quartz tube 4 min. ID containing about 0.4 g of sample fixed between two glass wool plugs. A carrier gas (usually nitrogen) was saturated with water vapor by bubbling through a water container where the temperature could be adjusted from 30°C to 95°C in order to vary the water vapor pressure. The flow rate could be varied between 4 and 20 ml/min. At the outlet of the reactor, the water vapor was condensed in a copper coil maintained at the melting ice temperature. Care was taken to avoid the condensation of water in other parts of the apparatus. The products were analyzed by gas chromatography.

The potassium hydroxide catalyzed reaction was studied from 525 to 1075K under a water vapor pressure ranging from 20 to 600 torr. The production of methane exhibited the same apparent activation energy of about 12 kcal/mole within the whole temperature range. This suggests that the catalytic mechanism involved remains the same at high temperature and has no relation to the (simultaneously occurring) reaction (1). The methane production appeared also to be first order with respect to the water vapor pressure.

Calcium oxide was also tried as catalyst in the temperature range 623-873K [5]. Single crystal graphite samples were impregnated with 1M solution of $\text{Ca}(\text{NO}_3)_2$ and dried in air. CaO was obtained from the decomposition of $\text{Ca}(\text{NO}_3)_2$ at the temperature of the reaction. No methane was detected when the sample was exposed only to 22 torr of H_2O and 730 torr of helium. XPS analysis showed, however, the appearance of a new peak at a binding energy of 290 eV. Methane was readily detected when the sample was subsequently exposed to 1 atm H_2 at the same temperature. The intensity of the peak at 290 eV decreased simultaneously with increasing time of reaction with hydrogen. We tentatively attribute this peak to a new form of active carbon that is hydrogenated to CH_4 by H_2 . A steady rate of production of methane was obtained when reacting the sample in a mixture of 22 torr of H_2O and 32 torr of H_2 . This reaction had an apparent activation energy of 16.3 kcal/mole and exhibited a first order dependence on the hydrogen pressure.

Alkali and calcium catalysts do not produce organic molecules other than methane under our experimental conditions. Studies are now in progress to determine if the combination of these catalysts with transition metal compounds could be utilized to produce higher molecular weight hydrocarbons.

This work is supported by the Director, Office of Energy Research, Office of Basic Energy Sciences, Materials/Chemical Sciences Division of the U.S. Department of Energy under Contract DE-AC03-76SF00098.

REFERENCES

1. Wen-Young Wen, Catal. Rev. Sci. Eng. 22, 1 (1980).
2. D.W. McKee, Chemistry & Physics of Carbon (P.L. Walker, Jr. and P.A. Thrower), Vol. 16, pg. 1, Marcel Dekker, New York (1981).
3. C.A. Mims and J.K. Pabst, Amer. Chem. Soc. Preprints, Div. of Fuel Chemistry, Vol. 25, 3, pg. 258 (1980).
4. A.L. Cabrera, H. Heinemann and G.A. Somorjai, J. Catalysis 75, 7 (1982).
5. R. Casanova, A. Cabrera, H. Heinemann and G.A. Somorjai, to be published.

CHARACTERIZATION OF COAL MACERALS ON THE BASIS OF THEIR FLUORESCENT SPECTRA

John C. Crelling* and David F. Bensley**

*Department of Geology, Southern Illinois University at Carbondale, Carbondale, Illinois, 62901

**Coal Research Section, The Pennsylvania State University, University Park, Pennsylvania, 16802

INTRODUCTION

One of the major problems of coal science is that very little is known about the basic properties of the various macerals that make up coal. Two of the main reasons for this lack of knowledge about the properties of coal macerals is that they are extremely difficult to separate from coal and that they are non-crystalline organic compounds and, therefore, not good subjects to analyze with such standard methods as x-ray diffraction or electron-microprobe analysis. Some of the most successful characterization of coal macerals to date has been by petrographic methods, in which the individual macerals do not have to be separated. In the steel industry, for example, petrographic techniques have proven so successful in allowing the prediction of the coking properties of coal that most major steel companies have now established petrographic laboratories. Another petrographic technique that has only recently been applied to coal analysis is qualitative and quantitative fluorescence microscopy. With this technique, the visible fluorescent light excited from the macerals reveals shapes, textures and colors not visible in normal white-light viewing. The technique also yields quantitative spectra that are characteristic of both the individual maceral type and the rank of the coal. It is now also well established that all of the liptinite macerals (derived from the resinous and waxy parts of plants) and some of the vitrinite macerals will fluoresce, and that some recently discovered liptinite macerals can only be identified by their fluorescence properties. Some of the first measurements of the absolute intensity of fluorescence of coal macerals at specific wavelengths were made by Jacob (1,2). Relative intensity measurements of fluorescent spectra of modern plant materials, peats and coals have been reported by van Gijzel (3,4,5). Teichmüller (6,7,8) described three new members of the liptinite group of macerals in part by demonstrating their distinctive spectral properties. Ottenjann, Teichmüller and Wolf (9) illustrated the correlation of changes in fluorescence spectra of sporinite with rank, and Crelling and others (10) and Crelling (11) have demonstrated the use of fluorescence spectra to discriminate macerals. In addition, Ottenjann, Wolf, and Wolff-Fischer (12) have been able to relate the fluorescence spectra of vitrinite macerals to the technological properties of coal. These studies have shown the potential of using fluorescence measurements in the study of liptinite and vitrinite macerals.

EQUIPMENT AND METHODS

The fluorescence microscopy system used in the SIUC Coal Characterization Laboratory is a Leitz MPV II reflectance microscope which is fitted with a 100 watt mercury arc lamp, a Ploem illuminator and a Leitz oil immersion 40X objective with a 1.3 numerical aperture. For spectral measurements the light from the mercury arc passes through a UGL ultra-violet filter to a TK400 dichroic mirror which reflects light less than 400 nm to the sample. The fluorescent light excited from the sample is passed through a 430 nm barrier filter to a motorized interference wedge in front of the photometer. The interference wedge controls the wavelength of the fluorescent light hitting the photometer so that the intensity variations from 430 to 700 nm can be scanned and recorded in about 40 seconds.

The spectral data are then fed into a computer from the microscope system and digitized, corrected and analyzed. Each spectrum is corrected for the effects of background fluorescence and for the effects of the microscope system, especially the sensitivity of the photo-multiplier tube, following correction procedures described by van Gijzel (13). For comparison the various spectra are normalized and reduced to a number of parameters such as: 1) the wavelength of maximum intensity peak (λ_{max}); 2) the red/green quotient (Q) where Q = relative intensity at 650 nm/relative intensity at 500 nm; 3) the area below λ_{max} ; 4) the area above λ_{max} ; 5) area blue (430 to 500 nm); 6) area green (500 to 570 nm); 7) area yellow (570 to 630 nm); and 8) area red (630 to 700 nm).

RESULTS AND DISCUSSION

In coals of the Illinois Basin, standard white-light petrographic methods generally reveal three types of liptinite macerals, resinite, sporinite and cutinite. These macerals are identified on the basis of their petrographic properties such as reflectance, size, shape and texture. When qualitative fluorescence analysis is used, the fluorescence colors and intensity commonly reveal an additional maceral, fluorinite. When fluorescence spectral analysis is used, the spectral data distinguish these four types of liptinite macerals plus additional varieties of resinite, sporinite and cutinite. Also, altered or weathered varieties of these macerals can be distinguished in some coals. For example, spectral analysis of the various liptinite macerals in samples of the Herrin (No. 6) coal seam with a reflectance of 0.65% (in oil at 546 nm) showed distinctive spectra for the macerals fluorinite, resinite, sporinite and cutinite. In this case, the spectra were assigned to maceral groups on the basis of the petrographic identification of macerals from which the spectra were obtained. When the groups of spectral data for each maceral type were subjected to discriminant function analysis of the eight different parameters for each spectrum, the maceral types were well separated. From this analysis it was easily seen that there were two different groups of resinite macerals. Thus, the statistical analysis of the spectral parameters of the macerals revealed two varieties of the resinite maceral group that could not be readily distinguished by normal petrographic means. The average spectra of the various maceral types distinguished by the discriminant function analysis are plotted in Figure 1. The combined results of maceral analyses in both white-light and fluorescent light as well as the reflectance value for the Herrin (No. 6) coal are given in Table 1.

Table 1.

RESULTS OF COMBINED WHITE-LIGHT AND FLUORESCENT LIGHT PETROGRAPHIC ANALYSES

<u>Coal Seam</u>	<u>Herrin (No. 6)</u>	<u>Brazil Block</u>	<u>Hiawatha</u>
Reflectance (in oil at 546 nm)	0.65	0.58	0.52
Vitrinite	65.1	56.3	73.7
Pseudovitrinite	19.8	8.7	7.8
Fluorinite	0.3	0.2	0
Resinite	0.1	0.7	6.9
Sporinite	3.0	14.1	0.5
Cutinite	0.4	2.0	0.8
Amorphous Liptinite	1.8	4.2	1.0
Semi-fusinite	5.7	4.9	4.2
Fusinite	2.1	3.4	1.3
Micrinite	1.7	5.5	3.8

In a study on the fluorescence properties of the Brazil Block seam, a somewhat different approach was used. In this case, about a hundred individual spectra were taken on all fluorescing liptinite macerals. Although the macerals from which the spectra were taken were not identified at that time, photomicrographs in both normal white-light and fluorescent light were taken for documentation. The spectral parameters for each spectrum were calculated and these data were subjected to cluster analysis to generate groupings of spectra on the basis of the spectral parameters. When these groups were identified they were subjected to discriminant function analysis to test degree to which the groups could be separated on the basis of their spectral parameters. It was found that seven groups could be distinguished. The basic petrographic data for the Brazil Block coal seam are given in Table 1 and the average spectral parameters for each group are given in Table 2. When the macerals from which the spectra were taken were identified from the photomicrographs, it was found that each group corresponded to a separate maceral type or a variety of a maceral type. There was one type of fluorinite, one type of resinite, three types of sporinite and two types of cutinite. While this correspondence of maceral types and varieties to statistical groupings of spectral data was not unexpected, it is further confirmation that the spectral parameters of macerals are unique to maceral type and variety.

Table 2.

SPECTRAL PARAMETERS OF AVERAGE SPECTRA
OF THE BRAZIL BLOCK COAL SEAM

Parameter	Fluorinite	Resinite	Sporinite			Cutinite	
			I	II	III	I	II
Peak (nm)	480	520	550	590	690	610	650
Red/Green Quotient	0.32	0.58	0.85	1.00	1.22	1.47	2.27
Area Blue (%)	37	19	16	14	13	12	7
Area Green (%)	38	43	36	34	31	32	29
Area Yellow (%)	15	23	25	28	26	28	29
Area Red (%)	10	15	23	24	30	28	35
Area Left of Peak (%)	21	33	40	53	93	59	60
Area Right of Peak (%)	79	67	60	47	7	41	40

An interesting result of this analysis is that one of the sporinite varieties and one of the cutinite varieties distinguished by statistical means showed petrographic evidence of alteration (weathering). Because the coal sample itself was collected from a fresh exposure at an active mine, it appears as if the weathered maceral varieties were weathered before they were incorporated into the peat that was later coalified.

The results of these two studies show that fluorescence spectral analysis can distinguish on a quantitative basis the various types of liptinite macerals and, indeed, even varieties of each type. That the various spectra are unique to the individual macerals is further indicated by the recurrent order of the spectral parameters, especially the wavelength of maximum intensity (λ_{max}) and the red/green quotient in any given coal. For example, as shown in Figure 1 for the Herrin (No. 6) seam and in Table 2 for the Brazil Block seam the order of the maceral types on the basis of increasing λ_{max} and Q is fluorinite, resinite, sporinite and cutinite. It should be noted, however, that as the rank of coal increases, all of the spectral peaks shift toward longer wavelengths and diminish in intensity and are thus difficult or impossible to distinguish from each other. Weathering of the macerals has a similar effect.

However, even when macerals have been altered by increases in rank, or weathering, or other processes, fluorescence microscopy can sometimes still be quite useful in characterizing coal macerals. For example, in some coal seams in the western U.S. there is an abundance of resinite. In fact, the resinite is being extracted from some of these coals and commercially exploited as a chemical raw material. In these seams the resinite most often occurs as a secondary material, filling fissures and voids in the coal. Numerous flow textures, inclusions of coal in resinite veinlets, and intrusive relationships throughout coal seams indicate that the resinite was mobilized at some point in its history. These secondary resinites are often difficult to detect in normal white-light viewing, however, they all tend to fluoresce strongly in a variety of colors and are therefore, quite amenable to fluorescence analysis. When samples of the Hiawatha seam from Utah are so examined, four types of secondary resinites, each with a different fluorescence color -- green, yellow, orange, red-brown -- are seen. Each type has a spectra that is distinctive and the various types can also be statistically separated on the basis of their spectral parameters. The average spectra of the four resinite types are shown in Figure 2 and the basic petrographic analysis of the sample from the Hiawatha seam is given in Table 1. It should be noted that at this time the only way to distinguish the various types of secondary resinite is with fluorescence microscopy. Work is now underway to separate these various resinite types and chemically characterize them.

SUMMARY

Although the characterization of coal macerals on the basis of their fluorescence spectral is a recent innovation, it has already proven to be an excellent fingerprinting tool for the various macerals. In some cases, it is even more sensitive than normal petrographic analysis. The initial results of fluorescence spectral studies show that the various fluorescent macerals in single coals can be statistically separated on the basis of their spectral parameters and that even varieties of one type of maceral can be so separated. Although the spectra obtained at this time are rather broad and not suitable for chemical structure analysis, the potential for structural analysis exist and may be realized with improvements in instrumentation.

REFERENCES

- 1) Jacob, H., (1964), Neue Erkenntnisse auf dem Gebiet der Lumineszenzmikroskopie fossiler Brennstoffe. -Fortschr. Geol. Rheinl. u. Westf., v. 12, p. 569-588.
- 2) Jacob, H., (1972), Mikroskop-Photometrie der organischen Stoffe von Boden I. Organopetrographische Nomenklatur und mikroskop-photometrische Methodik.- Die Bodenkultur, v. 23, p. 217-226.
- 3) van Gijzel, P., (1967), Autofluorescence of fossil pollen and spores with special reference to age determination and coalification. Leidse Geol. Meded., v. 50, p. 263-317.
- 4) van Gijzel, P., (1971), Review of the UV-fluorescence microphotometry of fresh and fossil exines and exosporia. In: Brooks et al.: Sporopollenin, p. 659-685, London, New York (Academic Press).

- 5) van Gijzel, P., (1975), Polychromatic UV-fluorescence microphotometry of fresh and fossil plant substances with special reference to the location and identification of dispersed organic material in rocks. In: Petrographic Organique et Potential Petrolier (Ed. by B. Alpern), p. 67-91, CNRS, Paris.
- 6) Teichmuller, M., (1974a), Uber neue Macerale der Liptinit-Gruppe und die Entstehung von Micrinit: Fortschr. Geol. Rheinld. u. Westf., v. 24, p. 37-64.
- 7) Teichmuller, M., (1974b), Entstehung und Veranderung bituminoser Substanzen in Kohlen in Beziehung zur Entstehung und Umwandlung des Erdols: Fortschr. Geol. Rheinld. u. Westf., v. 24, p. 65-112.
- 8) Teichmuller, M., (1974c), Generation of petroleum-like substances in coal seams as seen under the microscope. In: Advances in Organic Geochemistry 1973 (Ed. by B. Tissot and F. Bienner), p. 379-407, Editions Technip, Paris.
- 9) Ottenjann, K., Teichmuller, M. and Wolf, M. (1975), Spectral fluorescence measurements in sporinites in reflected light and their applicability for coalification studies. In: Petrographie Organique et Potentiel Petrolier (Ed. by B. Alpern), p. 49-65, CNRS, Paris.
- 10) Crelling, John C., Dutcher, Russell R. and Lange Rolf V., (1982), Petrographic and fluorescence properties of resinite macerals from western U.S. coals: Proceedings of the Fifth Symposium on the Geology of Rocky Mountain Coal - 1982: ed. Klaus D. Gurgel, Bulletin 118, Utah Geological and Mineral Survey, p. 187-191.
- 11) Crelling, John C., (1982), Current uses of fluorescence microscopy in coal petrology: Journal of Microscopy (in press).
- 12) Ottenjann, K., Wolf, M. and Wolf-Fischer, E., (1981) Beziehung zwischen der Fluoreszenz von Vitriniten und den technologischen Eigenschaften von Kohlen: Proceedings of International Conference on Coal Science - Dusseldorf, IEA, p. 86-89.
- 13) van Gijzel, P., (1979), Manual of the techniques and some geological applications of fluorescence microscopy. Workshop sponsored by Am. Assoc. of Strat. Palynologist, Core Laboratories, Inc., Dallas.

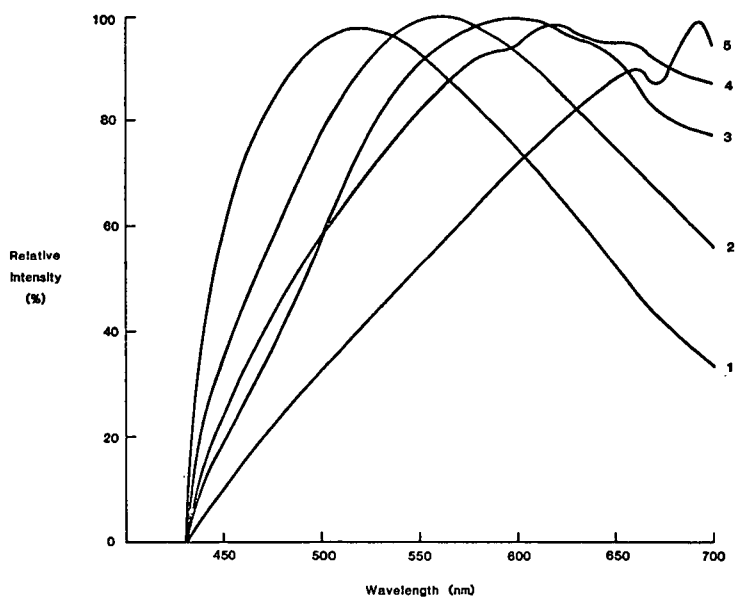


Figure 1. Average fluorescence spectrum for various macerals in the Herrin (No. 6) coal seam: 1) fluorinite; 2) low-peaking resinite; 3) high-peaking resinite; 4) sporinite; 5) cutinite. Vitrinite reflectance of the seam is 0.65%.

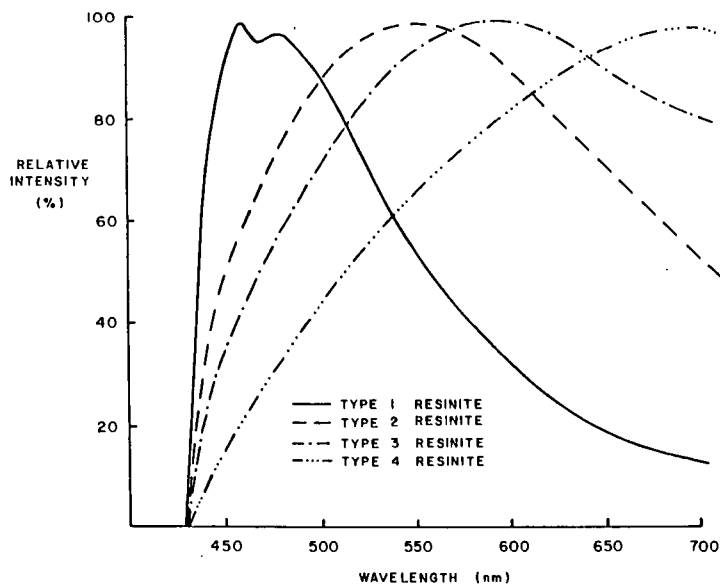


Figure 2. Average fluorescence spectra of resinite macerals in the Hiawatha seam, Utah after Crelling, et al. (10)

MICROSCOPIC INFRARED SPECTROSCOPY OF COALS

D. Brenner

Exxon Research and Engineering Company
P.O. Box 45
Linden, New Jersey 07036

Introduction

Most IR (infrared) spectroscopy of coal involves the use of finely crushed particles. Techniques in common use include incorporating the particles in potassium bromide disks (1) or slurrying them in a hydrocarbon oil such as Nujol (2). Such particulate samples generally include a wide range of types of vitrinite and other macerals which are derived from different plants (such as trees, bushes, and grasses) and from various parts of each plant (such as trunks, stems, roots, leaves, etc). In addition, inorganic substances of various types and degrees of dispersion are generally mixed in. Because of their different derivations, the various organic plant remnants are likely to have different physicochemical characteristics; however, because of the intimate mixing of these subcomponents, which usually occurs on a microscopic scale, it is difficult to separately characterize the different maceral components. In particular, IR spectra obtained on pulverized coal samples give averaged information rather than being characteristic of any individual component in the coal. A few techniques have been utilized in the past to overcome this problem. These include the hand separation of macerals (3,4), sink-float techniques, and the recently developed method of centrifugal separation of very finely pulverized coal (5). These preparation techniques provide a mixture of material which is highly enriched in a selected maceral type. These maceral concentrates can then be analyzed by a variety of chemical procedures. The averaged properties of a maceral type can be characterized using these procedures, but they do not enable the IR analysis of individual microscope macerals.

The particulate samples of coal used for infrared analysis must be finely ground because of the high absorbance of the coal. The particles must be less than roughly 20 micrometers thick (depending on the rank) for substantial transmission of the IR radiation in the more absorbing regions of the spectrum. The small particles of coal cause considerable scattering to appear in the IR spectrum. Other complications are the differences in the thicknesses of the various particles of the sample, and the variations in thickness along each particle. For example, the thinner edges (with respect to the illuminating beam) of the particles will be more transparent than the central regions, so the volume of the particles may not be sampled uniformly. This can be a problem for a heterogeneous material such as coal. Thin section samples of coal having a relatively uniform thickness of 20 micrometers or less have been used occasionally in the past (6). However, the difficulties in preparing these thin section samples and problems of contamination with the adhesives used in the preparation of the sections (7) has limited their usage. Also, because the cross sectional area of the samples must be several square millimeters or more for analysis with most IR spectrometers, microscopic components of the thin sections can not be individually analyzed.

In this paper a technique for the IR spectroscopic analysis of individual microscopic components in coal is described. This method combines new procedures for preparing uncontaminated thin section specimens of coal with a sensitive IR microspectrophotometer which has recently become commercially available. Details of this new technique are discussed and some representative spectra are described.

Experimental

The coal used in this study was Illinois No. 6 which is a high volatile C bituminous coal. To prepare thin sections, a chunk of coal about 1.5 cm across was cut perpendicular to the bedding plan to produce a roughly flat surface. This surface was ground smooth on a 20 cm diameter wheel using 600 grit and then 8 micrometer silicon carbide on disks. The flat surface was cemented to a glass slide with a thermoplastic hydrocarbon-based adhesive (Paraplast, manufactured by the Lancer Company) which is soluble in hexane. A temperature of about 70°C was used in melting and applying the adhesive. The coal was exposed to this temperature for only about a minute before cooling was started. The coal on the slide was ground to a thickness of 15 micrometers using the abrasives described above. The sample was then soaked in hexane at room temperature until the thin specimen floated off of the slide. The sample came off as a number of small pieces of various sizes from less than a millimeter across to several millimeters long. Although no residual adhesive could be observed on the pieces of coal, to insure complete removal of the adhesive the samples were immersed in a large excess of fresh solvent for several days. Then the hexane was decanted off and the specimens were stored in nitrogen at room temperature until they were used.

The microscopic infrared spectrophotometer used in this work (NanoSpec/20IR manufactured by Nanometrics Inc.) operates in transmission and contains reflecting lenses. Because of the reflecting optics, the visual and IR images of the sample correspond and the region of the sample being analyzed can readily be identified visually while it is in place in the IR microscope. This enables unambiguous correlation of visual microscopic characterization and IR analysis for the same area of the sample. The condenser and the objective of the microscope are both 15 power, 0.28 numerical aperture reflecting lenses. The part of the sample to be IR analyzed is optically delineated by an adjustable aperture at the image plane of the objective, so no masking is needed at the sample itself to define the analyzed area. The useful IR range of the instrument is from about 4000 to 700 cm^{-1} (2.5 to 14 micrometers). The IR monochromator is a variable interference filter. The resolution is only about 1% of the wave number value over the IR range; however, this should be adequate for many applications with coal because of the breadth of most of the absorbances. The IR source is a Nerst Glower and the detector is a liquid nitrogen cooled mercury cadmium telluride photodetector having high sensitivity. The operation of the spectrometer is computer-controlled and the data, which is stored digitally, can be automatically averaged and difference spectra can be obtained.

Results

In this preliminary study, spectral characteristics of vitrinite and exinite macerals in Illinois No. 6 coal were examined to evaluate the utility of this new technique for microscopic IR analysis of coals. In Figure 1, a photomicrograph of a thin section specimen consisting of a megaspore (a form of liptinite) surrounded by relatively homogeneous vitrinite is shown. The thin section was placed on a barium fluoride disk on the stage of the IR microscope. The megaspore and a region of the vitrinite lying close to the megaspore on the same specimen were analyzed with the IR microscope. The analyzed regions are indicated by rectangles drawn on the photograph of the sample; they are each about 55 micrometers wide by 180 micrometers long. Spectra of the two regions were taken in air at room temperature; they are compared in Figure 2. The spectra are displaced vertically to avoid overlapping. The displayed spectra actually involve a reference scan which was taken without the sample present but with all other conditions the same. The subsequent sample spectra are automatically normalized with respect to the reference spectrum. Each of the two sample spectra in Figure 2 are 2 minute scans.

A number of differences between the liptinite and vitrinite spectra are apparent. Note that since the thicknesses of the liptinite and vitrinite regions are the same and since scattering is minimal, these spectra can be directly compared quantitatively on a per unit volume basis. Some of the more prominent of the differences are as follows. The broad hydroxyl peak around 3350 cm^{-1} is much deeper for the vitrinite. This probably is caused chiefly by a much larger number of phenols in the vitrinite, but it may also indicate more water absorbed on the vitrinite. Between 2800 and 2975 cm^{-1} the liptinite shows a much stronger absorption than the vitrinite. This indicates much more aliphatic hydrogen in $-\text{CH}$, $-\text{CH}_2$, AND $-\text{CH}_3$ groups in the liptinite. Also, at about 2850 cm^{-1} the liptinite shows a substantially larger peak than the vitrinite on the side of the larger absorption. At about 1600 cm^{-1} the vitrinite peak is much larger than the liptinite peak probably indicating much more aromatic character in the vitrinite. Conversely, the CH_2 , CH_3 peak around 1440 cm^{-1} is much more pronounced for the liptinite. The spectra clearly contrast the more aromatic and hydroxyl-containing structure of the vitrinite to the more aliphatic structure of the liptinite.

Mention should be made of some artifacts which appear in the spectra of Figure 2. At about 2350 cm^{-1} there is a peak caused by CO_2 in the air. (This peak could be eliminated, if desired, by sealing the region of the beam path and maintaining a nitrogen atmosphere). At about 2250 cm^{-1} and 1230 cm^{-1} are peaks caused by changes in the IR filters. Three filters are used to obtain the full spectrum, and small peaks occur where the second and third filters are brought into use. Another artifact is broad peaks seen around 2100 cm^{-1} in the liptinite spectrum, 1950 cm^{-1} in the vitrinite spectrum and in some other areas. These peaks are caused by interference fringes which arise from the IR radiation being internally reflected from the top and bottom surfaces of the sample. The fringes can be misleading if they are not correctly identified.

The applicability of this technique for "in situ" IR analysis during chemical treatments and the ability to perform kinetic measurements was tested by observing the effect of applying deuterated pyridine to a thin section of vitrinite and then allowing it to dry. An area 40×180 micrometers was analyzed. First a spectrum was taken of the untreated sample. Then the solvent was placed on the sample and repetitive scans were made to monitor changes in the IR spectrum as the deuterated pyridine evaporated. Figure 3 shows spectra of the untreated sample, the sample wet with pyridine, and the sample after drying for about 20 minutes. For the latter spectrum, peaks characteristic of deuterated pyridine are still prominent, such as those at about 950 and 820 cm^{-1} . Later scans showed no appreciable lessening of the peaks. The retention of some of the pyridine is consistent with the results of Collins *et. al.* (8).

Tests were made to determine the minimum area of analysis which could be conveniently used with thin sections of coal in this technique. Figure 4 shows spectra of regions of a tiny roughly 30×30 micrometer piece of vitrinite. One spectrum was taken using a 21×21 micrometer analyzing area, and the other spectrum was taken using a 20×30 micrometer analyzing area. Four minutes were used for each scan. For this scan time, the smaller area gives quite a noisy spectrum, but the 20×30 micrometer spectrum is much better. By using a longer scanning time or by accumulating repetitive scans this spectrum could probably be made quite respectable. The spectral region having the greatest problem in the analysis of such very small areas is beyond 1000 cm^{-1} where the sensitivity of the spectrometer falls off. Subcomponents or macerals in the coal which are somewhat less than 25 micrometers across can probably be IR analyzed by using long data accumulation times. Preferably such small subcomponents should be physically separated from the surrounding material. Alternatively, the spectrum of a region including the subcomponent as well as some of the surrounding material could be subtracted (using an appropriate normalization factor) from a spectrum only of the surrounding

material in order to isolate the contribution of the subcomponent. Note, however, that for subcomponent sizes near the wavelength of the IR radiation the possibility of interference effects from the edges of the sample must be considered. Such effects ought to be made apparent by comparing spectra from subcomponents having different sizes or shapes.

Discussion

Infrared spectra of good quality have been obtained on uncontaminated individual microscopic macerals and microscopic subregions in coal. This development enables the infrared characterization of microscopic individual subcomponents of coals and other solid fossil fuels as opposed to obtaining statistically averaged data on complex mixtures. In addition, variations in functionalities over microscopic distances can be studied. The technique should also be applicable for the analysis of virtually any chemical process or chemical treatment of coal which causes changes in the IR spectrum and in which the area of interest is identifiable after the treatment. For example, the initial chemical functionality of an individual microscopic maceral or subregion can be determined with the microspectrometer; the maceral can be reacted; and the effect of the treatment on that same microscopic subregion can be determined.

In Figure 2 the IR spectrum of a subregion of vitrinite about 0.010 mm^2 in area is compared with the IR spectrum from an equal area which is within a single megaspore. The two regions of analysis are on the same piece of thin section and they are separated by only about 160 micrometers. The two minute scans of the 15 micrometer thick samples give excellent signal to noise. As described in the results section, these spectra clearly contrast the more aromatic and hydroxyl-containing structure of the vitrinite to the more aliphatic structure of the megaspore. The ability to analyze closely lying regions having identical preparation, equal areas being analyzed, and the same thickness, facilitates quantitative comparisons of the regions. Thus, while these data are generally consistent with the results of Bent and Brown (9) taken on maceral concentrates, the present technique enables a more direct quantitative comparison of the spectra.

The spectra in Figure 3 demonstrate the "in situ" treatment of an uncontaminated thin section of coal. One operational difficulty is the possibility of movement of the sample during treatment which would make analysis of the same microscopic region before and after treatment difficult. For example, application of a drop of solution to the coal is likely to cause movement. Movement can be avoided by securing the sample, but this may be difficult for small samples or it may affect the sample. Alternatively, if the region under analysis is carefully recorded, such as on a photograph, then during or after treatment the sample can be accurately repositioned on the stage.

Figure 4 demonstrates that isolated samples of coal less than 30 micrometers across can be satisfactorily IR analyzed and that delineated regions of a sample less than 25 micrometers across can be characterized by IR. Signal to noise levels which are improved over those shown in Figure 4 can be obtained by using longer data accumulation times. Alternatively, if better quality data is required only for some small regions of the spectrum, then those regions alone can be scanned to shorten the time needed to obtain an acceptable signal to noise level. The ability to analyze small regions of a coal sample is important even for a single maceral type such as vitrinite. For example, substantial variations occur in the structure (10,11) and swellability (12) of different microscopic areas of vitrinite from the same coal.

In the IR microscope the region of the sample being analyzed is delineated by a variable aperture at the image plane of the objective. Therefore, no spacial

restrictions are placed around or near the sample itself. Since the image of the sample has been substantially magnified at this image plane, it is relatively easy to accurately define even very small subregions of the sample for analysis with the aperture. However, the geometrical region delineated by the variable aperture which is observed visually is not nearly so well defined for the infrared radiation because of diffraction effects. The spacial uncertainty is proportional to the wavelength, so the resolution is considerably poorer near the long wavelength end of the IR range. The divergence or angular spread of the IR beam passing through the sample, which is determined by the numerical aperture, will further diminish the spacial specificity of the delineated area. This, of course, becomes more of a problem for thick samples. For analysis of a very small subregion in the coal, the most unambiguous way to avoid contributions from contiguous material is to physically remove the subcomponent from the surrounding material.

The 15 micrometer thickness for the Illinois No. 6 coal is quite satisfactory since the percent transmissions of a number of the larger peaks are below 40 percent, but without saturation. Also, at this thickness the thin sections can be conveniently manipulated without fracturing. Using the described grinding technique for preparation, samples containing any maceral types and even substantial amounts of mineral matter can be prepared. A wide range of coals (with the possible exception of very low or very high ranks) can be handled by these techniques.

The interference peaks which occur in the spectra of Figure 2 can be misleading when trying to interpret the spectra. These fringes occur when some of the IR radiation reflects from the top and bottom surface of the sample and then interferes with the unreflected beam. The fringes are particularly a problem where the top and bottom surfaces are nearly parallel and where the thickness of the sample is comparable to the wavelengths of the radiation such as for the thin section specimens used in the technique described here. However, the intensity of the interfering beam is not large since it is reflected twice and it passes through the sample three times instead of once. Thus, as seen in Figure 2, the fringes are most prominent in the spectral regions having low absorbance. The fringes can be partially compensated for by determining their position and intensity in a low absorbance region and then calculating and subtracting out their contribution to other parts of the spectrum where their presence is less obvious. Alternatively, tilting the sample, or using samples of different thicknesses and of higher absorbance can be used to identify the effects of the fringes on a spectrum so that they can be compensated for.

Summary and Conclusions

Microscopic macerals and subregions in coal have been characterized by infrared spectroscopy using a new technique. Individual macerals or subregions of the coal as small as 25 micrometers across can be analyzed. The technique utilizes new procedures for preparing uncontaminated thin sections of coal in combination with a recently available microscopic IR spectrometer.

Because the thin section specimens are not contaminated with adhesives or embedding materials, and because the samples are readily accessible on the stage of the IR microscope, this technique is well suited for "in situ" treatments of the coal. Alternatively, since the 15 micrometer thick specimens of coal can ordinarily be handled and transported without damage (if proper care is taken), an untreated sample can be initially analyzed, then it can be removed from the instrument for chemical or thermal treatment, and finally, the same specimen can be returned to the microspectrometer for determination of the changes in the IR spectrum. The analysis of the same spectrum before and after treatment is highly desirable for micro-heterogeneous substances such as coal.

The microscopic IR spectroscopy technique described here differs from and complements prior IR work on maceral concentrates in being able to spatially delineate an individual subcomponent being IR analyzed and to characterize it visually in the context of its surroundings.

Preliminary IR measurements on microscopic subregions of individual macerals of homogeneous-appearing vitrinite and of megaspores in Illinois No. 6 coal clearly demonstrate quantitative as well as qualitative chemical differences between these macerals. This work demonstrates that good quality IR spectra of microscopic subregions of coal can be obtained.

Acknowledgement

The author wishes to acknowledge the excellent technical assistance of Mark S. Beam in the preparation of the samples for these studies.

References

1. Gordon, R. R., Adams, W. N., Pitt, G. J., Watson, G. H., Nature, 174, 1098 (1954).
2. Brooks, J. D., Durie, R. A. and Sternhell, S., J. Appl. Sci., 9, 63 (1958).
3. Fenton, G. W. and Smith, A. H. V., Gas World, 149 (1959).
4. van Krevelen, D. W. and Schuyer, J., Coal Science, p. 240, Elsevier, Amsterdam (1957).
5. Dyrkacz, G. R., Horwitz, E. P., Fuel, 61, 3 (1982).
6. Cannon, C. G. and Sutherland, G. B. B. M., Trans. Faraday Soc., 41, 279 (1945).
7. Mackowsky, M.-Th., "Stach's Textbook of Coal Petrology," p. 243, Gebruder Bontraeger, Berlin (1975).
8. Collins, C. J., Hagaman, E. W., Jones, R. M., and Raaen, V. F., Fuel, 60, 359 (1981).
9. Bent, R. and Brown, J. K., Fuel, 40, 47 (1961).
10. Taylor, G. H., Coal Science, Advances in Chemistry Series 55, p. 274, edited by Given, P. H., Am. Chem. Soc., Washington D.C. (1966).
11. Brenner, D., Proceedings of the International Conference on Coal Science, p. 163, Verlag Gluckauf GmbH, Essen (1981).
12. Brenner, D., Preprints of the Division of Fuel Chemistry, ACS National Meeting, Vol. 27, No. 3-4, 244 (1982).

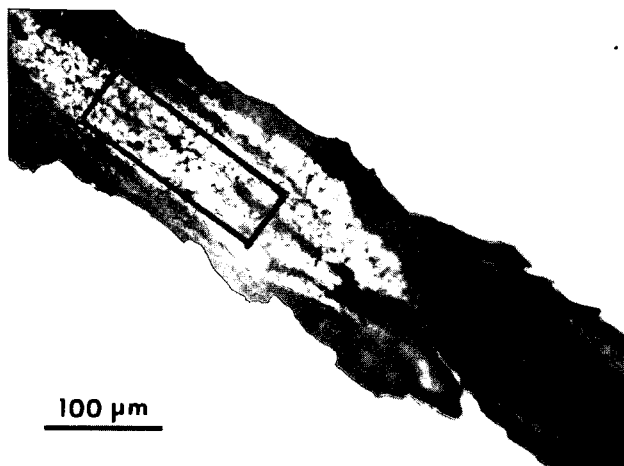


Fig. 1. Thin Section Sample of Illinois No. 6 Coal Containing Regions of Vitrinite and Liptinite

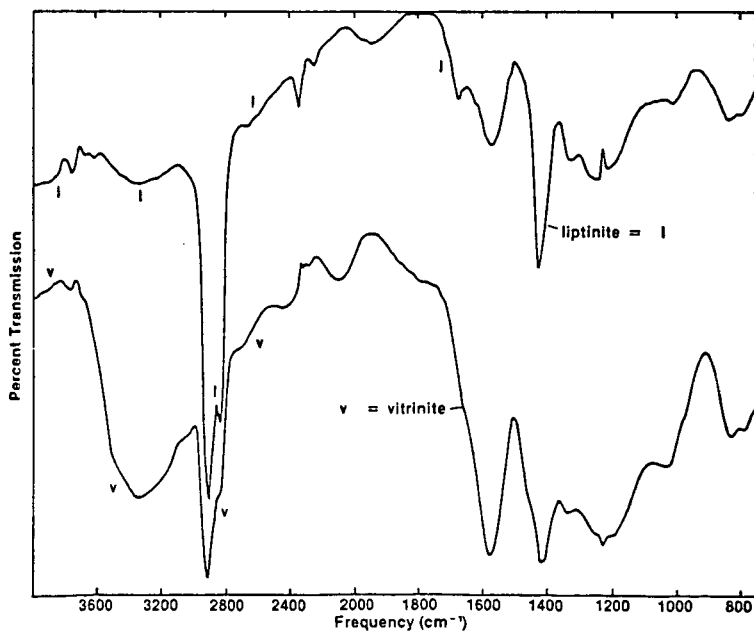


Fig. 2. IR Spectra of Microscopic Regions of Vitrinite and Liptinite in the Same Thin Section Sample of Illinois No. 6 Coal

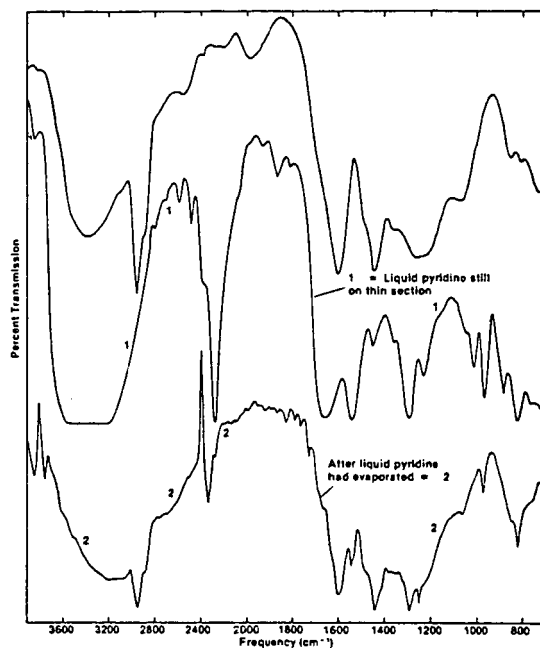


Fig. 3. IR Spectra of a Microscopic Region of Vitrinite in a Thin Section of Illinois No. 6 Coal
 Top ---- Untreated Sample
 Middle -- Liquid Deuterated Pyridine on the Sample
 Bottom -- After Pyridine has Evaporated

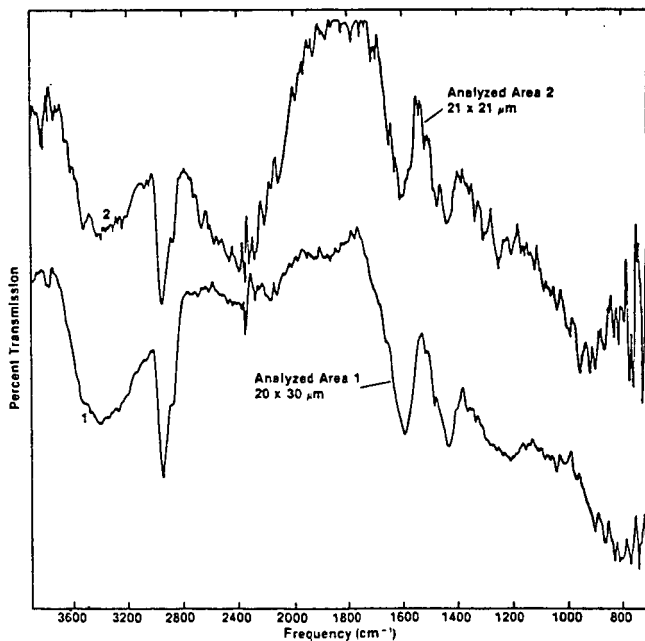


Fig. 4. IR Spectra of a Thin Section Sample of Illinois No. 6 Coal having an Area of $30\mu\text{m} \times 30\mu\text{m}$
 Top ---- Delineated Area is $21\mu\text{m} \times 21\mu\text{m}$
 Bottom -- Delineated Area is $20\mu\text{m} \times 30\mu\text{m}$